

Microbial metabolisms and calcification in freshwater biofilms

Dissertation
zur Erlangung des Doktorgrades
der Mathematisch-Naturwissenschaftlichen Fakultäten
der Georg-August-Universität Göttingen

vorgelegt von

Fumito Shiraishi

Aus Imabari / Japan

Göttingen März 2008

D 7

Referent: Prof. Dr. Joachim Reitner

Korreferent: Prof. Dr. Volker Thiel

Tag der mündlichen Prüfung:

Table of contents

Acknowledgements

1. Introduction	1
2. Microenvironmental effects of biofilms and calcium mass balance	15
Photosynthesis, respiration and exopolymer calcium-binding in biofilm calcification (Westerhöfer and Deinschwanger Creek, Germany)	
3. Microenvironmental effects of biofilms and trace of calcium	38
Microbial mediation of stromatolite formation in karst-water creeks	
4. Effects of pH and temperature on biofilm calcification	57
The affect of bulk water pH and temperature on calcium precipitation in tufa	
5. Microbial effects on bulk water chemistry, stable isotopes and fabrics	71
Microbial effects on biofilm calcification, ambient water chemistry and stable isotope records in a highly supersaturated setting (Westerhöfer Bach, Germany)	
6. Development of new hybridization technique for calcified biofilms	105
<i>In situ</i> co-localization of microorganisms and calcite in calcified biofilm by using FISH and CARD–FISH	
7. Discussion	115
Preconditions of photosynthesis induced carbonate precipitation	
Summary	125

Acknowledgements

The work of this thesis was strongly supported by many people. First of all, Dr. Gernot Arp provided me a great opportunity to come and study in Germany. He helped me very much through the whole period of my three years German life, including university registration, coordination of my daily life and scientific supervising. Especially, I am grateful that he kindly attended me whenever I visited him. Dr. Andreas Reimer supervised my study together with Dr. Gernot Arp, and he introduced me various kinds of chemical analysis. Prof. Dr. Joachim Reitner, the leader of our working group, provided me many useful advises, and occasionally encouraged me by cool beer during very hot summertime.

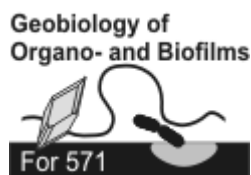
Dipl.-Geol. Nadine Schäfer who was sitting in the same office for three years frequently helped me, and provided a lot of essential information for German life. Mr. Wolfgang Dröse provided instructions of various kinds of techniques including histological stainings, sample embedding and hybridization. He also taught me many German words. Mr. Alexander Satmari provided instructions of the polish machine and rock cutting instruments. Dr. Andreas Kronz provided the instructions of electron microprobe and micromill microsampling device. Drs. Daniel Jackson and Nadia Queric provided many advises for the development of CARD–FISH protocols.

Drs. Dirk de Beer and Andrew Bissett provided the instructions of microelectrode measurements and supported my short staying in Bremen. Drs. Thomas Neu and Barbara Zippel supported my short staying in Magdeburg.

Parts of the present study have been published or submitted as papers. Chapter 2 was published in *Geomicrobiology Journal*, Chapter 3 was published in *Limnology and Oceanography*, Chapter 5 was submitted to *Palaeogeography Palaeoclimatology Palaeoecology*, and Chapter 6 was submitted to *Journal of Microbiological Methods*.

My entire study in Germany was funded by DFG project (DFG-Ar 335/5 "Steuerung von Mineralisationsprozessen durch heterotrophe und autotrophe Prokaryota in Hoch-pCO₂-Biofilmen von Kalktuffsystemen", Research Unit 571 "Geobiology of Organo- and Biofilms").

A contribution to



Chapter 1

Introduction

Microbialites: key structures for understanding ancient Earth environments

The life, appeared at least before 3.8 Ga (e.g., Mojzsis et al., 1996), had been microscopic size for about 3.0 Ga until when they evolved to relatively bigger size in the late Proterozoic. However, the activities of such microorganisms had strong impacts on the ancient Earth environment, and particularly O₂-producing photosynthetic bacteria such as cyanobacteria changed the environment from anoxic to oxic (Fig. 1).

The evidence of microbial activities through the Earth history is recorded in the geological successions as e.g. chemical fossils and microbialites. Especially microbialite, formed by the interactions between sediments and microorganisms, was only the macroscopic structures produced by organisms for 3.0 billion years after the appearance of life on the Earth (Burne and Moore, 1987), which is very interesting material for Earth science.

Microbialites mainly composed of carbonate (stromatolites) and iron (BIF), and other type of minerals such as phosphate and silicate are minor. Although the contribution of microorganisms for BIF formation is still matter of controversy (e.g., Konhauser et al., 2007, and references therein), there is general agreement that the activity of O₂-producing photosynthetic bacteria had strong impact on the BIF distribution through the Earth history. BIF appeared from middle Archean, attained the maximum at late Archean to Paleoproterozoic, followed by sharp decline when pO₂ increased, and no extensive

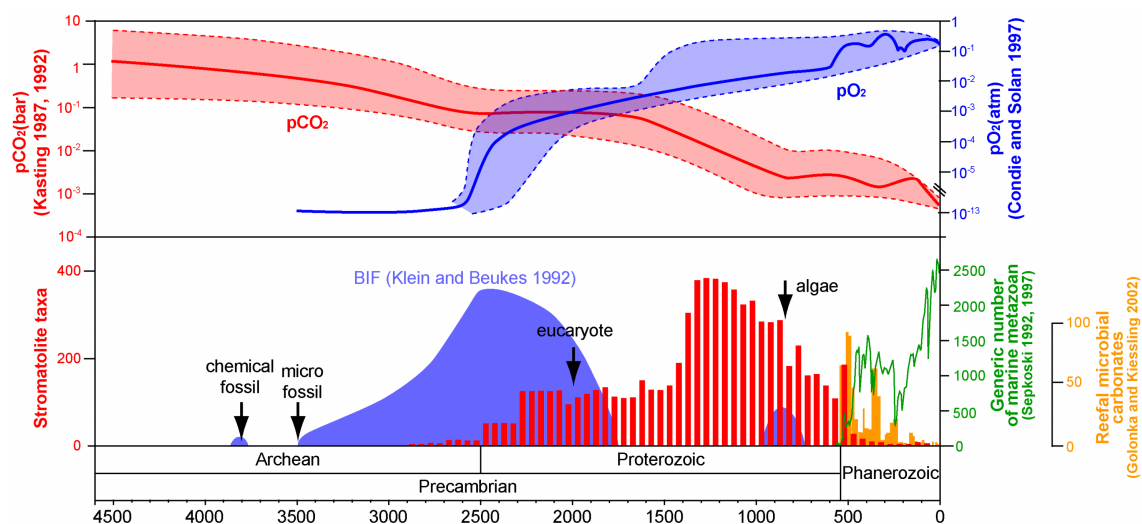


Fig. 1 Integrated time distributions of microbialite (BIF, stromatolite and reefal microbial carbonates) and the number of metazoan over geologic time. Estimated changes of pCO₂ and pO₂ are also shown. Partly based on Riding (2006)



Fig. 2 Recent marine stromatolites in Hamelin Pool, Shark Bay in western Australia. (A) The view of low tide state. (B) The view of underwater. Photo courtesy of Dr. Akihiro Kano (Hiroshima Univ.).

development after that except for 0.8-0.6 Ga (Klein and Beukes, 1992; Fig. 1). Stromatolites, the carbonate microbialite, appeared at late Archean, of which development almost overlapped with the decline of BIF. Stromatolite attained the maximum at Mesoproterozoic, followed by decrease in Neoproterozoic, and abruptly decrease at the beginning of Phanerozoic because of the interferences by skeletal algae and invertebrates which disturbed the lamination (Riding, 2000). Although calcareous microbialite without lamination appeared in Phanerozoic together with other reef builders, their appearance decreased toward Recent with some fluctuations. In the Recent ocean, microbialites are restricted in some localities including the stromatolites in Shark Bay and Bahamas, which would retain the view of ancient shoreline (Fig. 2). Mineralization processes by microorganisms are less controlled if compared to the biomineralization of higher organisms such as corals, calcareous algae and vertebrates, and thought to be strongly affected by surrounding environment, and therefore the occurrence pattern of microbialite is thought to provide important information for understanding the evolution of seawater chemistry. This thesis focuses on the carbonate microbialites including stromatolites.

A number of mechanisms for constructing the carbonate microbialite have been suggested, which are largely divided into three: grain trapping, nucleation and precipitation.

Grain trapping: Detritus particles are trapped into the biofilms by the growth of filamentous microorganisms and stabilized, which is suggested from the studies of Recent marine stromatolites (e.g., Gebelein, 1969). Particles are also trapped in the biofilms by simple physical trapping (baffling) and/or sticky exopolymers produced by microorganisms (e.g., Riding, 2000). However, trapped particles must be strengthened by early lithification in any case to remain as a construction.

Nucleation: Exopolymer produced by microorganisms and microbial cell walls contain a

number of acidic functional groups which can bind positively charged cations such as Ca^{2+} , and it is suggested that this binding results in the mineral nucleation (e.g., Pentecost and Riding, 1986). Indeed, it is demonstrated that different composition of exopolymer leads to different crystal type (e.g., Kawaguchi and Decho 2002a; Braissant et al. 2003). Although the inhibition of precipitation by exopolymer Ca^{2+} binding is also suggested (e.g., Kawaguchi and Decho, 2002b), the binding capacity must be considered quantitatively because exopolymers are not infinitive sponge for cations (see also Arp et al., 2001).

Precipitation: It is suggested that saturation state of carbonate minerals is increased by the microbial metabolisms, and results in the mineral precipitation. A number of mechanisms have been suggested: photosynthetic CO_2 assimilation (e.g., Pentecost and Riding, 1986), alkalinity increasing by ammonification, denitrification, sulphate reduction and anaerobic sulphide oxidation (see Dupraz and Visscher, 2005). In addition, mineral precipitation induced by non-living organic molecular is also suggested (organomineralization; e.g., Trichet and Defarge, 1995; Reitner et al., 1995).

The most convincing material for understanding the mechanisms of ancient microbialite formation is the recent analogues. Especially stromatolites, fortunately still remain in the Recent ocean, have been intensively investigated, and these studies revealed that grain trapping and sulfate reduction by microorganisms are important for the stromatolite formation (e.g., Gebelein, 1969; Reid et al., 2000). However, Recent marine stromatolites mainly formed by grain trapping, while ancient stromatolites, particularly pre-Phanerozoic stromatolites are formed by *in situ* mineral precipitation (Awramik and Riding, 1988). Therefore, the investigation of Recent stromatolite analogous formed by *in situ* precipitation is required to understand the ancient stromatolite formation. In addition to the selection of optimum materials, the methods for investigating the microbial composition and their influences on the surrounding water chemistry are also important. In this study, the effects of microbial metabolisms and products on the mineral precipitation in the recent stromatolites formed by *in situ* precipitation are investigated by using the latest tools in environmental microbiology including microelectrodes, fluorescence *in situ* hybridisation (FISH) and confocal laser scanning microscopy (CLSM).

By applying optimum tools for optimum samples, this study aims for understanding the formation mechanisms of stromatolites and its implication for the pre-Phanerozoic ocean.

Tufa: an analogue of ancient stromatolites

Although there is no suitable analogue for the ancient stromatolite in the Recent ocean, there are a number of stromatolites formed by *in situ* precipitation in non-marine settings, one of which is the freshwater carbonate deposit in the karst creeks, called as tufa.

There is terminological confusion in the freshwater carbonate deposits, and the terms “sinter” and “travertine” have been used for the carbonate deposits which have completely the same features of “tufa” (Julia, 1983). In this study, the term “tufa” is restricted for the freshwater deposits precipitated from karst water of meteoric origin, by following the definition of Ford and Pedley (1996). It is worth separating tufa from other non-marine carbonate deposits such as hot spring deposits by means of water source. Tufa-depositing water originated from meteoric water and pass through relatively shallow subsurface, and hence the concentrations of dissolved components are relatively low and its deposition is strongly influenced by climatic conditions. On the other hand, the water chemistry of hot spring reflects water-rock interactions in the deep subsurface, and contains higher $p\text{CO}_2$ and various metal ions if compared to that of tufa, and hence fabric and mineralogy of deposits are very diverse.

The depositional process of tufa has been explained as follows. First, meteoric water pass through the soil, and equilibrate with soil atmosphere that has high $p\text{CO}_2$ originated from the respiration of microorganisms. This water dissolves underlying limestone. When water recharged from subsurface, CO_2 degasses from the water because $p\text{CO}_2$ of normal atmosphere is much lower than that of subsurface. As CO_2 degasses from the water, carbonate equilibrium shifts to increase CaCO_3 supersaturation (Fig. 3). Tufa deposits, especially of which contentiously developing on the creek floor, are colonized mainly by filamentous cyanobacteria, and sometimes exhibit annual lamination. Although some researcher thought that microorganisms have strong influence on tufa precipitation, tufa-depositing water attains high supersaturation by physicochemical processes as described above, and there is no microbial effect on bulk water chemistry and isotopic records. Therefore many researchers nowadays are convinced that inorganic precipitation is the major process on tufa deposition, and microbial effects are negligible. However, the investigations of this thesis revealed that tufa is very interesting analogue of ancient stromatolites. As described in following chapters, microbial metabolisms controlled *in situ* mineral precipitation in the biofilm, and result in the stromatolite formation.

In this study, two tufa-forming creeks in Germany were investigated. One is the Westerhöfer Bach in central Germany, and another is the Deinschwanger Bach in the

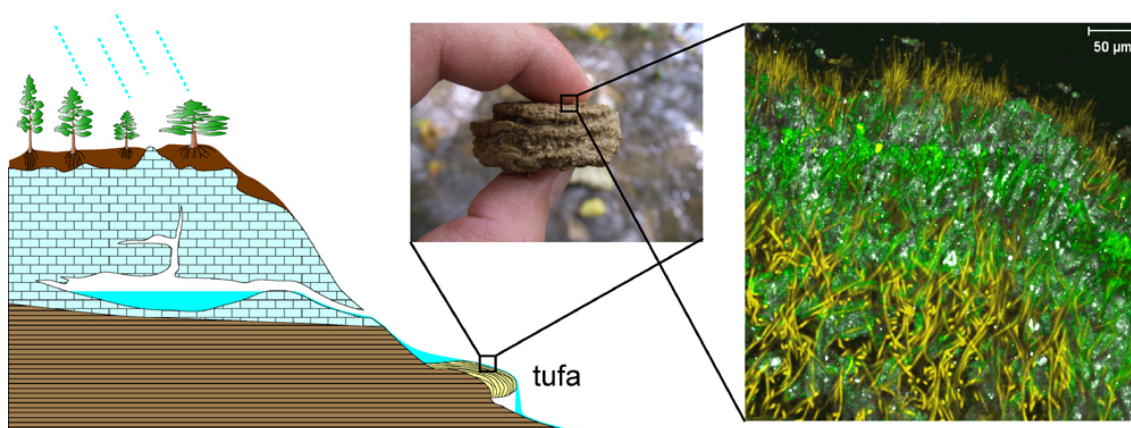


Fig. 3 Schematic view of tufa deposition. Water is meteoric origin which passed through the limestone bed. Tufa deposits in the center of flow path sometimes show annual laminations (tufa stromatolite), and its biofilm mainly composed of filamentous cyanobacteria.

southern Germany.

Equilibrium of aqueous carbonate system

It is necessary to understand the behaviors of carbonate species and cations (e.g., Ca^{2+} , Mg^{2+}) in water when we try to understand the precipitation of carbonate minerals, regardless of inorganic or organic processes involved. Particularly the nature of carbonate species is far from straightforward, and would be an important key for understanding carbonate precipitation. Here, the equilibrium of carbonate species will be briefly explained, and see the text books for the further details (e.g., Stumm and Morgan, 1996; Zeebe and Wolf-Gladrow, 2001).

When CO_2 dissolve in the water, it react with water and dissociate to form three different chemical species (Fig. 4): dissolved CO_2 ($\text{CO}_{2(\text{aq})}$), bicarbonate (HCO_3^-) and carbonate (CO_3^{2-}). Strictly there is also the form of carbonic acid (H_2CO_3) but its amount is much lower than the other species and here it is ignored for simplicity. Equilibrium constants of each reaction (K_H , K_1 and K_2) are expressed as followings (each ion is expressed by

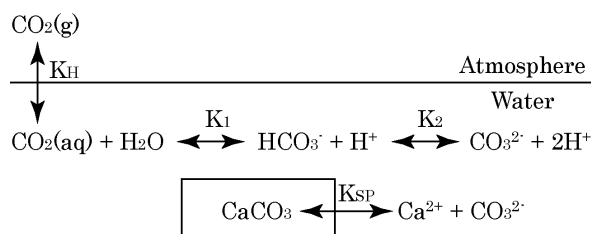


Fig. 4 Schematic illustration of the carbonate system.

Table 1 Equilibrium constants delivered from Plummer and Busenberg (1982). T is in °K.

$$\log K_H = 108.3865 + 0.01985076T - 6919.53 / T - 40.45154 \log T + 669365 / T^2$$

$$\log K_1 = -356.3094 - 0.06091964T + 21834.37 / T + 126.8339 \log T - 1684915 / T^2$$

$$\log K_2 = -107.8871 - 0.03252849T + 5151.79 / T + 38.92561 \log T - 563713.9 / T^2$$

$$\log K_{SP(\text{calcite})} = -171.9065 - 0.077993T + 2839.319 / T + 71.595 \log T$$

concentration for simplicity),

$$K_H = \frac{[\text{CO}_2]}{p\text{CO}_2} \quad (1.1)$$

$$K_1 = \frac{[\text{HCO}_3^-][\text{H}^+]}{[\text{CO}_2]} \quad (1.2)$$

$$K_2 = \frac{[\text{CO}_3^{2-}][\text{H}^+]}{[\text{HCO}_3^-]} \quad (1.3)$$

Similarly, the solubility product (K_{SP}) of calcium carbonate is expressed as follows,

$$K_{SP} = [\text{Ca}^{2+}][\text{CO}_3^{2-}] \quad (1.4)$$

These equilibrium constants and solubility product are the functions of temperature, which are available from literatures (Table 1 shows the equilibrium constants for freshwater; Plummer and Busenberg, 1982). The sum of $\text{CO}_{2(\text{aq})}$, HCO_3^- and CO_3^{2-} is called as total dissolved inorganic carbon, which is denoted either by DIC or ΣCO_2 .

$$\text{DIC} \equiv \sum \text{CO}_2 = [\text{CO}_2] + [\text{HCO}_3^-] + [\text{CO}_3^{2-}] \quad (1.5)$$

From equations (1.2), (1.3) and (1.5), following relationships are obtained,

$$[\text{CO}_2] = \text{DIC} \left(1 + \frac{K_1}{[\text{H}^+]} + \frac{K_1 K_2}{[\text{H}^+]^2} \right) \quad (1.6)$$

$$[\text{HCO}_3^-] = \text{DIC} \left(1 + \frac{[\text{H}^+]}{K_1} + \frac{K_2}{[\text{H}^+]} \right) \quad (1.7)$$

$$[\text{CO}_3^{2-}] = \text{DIC} \left(1 + \frac{[\text{H}^+]}{K_2} + \frac{[\text{H}^+]^2}{K_1 K_2} \right) \quad (1.8)$$

It is clear from these equations that the concentrations of carbonate species are the functions of $[\text{H}^+]$, and thereby of pH ($[\text{H}^+] = 10^{-\text{pH}}$), when the temperature is constant (Fig. 5). The carbonate alkalinity, CA, is expressed as follows,

$$CA = [\text{HCO}_3^-] + 2[\text{CO}_3^{2-}] \quad (1.9)$$

In the freshwater settings, carbonate alkalinity is almost same as total alkalinity. If two of six parameters (DIC, CA, $[\text{H}^+]$, $[\text{CO}_2]$, $[\text{HCO}_3^-]$ and $[\text{CO}_3^{2-}]$) are given, it is theoretically possible to calculate the rest four parameters from equations (1.5)–(1.9).

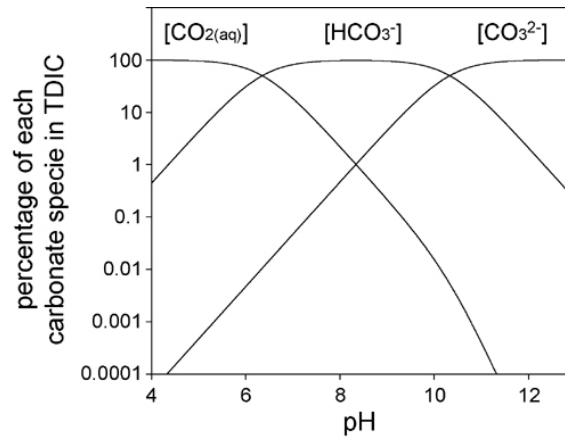


Fig. 5 Relative percentage of carbonate species as function of pH at 25°C.

Activity and ionic strength

Although equilibrium of carbonate species was expressed by using concentration for simplicity in the previous section, activity must be used for accurate thermodynamic calculation instead of concentration. The relationship between molar concentration $[i]$ and activity of dissolved chemical species $\{i\}$ is followings,

$$\{i\} = \gamma_i [i] \quad (1.10)$$

where γ_i is activity coefficient of dissolved species i . Activity coefficient relates with the interactions between ions, which is expressed by the concept, ionic strength I , as follows,

$$I = \frac{1}{2} \sum [i] Z_i^2 \quad (1.11)$$

where Z_i is electric charge of i . Generally, water of ionic strength <0.1 , $0.1-1$ and >1 are called as “diluted”, “intermediate” and “concentrated” respectively. In the natural settings, these three examples correspond to river water, seawater and brine respectively.

There are several methods for estimating activity coefficient that is the function of ion strength. Widely accepted method is following extended Debye–Hückel limiting law,

$$\log \gamma_i = \frac{-AZ_i^2\sqrt{I}}{1 + aB\sqrt{I}} \quad (1.12)$$

where, A and B are temperature-dependent constants, a is radius of given ion. PHREEQC, a computer program used for calculating ion activities and saturation state in this thesis, employs this equation. Activity coefficients delivered from Debye–Hückel's extended equation is accurate for the water with ionic strength of <0.1 , while more complex calculations are required for precisely estimating activity coefficients of more concentrated water such as seawater.

Similar to concentration and activity of ions, fugacity must be used for gases instead of partial pressure to calculate accurately. However, the fugacity of CO_2 in most natural conditions is almost same as partial pressure, and therefore $p\text{CO}_2$ was used in this thesis.

Kinetics in liquid–solid interface

Plummer et al. (1978) dissolved calcium carbonate, and obtained following rate equation,

$$R = -k_1\{\text{H}^+\} - k_2\{\text{H}_2\text{CO}_3^*\} - k_3 + k_4\{\text{Ca}^{2+}\}\{\text{HCO}_3^-\} \quad (1.13)$$

where k_1 – k_4 are the rate constants, and H_2CO_3^* is $\text{H}_2\text{CO}_3 + \text{CO}_{2(\text{aq})}$. It is also possible to apply this equation to precipitation (Plummer et al. 1979; Reddy et al. 1981). However, their experiments dissolved finely crushed spar in turbulence which caused rapid dissolution. Care has to be taken when we apply this equation to the natural conditions because there is diffusive boundary layer (DBL) at solid surface in most cases. DBL is a thin film of water adjacent to the liquid–solid interface and transfer of dissolved component takes place by molecular diffusion in DBL, while turbulent and/or convective flow prevails in the water column (Fig. 6). The thickness of DBL strongly affects the precipitation rates of minerals, which significantly decreases when DBL becomes thicker due to the slow diffusion of ionic species as indicated by the theoretical calculation of Dreybrodt and Buhmann (1991; Fig. 7). DBL becomes thinner when the flow speed of water column becomes faster, and vice versa. The thickness of DBL is also affected by the shape of solid, and small particles tend to attain thinner DBL. Therefore, the equation (1.10) is the highest possible rate of precipitation, and thereby the approximation of DBL thickness of 0.

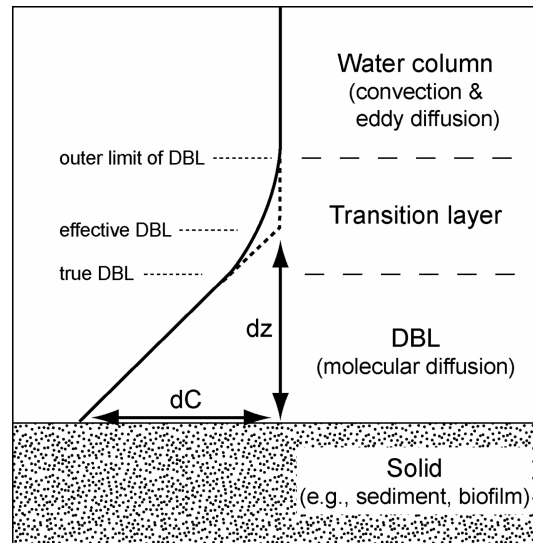


Fig. 6 Schematic of typical microprofile of dissolved component measured by microelectrodes. The interpretation concepts are also shown. After Jørgensen and Revsbech (1985).

As revealed in later chapters, there is DBL of $\sim 200 \mu\text{m}$ thick on the tufa surface even in fast flowing creeks. On the other hand, DBL enables steep chemical gradient upon the biofilm surface, which is measurable by microelectrode. Fig. 6 shows a typical microprofiles and the concept of its interpretation. As indicated in this figure, the concentration of dissolved component is stable in the water column due to the complete mixing by eddy diffusion and convection, while it changes in DBL due to the slow diffusion. The concentration decreases in DBL if biofilm consumes a component as a net, and vice versa. This results in the significant differences of concentrations between the water column, where the conventional water chemistry analysis measure, and DBL, of which chemistry is only measurable by microelectrode.

Concentration gradient measured by microelectrode allows flux calculation of dissolved components by using Fick's first law,

$$J = -D \frac{dC}{dz} \quad (1.14)$$

where D denotes the diffusion coefficient ($\text{m}^2 \text{s}^{-1}$), dC is the concentration difference of a given ion (mol m^{-3}), and dz is the diffusion distance (m).

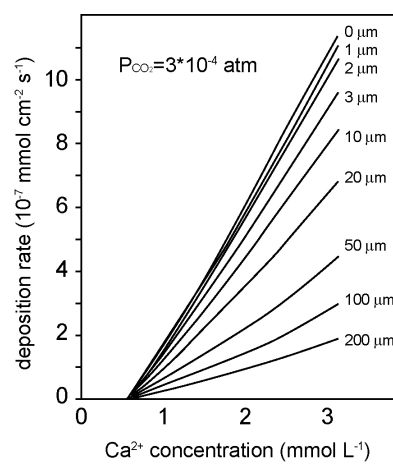


Fig. 7 Deposition rate of calcite in an open system as function of the calcium concentration at 20°C. The numbers on the curves are the thickness of diffusive boundary layer. After Dreybrodt and Buhmann (1991).

References

- Arp G, Reimer A, Reitner J. 2001. Photosynthesis-induced biofilm calcification and calcium concentrations in Phanerozoic oceans. *Science* 292:1701–1704.
- Awramik SM, Riding R. 1988. Role of algal eukaryotes in subtidal columnar stromatolite formation. *Proc Natl Acad Sci USA* 85:1327–1329.
- Awramik, S.M., Sprinkle, J., 1999. Proterozoic stromatolites: the first marine evolutionary biota. *Hist. Biol.* 13, 241–253.
- Braissant O, Cailleau G, Dupraz C, Verrecchia EP. 2003. Bacterially induced mineralization of calcium carbonate in terrestrial environments: the role of exopolysaccharides and amino acids. *J Sediment Res* 73:485–490.
- Burne RV, Moore LS. 1987. Microbialites: organosedimentary deposits of benthic microbial communities. *Palaios* 2:241–254.
- Condie, K.C., Sloan, R.E., 1997. *Origin and Evolution of Earth*. Prentice Hall, New Jersey.
- Dreybrodt, W., Buhmann, D., 1991. A mass transfer model for dissolution and precipitation of calcite from solutions in turbulent motion. *Chem. Geol.* 90:107–122.
- Dupraz C, Visscher PT. 2005. Microbial lithification in marine stromatolites and hypersaline mats. *Trends Microb* 13:429–438.
- Ford TD, Pedley HM. 1996. A review of tufa and travertine deposits of the world. *Earth-Sci Rev* 41:117–175.
- Gebelein, C.D., 1969. Distribution, morphology, and accretion rate of Recent subtidal algal stromatolites, Barmuda. *J. Sediment. Petrol.* 39, 49-69.
- Golonka, J., Kiessling, W., 2002. Phanerozoic time scale and definition of time slices. In: Kiessling, W., Flügel, E., Golonka, J. (Eds.), *Phanerozoic Reef Patterns*, SEPM Sec. Publ. 72, 11-20.
- Jørgensen, B.B., Revsbech, N.P., 1985. Diffusive boundary layers and the oxygen uptake of sediments and detritus. *Limnol. Oceanogr.* 30, 111-122.
- Juria, R., 1983. Travertine. In: Scholle, P.A., Bebout, D.G., Moore, C.H. (Eds.), *Carbonate Depositional Environments*. Am. Assoc. Petrol. Geol. Mem. 33, 64-72.
- Kasting, J.F., 1987. Theoretical constraints on oxygen and carbon dioxide concentrations in the Precambrian atmosphere. *Precambrian Res.* 34, 205–229.
- Kasting, J.F., 1992. Proterozoic climates: the effect of changing atmospheric carbon dioxide concentrations. In: Schopf, J.W., Klein, C. (Eds.), *The Proterozoic Biosphere: A Multidisciplinary Study*. Cambridge University Press, Cambridge, pp. 165–168.
- Kawaguchi T, Decho AW. 2002a. A laboratory investigation of cyanobacterial extracellular polymeric secretions (EPS) in influencing CaCO₃ polymorphism. *J Crystal Growth* 240:230–235.
- Kawaguchi T, Decho AW. 2002b. Isolation and biochemical characterization of extracellular polymeric secretions (EPS) from modern soft marine stromatolites (Bahamas) and its inhibitory effect on CaCO₃ precipitation. *Prep Biochem Biotechnol* 32:51–63.

- Klein, C., Beukes, N.J., 1992. The distribution, stratigraphy, and sedimentologic setting and geochemistry of Precambrian iron formations. In: Schopf, J.W., Klein, C., (Eds.), *The Proterozoic Biosphere; A Multidisciplinary Study*. Cambridge University Press, Cambridge, pp. 139–146.
- Konhauser, K.O., Amskold, L., Lalonde, S.V., Posth, N.R., Kappler, A., Anbar, A., 2007. Decoupling photochemical Fe(II) oxidation from shallow-water BIF deposition. *Earth Planet. Sci. Lett.* 258, 87–100.
- Mojzsis, S.J., Arrhenius, G., McKeegan, K.D., Harrison, T.M., Nutman, A.P., Friend, C.R., 1996. Evidence for life on Earth before 3,800 years ago. *Nature* 384, 55–59.
- Pentecost A, Riding R. 1986. Calcification of cyanobacteria. In: Leadbeater BSC, Riding R. editors. *Biom mineralization in Lower Plants and Animals*. Systematic Assoc Spec Vol 30, Oxford: Clarendon Press, p 73–90.
- Plummer LN, Busenberg E. 1982. The solubilities of calcite, aragonite and vaterite in CO₂–H₂O solutions between 0 and 90°C, and an evolution of aqueous model for the system CaCO₃–CO₂–H₂O. *Geochim Cosmochim Acta* 46:1011–1040.
- Plummer LN, Parkhurst DL, Wigley TML. 1979. Critical review of the kinetics of calcite dissolution and precipitation. In: Janne E. editor. *Chemical Modelling in Aqueous Systems: Speciation, Sorption, Solubility and Kinetics*. Washington DC: American Chemical Society, p 537–573.
- Plummer, L.N., Wigley, T.M.L., Parkhurst, D.L., 1978. The kinetics of calcite dissolution in CO₂–water systems at 5° to 60°C and 0.0 to 1.0 atm CO₂. *Am. J. Sci.* 278, 179–216.
- Reddy MM, Plumer LN, Busenberg E. 1981. Crystal growth of calcite from calcium bicarbonate solutions at constant pCO₂ and 25°C: a test of the calcite dissolution model. *Geochim Cosmochim Acta* 45:1281–1291.
- Reid RP, Visscher PT, Decho AW, Stolz JF, Bebout BM, Dupraz C, Macintyre IG, Paerl HW, Pinckney JL, Prufert-Bebout L, Steppe TF, Das Marais DJ. 2000. The role of microbes in accretion, lamination and early lithification of modern marine stromatolites. *Nature* 406:989–992.
- Reitner, J., Gautret, P., Marin, F., Neuweiler, F., 1995. Automicrites in a modern marine microbialite: formation model via organic matrices (Lizard Island, Great Barrier Reef, Australia). *Bull. Inst. Oceanogr. Monaco, Mun. Spec.* 14, 237–263.
- Riding R. 2000. Microbial carbonates: the geological record of calcified bacterial–algal mats and biofilms. *Sedimentology* 47:179–214.
- Riding R., 2006. Microbial carbonate abundance compared with fluctuations in metazoan diversity over geological time. *Sedimentary Geology* 185, 229–238.
- Sepkoski Jr., J.J., 1992. Proterozoic–early Cambrian diversification of metazoans and metaphytes. In: Schopf, J.W., Klein, C. (Eds.), *The Proterozoic Biosphere; A Multidisciplinary Study*. Cambridge University Press, Cambridge, pp. 553–561.
- Sepkoski Jr., J.J., 1997. Biodiversity: past, present, and future. *J. Paleontol.* 71, 533–539.
- Stumm, W., Morgan, J.J., 1996. *Aquatic Chemistry*. John Wiley & Sons, New York, pp. 1022.
- Trichet, J., Defarge, C., 1995. Non-biologically supported organomineralization. *Bull. Inst. Oceanogr. Monaco,*

Mun. Spec. 14, 203-236.

Zeebe, R.E., Wolf-Gladrow, D., 2001. CO₂ in Seawater: Equilibrium, Kinetics, Isotopes. Elsevier, Amsterdam, 346p.

Chapter 2

Photosynthesis, respiration and exopolymer
calcium-binding in biofilm calcification (Westerhöfer and
Deinschwanger Creek, Germany)

Photosynthesis, respiration and exopolymer calcium-binding in biofilm calcification (Westerhöfer and Deinschwanger Creek, Germany)

Fumito Shiraishi, Andrew Bissett, Dirk de Beer, Andreas Reimer, Gernot Arp

Abstract

The impact of microbial activity on biofilm calcification in aquatic environments is still a matter of debate, especially in settings where ambient water has high CaCO_3 mineral supersaturation. In this study, biofilms of two CO_2 -degassing karst-water creeks in Germany, which attain high calcite supersaturation during their course downstream, were investigated with regard to water chemistry of the biofilm microenvironment. The biofilms mainly consisted of filamentous cyanobacteria (*Phormidium* morphotype) and heterotrophic bacteria (including sulfate-reducing bacteria), which affect the microenvironment and produce acidic exopolymers. *In situ* and *ex situ* microelectrode measurements showed that a strong pH increase, coupled with Ca^{2+} consumption, occurred in light conditions at the biofilm surface, while the opposite occurred in the dark. Calcite supersaturation at the biofilm surface, calculated from *ex situ* Ca^{2+} and CO_3^{2-} microelectrode measurements, showed that photosynthesis resulted in high omega values during illumination, while respiration slightly lowered supersaturation values in the dark, compared to values in the water column. Dissociation calculation demonstrated that the potential amount of Ca^{2+} binding by exopolymers would be insufficient to explain the Ca^{2+} loss observed, although Ca^{2+} complexation to exopolymers might be crucial for calcite nucleation. No spontaneous precipitation occurred on biofilm-free limestone substrates under the same condition, regardless of high supersaturation. These facts indicate that photosynthesis is a crucial mechanism to overcome the kinetic barrier for CaCO_3 precipitation, even in highly supersaturated settings.

INTRODUCTION

Evidence of microbial activity may already be present in early sedimentary rocks as early as the Archean (Schidlowski 1988; Rosing 1999). Since that time, microbial activities have potentially been involved in mineral precipitation, recognizable as microbialites in geological successions. Stromatolites, one category of microbialite (Burne and Moore 1987),

appeared approximately 3.5 billion years ago (Allwood et al. 2006) and were dominant for 2.0 billion years and hence, they are expected to provide essential information about the evolution of the ancient earth-environment and early life (e.g., Awramik 1992). Indeed, microbial mineralization is strongly affected by the chemistry of surrounding environments, unlike biomineralization in higher plants and animals such as corals, coralline algae and vertebrates. This dependence on environmental chemical conditions is the reason why stromatolites and other microbialites are thought to provide important information about the ancient atmosphere and ocean chemistry (e.g., Riding 1982, 2006; Riding and Liang 2005; Grotzinger and Knoll 1999; Arp et al. 2001a).

Until now, several possible explanations have been provided for the mechanisms of stromatolite formation, including sediment trapping by bacterial filaments and adhesive extracellular polymeric substances (EPS), crystal nucleation by EPS, and *in situ* carbonate precipitation by CO₂ removal of photosynthesis (see Riding 2000 for a review). However, it has been difficult to precisely assess the impacts of microbial effects on mineralization for several reasons: 1) microbialites are rare in recent marine environments, and 2) it is difficult to directly measure the influence of microbial activity in the microenvironments where precipitation takes place. Therefore, mechanisms of microbial calcification and stromatolite formation are still a matter of controversy, which includes the discussion about their potential abiotic origin (Grotzinger and Rothman 1996; Grotzinger and Knoll 1999).

In order to overcome above-mentioned problems, a number of researchers have focused on one of the few present-day marine stromatolites, the Bahamian stromatolites, using microbiological methods, including microelectrodes, microautoradiography, fluorescence *in situ* hybridization (FISH), confocal laser scanning microscopy (e.g., Visscher et al. 1998, 2000; Reid et al. 2000; Kawaguchi and Decho 2002a, b; Decho et al. 2005; Baumgartner et al. 2006). These studies suggest that sulfate-reducing bacteria (SRB) play an important role in the gross calcification, while CO₂ assimilation by photosynthesis has only little or no affect (for more detail, see Dupraz and Visscher 2005). However, Awramik and Riding (1988) insisted that most of the pre-Phanerozoic stromatolites are composed of lime mud precipitated *in situ*, and are therefore different from recent marine stromatolites, which have mostly formed by trapping detrital particles (see also Kempe and Kazmierczak 1990). In order to understand the pre-Phanerozoic ocean it is, therefore, necessary to investigate recent stromatolites formed by *in situ* CaCO₃ precipitation, rather than detrital trapping.

While the CaCO₃ supersaturation of recent oceans is too low to support extensive biofilm calcification in open-marine settings, a number of non-marine or lagoonal settings show calcareous microbialites formed by *in situ* CaCO₃ precipitation when approximately an 8- to 10-fold calcite supersaturation in the macroenvironment is exceeded (Kempe and

Kazmierczak 1990; Arp et al. 2001a). Here, carbon assimilation by autotrophs, such as cyanobacteria, is considered to be the major factor in shifting the carbonate equilibrium towards higher $\{CO_3^{2-}\}$ (braces denote activity). Indeed, Awramik (1984) emphasized that non-marine stromatolites mainly constructed by *in situ* $CaCO_3$ precipitation are more suitable for the understanding of pre-Phanerozoic stromatolites than modern or Phanerozoic marine microbial mats and stromatolites. However, one question always arose in studies of environments where water already has a high supersaturation for $CaCO_3$: Is biofilm calcification actively promoted by microbial activity that increases $\{CO_3^{2-}\}$ or passively by providing crystal nucleation sites?

Tufa, formed by calcifying biofilms in CO_2 -degassing karst-water creeks (e.g., Ford and Pedley 1996), is one example of non-marine stromatolites (Riding 2000). The process of tufa formation has been explained as follows (Ford and Pedley 1996): First, meteoric water passes through the soil and equilibrates with the soil atmosphere that has high pCO_2 originating from the respiration of microorganisms. This water dissolves bedrock limestone. When the water is recharged from the subsurface, CO_2 degasses from the water because pCO_2 of the normal atmosphere is much lower than that of the subsurface. As the CO_2 degasses from the water, carbonate equilibrium shifts to increase $CaCO_3$ supersaturation.

Although Ford and Pedley (1996) considered both physical and biological processes to be important for tufa formation, some studies suggested that strong physical CO_2 degassing attains enough supersaturation of bulk water to cause spontaneous $CaCO_3$ precipitation (e.g., Jacobson and Usdowski 1975) and that biofilms of the tufa surface are calcified passively (e.g., Merz-Preiß and Riding 1999; Arp et al. 2001b). Indeed, stable carbon isotope records (e.g., Matsuoka et al. 2001) and uptake of radioactive-labeled CO_2 by cyanobacteria (Pentecost 1978) show only minor signatures of microbial activities, especially photosynthesis. In addition, it was thought that if photosynthetic removal of CO_2 can increase $CaCO_3$ supersaturation, pH should be increased in the bulk water during daytime. However, the bulk water chemistry of tufa-forming creeks does not show diurnal pH changes and it was concluded that the effect of photosynthesis on tufa precipitation is negligible (e.g., Merz-Preiß and Riding 1999).

Nonetheless, Arp et al. (2001a) have suggested that low concentrations of dissolved inorganic carbon (DIC), and consequently low carbonate-buffering of the tufa creek waters, imply that photosynthesis may significantly influence the carbon pool and $\{CO_3^{2-}\}$ within the microenvironment. The present paper attempts to evaluate the effects of photosynthesis, respiration and Ca^{2+} binding by EPS on $CaCO_3$ precipitation in these highly supersaturated settings. For this purpose, and with the aim of contributing to the understanding of pre-Phanerozoic ocean, the tufa biofilms of two karst-water creeks in Germany were

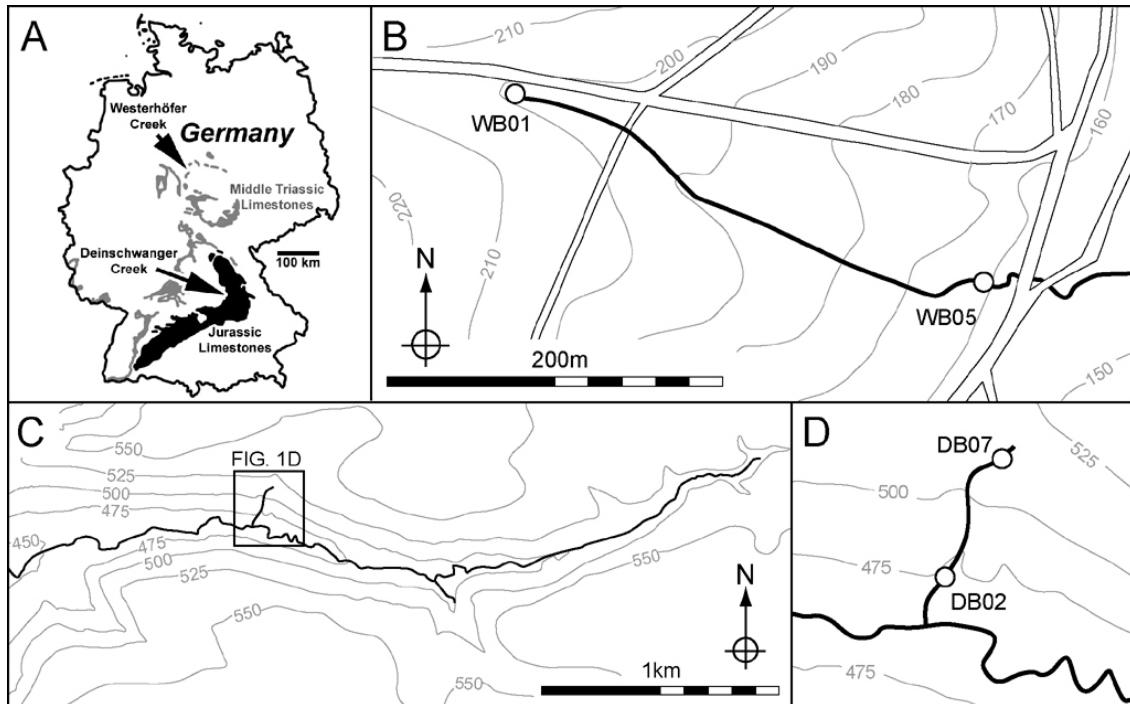


Fig. 1 Locations of the Westerhöfer and Deinschwanger Creek. (B) The map of the Westerhöfer Creek showing the locations of the two sampling sites (WB01 and WB05). (C) The map of Deinschwanger Creek, showing the position of the side creek studied. (D) The detailed map of the Deinschwanger Creek side creek. The locations of the two sampling sites (DB02 and DB07) are shown.

investigated by means of microbiological techniques including microelectrodes, FISH, and EPS staining.

MATERIALS AND METHODS

Study area

Two hardwater creeks, the Westerhöfer and Deinschwanger Bach, and their calcifying biofilms were investigated (Fig. 1). The Westerhöfer Creek, located in the West of the Harz Mountains ($51^{\circ}45'N$, $10^{\circ}5'E$) is less than 2 m wide and receives its waters from only one spring discharging from the Middle Triassic Muschelkalk-Group aquifer. The upstream, approximately 330 m long, section of this tufa-forming creek was investigated in this study (Fig. 1B). The spring site (WB01) and 300 m downstream (WB05) were chosen for the study sites. There is about 40 m difference in altitude between these two points. This creek has previously been investigated by Jacobson and Usdowski (1975), Usdowski et al. (1979), and Dreybrodt et al. (1992) with regard to hydrochemistry and oxygen and carbon stable isotopes. Their sampling site 9 corresponds to sampling site WB05 of this study.

The Deinschwanger Creek, located at the western margin of the Franconian Alb ($49^{\circ}23'N$, $11^{\circ}28'E$) has previously been investigated by Arp et al. (2001b). This tufa-forming creek is

fed by three main springs and a number of side springs (Fig. 1C), most of them discharging from the Upper Jurassic Weißjura-Group aquifer. The side creek flowing from the northern slope into the main creek was chosen as study site; the spring site (DB07) and 132 m downstream (DB02) of this side creek were selected for sampling (Fig.s 1CD). There is approximately 40 m altitude difference between these two points.

Water chemistry analysis

Samples for water chemistry were taken in May 2006 at the Westerhöfer Creek, and October 2005 at the Deinschwanger Creek. The pH of creek water was measured in the field with a portable pH meter (WTW GmbH) calibrated against standard buffers (pH 7.01 and 10.01; HANNA instruments). Water samples were collected for measuring total alkalinity, cation and anion concentrations, and stored cool and dark until analysis. The samples for cation measurements were fixed by adding 50 µl concentrated methane sulfonic acid to 50 ml sample water. Total alkalinity was determined by acid-base titration using a hand-held titrator and 1.6 N H₂SO₄ cartridges (Hach Corporation), and measured within 48 h from sampling. Cation and anion concentrations were measured by ion chromatography (Dionex Corporation). Dissolved silica concentrations were measured by photometric methods according to Grasshoff et al. (1983).

Measured values were processed with the computer program PHREEQC (Parkhurst and Appelo 1999) in order to calculate ion activities and pCO₂ of the water samples as well as saturation state with respect to calcite which is given by

$$\Omega_{(\text{calcite})} = \{\text{Ca}^{2+}\} \times \{\text{CO}_3^{2-}\} / \text{Ksp}_{(\text{calcite})} \quad (2.1)$$

where the numerator is the ion activity product and Ksp_(calcite) denotes the solubility product of calcite.

Biofilm sectioning, staining and microscopy

In order to investigate the compositions of tufa biofilms, biofilm samples were collected from the downstream sites of both creeks. Samples were collected from the Westerhöfer Creek (WB05) in June 2005 and from the Deinschwanger Creek (DB02) in October 2005. Resin-embedded, non-decalcified sections were prepared as described by Arp et al. (1998). Samples for FISH and EPS staining were decalcified in 20 % Formical–2000 (Decal Chemical Corporation Ltd.) and embedded in paraffin as described by Hoffmann et al. (2003).

In this study, the acidic groups of EPS were stained using Alcian Blue, which is the

cationic dye that detects anionic substances (Scott et al. 1964; Ramus 1977). Although there are several methods for Alcian Blue staining with regard to solution pH, the method of pH 2.5 introduced by Romeis (1989) was applied. First, paraffin sections were treated with 3 % acetic acid for 3 min., then transferred to 1 % Alcian Blue in 3 % acetic acid and stained for 30 min. followed by washing with 3 % acetic acid and 3 times distilled water. Sections were then stained by Nuclear Fast Red for 3 min., washed with distilled water 3 times, followed by ethanol series dehydration, 2 min. xylol treatment, and dropped Biomount (British Biocell International Ltd.), and enclosed by a cover glass.

For FISH, the following rRNA-targeted oligonucleotide probes labeled by Cy3 were applied: EUB338 (specific for the domain *Bacteria*; Amann et al. 1990), SRB385 (specific for most members of delta subclass *Proteobacteria* including *Desulfobacteriaceae*; Rabus et al. 1996), non-EUB338 (complementary sequence to EUB338; Wallner et al. 1993). Hybridization procedures were based on those described by Manz et al. (2000).

Alcian Blue stained sections were examined with a Zeiss Axioplan microscope. Other sections were examined with a Zeiss 510 Meta laser scanning microscope, equipped with Ar laser (458, 477, 488 and 514 nm) and He-Ne laser (543 and 633 nm).

Organic and inorganic carbon analysis

Organic and inorganic carbon deposition rates of tufa were measured in order to estimate annual CaCO_3 deposition per unit area. Coring of tufa samples was conducted at the downstream sites of the Westerhöfer Creek (WB05) in June 2005 in October 2005 and October 2006 at the Deinschwanger Creek (DB02). Core samples were taken from the centre of the flow path, and annually laminated and flat deposits were chosen for the measurements. Cores were then divided into each layer, one layer hereof representing a one-year-deposit, except for currently developing surface layers which were also analysed for comparison. Pictures of samples were taken by conventional digital camera and surface area was measured with the image-processing software Scion Image (Scion Corporation). Samples were dried at 50°C for 24 h and weighed. They were then ground to powder in a mortar and pestle, and weight % of organic and inorganic carbon were measured by Multiphase Carbon Determinator LECO RC-412. In our protocol, samples were heated to 500°C, and organic carbon counted for 120 sec., after which samples were heated to 900°C and inorganic carbon counted.

In the tufa samples inorganic carbon originates from CaCO_3 . Therefore CaCO_3 depositional amount per unit area was calculated as follows:

$$\text{CaCO}_3 \text{ deposition} = (M_{\text{CaCO}_3} \times C_{\text{inorg}} \times W) / (M_C \times S) \quad (2.2)$$

where M_{CaCO_3} and M_{C} are the molecular and atomic weights of CaCO_3 and carbon respectively, C_{inorg} is the weight ratio of inorganic carbon, W is the dry weight of tufa (g), and S is the surface area of the sample (m^2). Because of the chemical variability of organic matter it is impossible to calculate the depositional amount of organic compounds directly from weight % of organic carbon. The maximum organic contents were, therefore, estimated by subtracting the weight of CaCO_3 from the total sample weight, because the main components of tufa other than CaCO_3 seem to be organic compounds and clay minerals. However, these values cannot be regarded as annual production of organic compounds, since all organics produced by surface tufa biofilms would not remain in deposits.

Microelectrode measurements

In situ and *ex situ* microelectrode profiles of pH, O_2 , Ca^{2+} and CO_3^{2-} were measured in order to evaluate microbiological effects at the tufa surface; the site of calcite precipitation. O_2 microelectrodes (tip diameters of 10 μm) were prepared according to Revsbech (1989). pH, Ca^{2+} and CO_3^{2-} were measured with ion-specific liquid ion-exchange (LIX) membrane glass microelectrodes with tip diameter of 10 μm (de Beer et al. 2000; Gieseke and de Beer 2004). Microelectrodes positioning was controlled by a motorized micromanipulator (VT-150, Micos, Eschbach). The microelectrodes were connected to a picoammeter (for O_2) or millivoltmeter (for the rest) and output was collected by a data acquisition box (NI DAQPad-6015, National Instruments, Austin). *In situ* pH and O_2 microprofiles were measured at site DB02 (11:00–15:00, October 2005). Light intensity was almost constant through the measurements ($\sim 200 \mu\text{E m}^{-2} \text{ s}^{-1}$). In addition, *ex situ* measurements of pH, O_2 , Ca^{2+} and CO_3^{2-} concentration profiles were also carried out. For *ex situ* measurements, biofilm samples were taken from site WB05 three days before the measurement (October 2006) and incubated at 10°C under a light:dark cycle of 12:12 h until the measurements. *Ex situ* measurements were conducted at room temperature ($\sim 25^\circ\text{C}$), in a recirculating aquariums filled with spring water (WB01). For comparison, pH and Ca^{2+} profiles of a limestone substrate devoid of a biofilm were also measured under the same conditions. Light measurements were performed using a fiber-optic lamp (KL 1500, Schott; $500 \mu\text{E m}^{-2} \text{ s}^{-1}$). The tips of microelectrodes were set to the biofilm surface using a dissection microscope (SV6, Zeiss).

Fluxes were calculated from measured profiles using Fick's first law,

$$J = -D \times dC / dz \quad (2.3)$$

Table 1 Water chemistry of the spring and the downstream sites in the investigated creeks, and experimental water used for *ex situ* microelectrode measurements

location/ experiment	Temp. (°C)	pH	Ca ²⁺ (mmol L ⁻¹)	Mg ²⁺ (mmol L ⁻¹)	Na ⁺ (mmol L ⁻¹)	K ⁺ (mmol L ⁻¹)	Si (mmol L ⁻¹)	TA (meq L ⁻¹)	Cl ⁻ (mmol L ⁻¹)	SO ₄ ²⁻ (mmol L ⁻¹)	NO ₃ ⁻ (mmol L ⁻¹)	pCO ₂ (×10 ⁻³ atm)	Ω _{calcite}
WB01 (spring)	8.9	7.33	3.95	1.72	0.34	0.05	0.15	5.40	0.29	2.94	0.09	11.48	1.6
WB05 (downstream)	10.1	8.22	3.57	1.69	0.33	0.05	0.15	4.82	0.29	2.87	0.08	1.31	10.2
DB07 (spring)	9.2	7.90	2.39	0.82	0.44	0.09	0.10	5.28	0.70	0.14	0.64	3.16	4.5
DB02 (downstream)	10.4	8.48	2.28	0.78	0.43	0.09	0.10	5.00	0.67	0.14	0.61	0.74	15.4
tufa biofilm	26.0	8.25	3.46	1.55	0.31	0.05	0.16	5.64	0.29	2.27	0.08	1.69	20.8
limestone	26.0	8.19	2.05	1.55	0.31	0.05	0.16	4.04	0.29	2.27	0.08	1.44	8.3

where D denotes the diffusion coefficient ($\text{m}^2 \text{s}^{-1}$), dC is the concentration difference of a given ion (mol m^{-3}), and dz is the diffusion distance (m). The diffusion coefficients of O_2 and Ca^{2+} are derived from literature values as follows: O_2 at 25°C is $2.35 \times 10^{-9} \text{ m}^2 \text{ s}^{-1}$ (Broecker and Peng 1974), Ca^{2+} at 25°C is $0.793 \times 10^{-9} \text{ m}^2 \text{ s}^{-1}$ (Li and Gregory 1974).

Ca^{2+} and CO_3^{2-} concentration microprofiles were used to calculate saturation with respect to calcite. $K_{\text{sp}(\text{calcite})}$ (3.31×10^{-9} at 25°C , consistent with the PHREEQC database) was given by Plummer and Busenberg (1982). $\{\text{Ca}^{2+}\}$ and $\{\text{CO}_3^{2-}\}$ were estimated by applying the activity coefficients provided by PHREEQC for experimental water (0.62 for Ca^{2+} and 0.66 for CO_3^{2-}).

RESULTS

Water chemistry

Both investigated creeks displayed the typical hydrochemical evolution of high pCO_2 hard-water creeks. In the Westerhöfer Creek, pCO_2 rapidly decreased from the spring site ($11.4 \times 10^{-3} \text{ atm}$, WB01) to the site 300 m downstream ($1.31 \times 10^{-3} \text{ atm}$, WB05). Coupled with CO_2 degassing pH increased from 7.33 to 8.22 (Table 1). Accordingly, saturation state of calcite increased along the flowpath reaching more than 10-fold supersaturation. At the downstream site, ongoing carbonate precipitation was evident from the decrease of calcium concentration and total alkalinity. Water of the Westerhöfer Creek tended to have high SO_4^{2-} concentrations, reflecting the discharge from the evaporite-containing limestones of the Middle Triassic Muschelkalk-Group.

At the side creek of Deinschwanger Creek, changes of water chemistry along the creek were similar to that observed in the Westerhöfer Creek apart from high NO_3^- concentrations due to agricultural run-off. In comparison to the Westerhöfer Creek, slightly higher pH-value (8.48) and calcite supersaturation (15-fold) were recorded at the downstream site (DB02, Table 1), where loss of calcium and total alkalinity due to carbonate precipitation was observable.

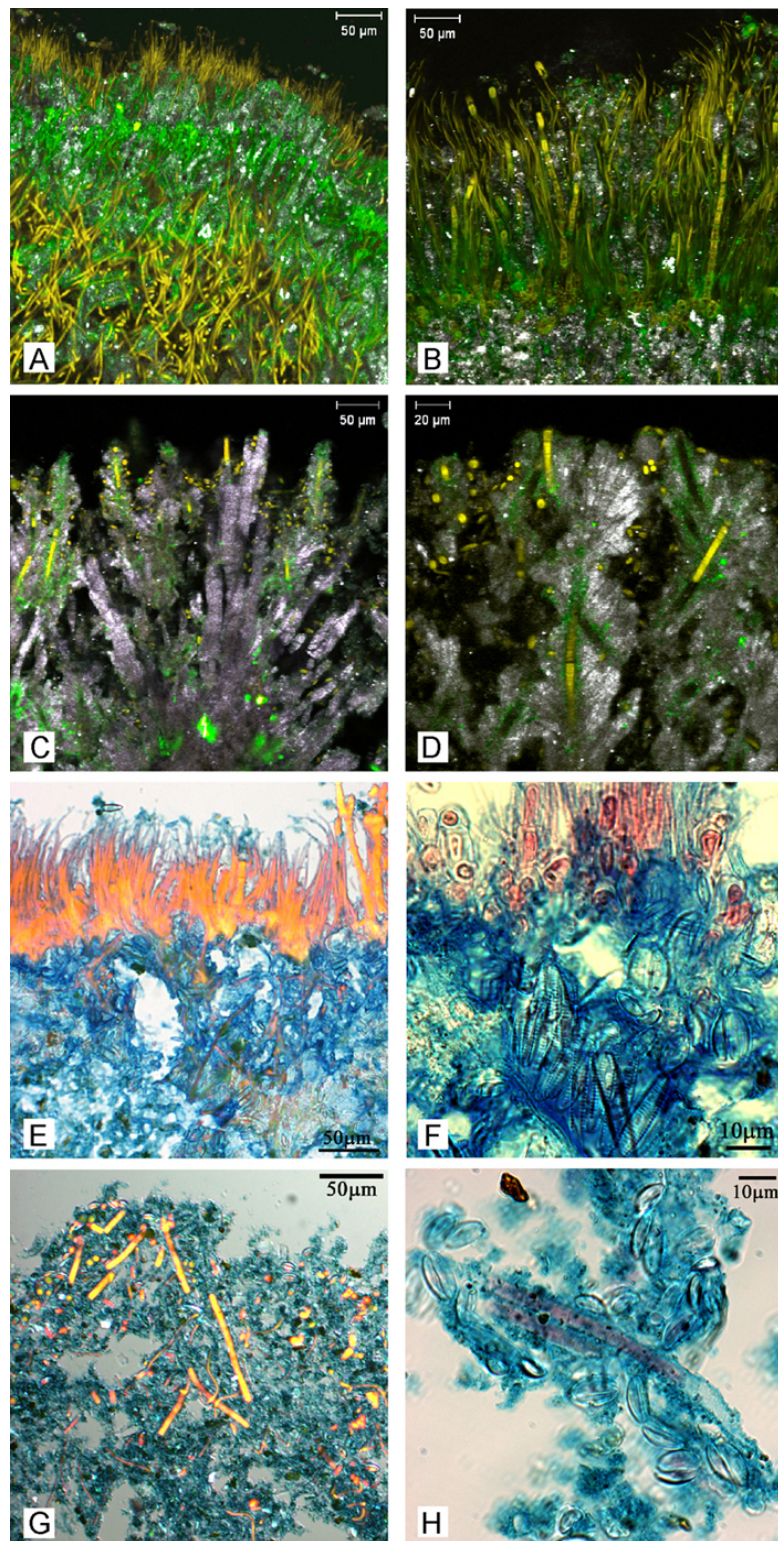


Fig. 2 Micrographs of the topmost tufa biofilms of the Westerhöfer (A, B, E and F) and Deinschwanger Creek (C, D, G and H). A–D are resin embedded sections viewed under CLSM. Yellow represents autofluorescence, green calcein staining, and white reflected signal (mostly derived from carbonate crystals). E–H are paraffin sections stained by Alcian Blue, and viewed under transmitted light microscopy. E and G are composite photographs produced by overlapping epifluorescence and transmitted images. Red–yellow represent autofluorescence.

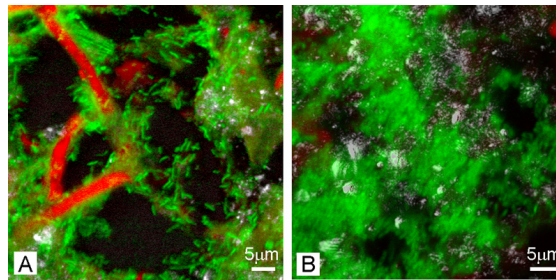


Fig. 3 FISH micrographs of Westerhöfer tufa viewed under CLSM. Green indicates probe signal, red indicates autofluorescence of cyanobacteria, and white indicates reflected signal (probably mostly clay minerals). (A) EUB338. (B) SRB385.

Biofilm composition

Biofilm compositions at the downstream sites of both creeks (WB05 and DB02) were very similar. Major primary producers were filamentous cyanobacteria (3–5 μm wide) of morphotype “*Phormidium incrustatum*” (Figs. 2A–D). They formed thick (200–500 μm) biofilms at the top of the deposits and left empty calcareous tubes behind. They were accompanied by *Lyngbya*-type and coccoid cyanobacteria and filamentous green algae of genus *Cladophora* (Fig. 2B). In addition, many diatoms such as *Achnanthes*, *Gomphonema*, *Nitzschia*, and *Navicula* occurred at the biofilm top and scattered around the cyanobacterial filaments (Figs. 2E–H). FISH results showed the presence of heterotrophic bacteria including sulfate-reducing bacteria (Fig. 3). The EPS matrix within the biofilm exhibited an acidic property, as demonstrated by Alcian Blue staining (Figs. 2E–H).

Microprofiles of tufa biofilm

In situ pH and O_2 microprofiles at daytime showed constant values in the water column (pH 8.5 and 350 $\mu\text{mol L}^{-1}$ O_2) with a strong increase in the diffusive boundary layer (DBL) at the tufa surface (pH 9.5 and 900 $\mu\text{mol L}^{-1}$ O_2 ; Fig. 4).

Microprofiles of pH, O_2 , Ca^{2+} and CO_3^{2-} under light and dark conditions were also measured *ex situ* (Fig. 5). They showed a thicker DBL (400–800 μm) than *in situ* (200 μm), due to slower flow rates in the laboratory experiment. Nonetheless, pH and O_2 microprofiles were comparable to *in situ* microprofiles, and all *ex situ* microprofiles showed a clear diurnal pattern. Upon illumination, pH, O_2 and CO_3^{2-} concentrations increased from the water column (pH 8.2; O_2 250 $\mu\text{mol L}^{-1}$; CO_3^{2-} 20 $\mu\text{mol L}^{-1}$) to the biofilm surface (pH 9.0; O_2 700 $\mu\text{mol L}^{-1}$; CO_3^{2-} 100 $\mu\text{mol L}^{-1}$), while Ca^{2+} concentrations showed a decrease from 3.5 to 2.1 mmol L^{-1} . As a result, calcite supersaturation calculated from Ca^{2+} and CO_3^{2-} microprofiles exhibited a strong increase from 8-fold in the water column to 27-fold at the biofilm surface (Fig. 5). The opposite took place in the dark: pH, O_2 and CO_3^{2-} decreased toward the biofilm surface (pH from 8.2 to 8.0; O_2 from 250 to 130 $\mu\text{mol L}^{-1}$; CO_3^{2-} from 20 to 13 $\mu\text{mol L}^{-1}$), coupled with a minor Ca^{2+} increase from 3.4 to 3.6 mmol L^{-1} . Consequently, calcite

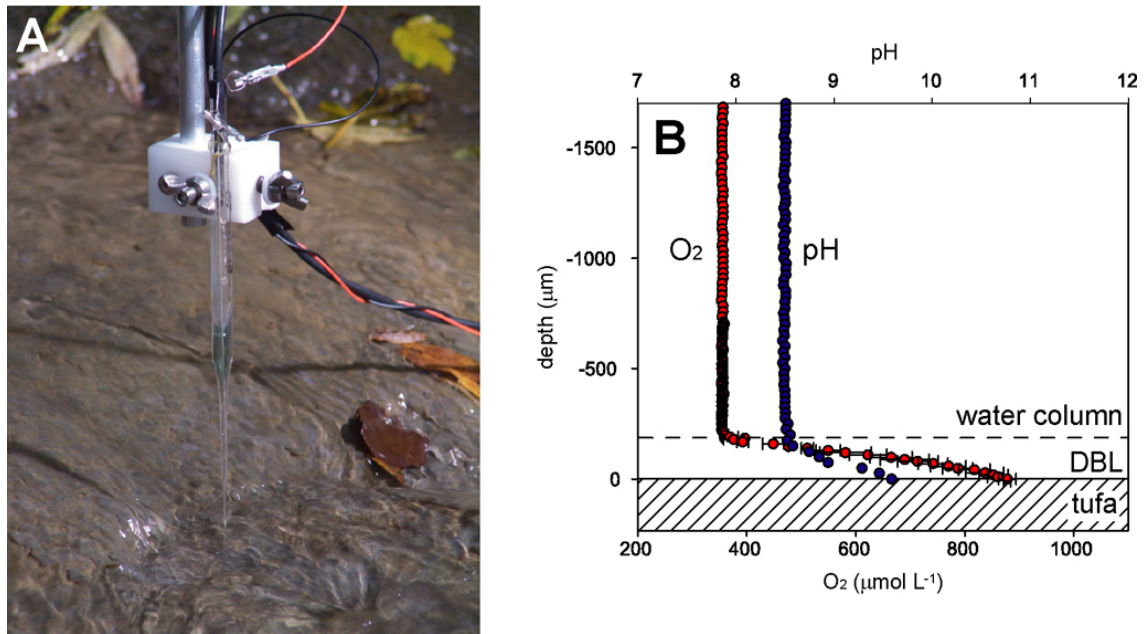


Fig. 4 *In situ* microelectrode measurements of pH and O₂ in the Deinschwanger Creek (DB02). (A) Picture of *in situ* measurement, which shows exact measuring point in a flow fast zone of the creek. (B) Microprofiles of pH and O₂. Dashed line represents diffusive boundary layer (DBL), the solid line the tufa surface.

supersaturation decreased from 8-fold in the water column to 6-fold at the biofilm surface under dark conditions (Fig. 5).

On the other hand, pH and Ca²⁺ microprofiles of limestone substrate without biofilm showed no change on the surface. Ca²⁺ concentration of the experimental water during these measurements was lower than that of biofilm measurements, because previous measurements of the tufa biofilm and inorganic precipitation by CO₂ degassing reduced Ca²⁺ concentration (Table 1).

O₂ and Ca²⁺ fluxes calculated from the *in situ* and *ex situ* microprofiles of the tufa biofilm are shown in Table 2.

Annual depositional rates

Table 3 shows depositional amounts of CaCO₃ per unit area calculated from weight % of inorganic carbon, surface area, and dry weight of laminated tufa samples. These values are regarded as annual depositional amounts, except for developing surface samples. The resulting annual depositional rates were 2934–4514 g m⁻² year⁻¹ (mean is 3935 g m⁻² year⁻¹) at downstream sites of the Westerhöfer Creek (WB05), and 2148–3598 g m⁻² year⁻¹ (mean is 2867 g m⁻² year⁻¹) at downstream sites of the Deinschwanger Creek side creek (DB02). Maximum organic contents were 210–615 g m⁻² in WB05 and 373–693 g m⁻² in DB02. Surface samples tended to contain higher amounts of organic components, but this was not always the case.

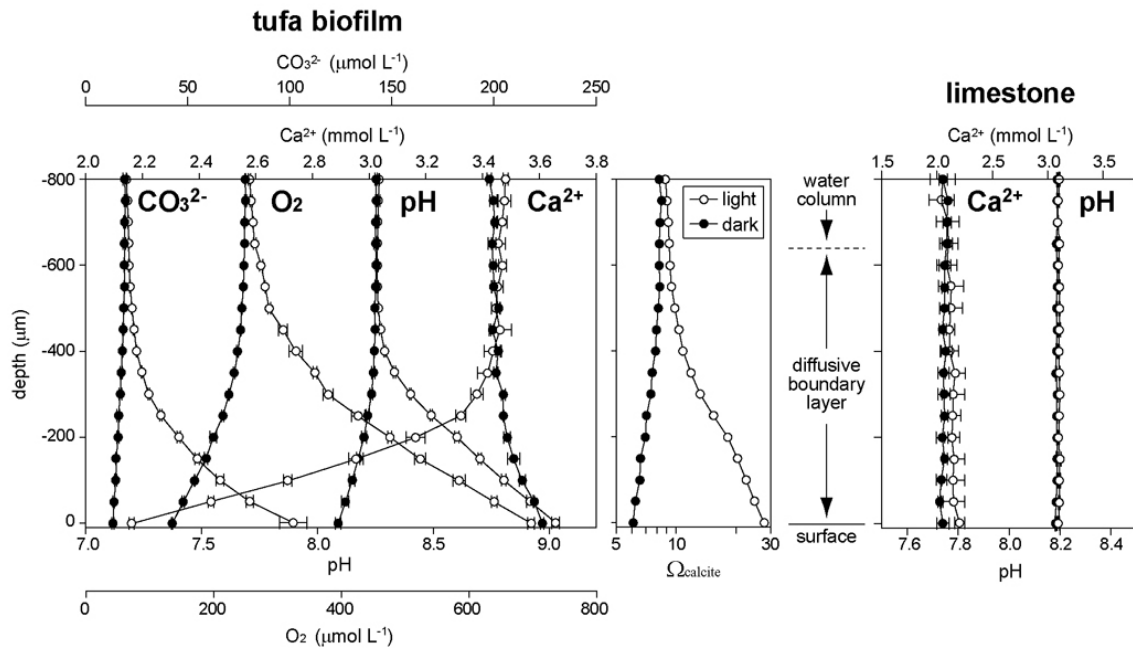


Fig. 5 *Ex situ* microprofiles of tufa biofilm (pH, O₂, Ca²⁺ and CO₃²⁻) and biofilm-free limestone substrate (pH and Ca²⁺) from the Westerhöfer Creek (WB05). Open circles indicate light profiles, and closed circles indicate dark profiles. Saturation state (Ω_{calcite}) calculated from Ca²⁺ and CO₃²⁻ profiles is also shown.

DISCUSSION

Photosynthesis and Ca²⁺ complexation by EPS

Non-marine stromatolites are formed by calcifying biofilms in highly supersaturated environments. Such environments are achieved by physicochemical processes such as mixing of Ca²⁺-supplying freshwaters with highly alkaline waters, evaporation, and degassing of CO₂. In the sites studied herein, physicochemical mechanisms and photosynthetic CO₂ assimilation, which both potentially affect carbonate equilibrium and cause CaCO₃ precipitation, take place simultaneously. Therefore, considerable controversy exists regarding whether biofilm calcification in such environments is physicochemically (inorganically) or biologically controlled, including the discussions on tufa formation. However, a number of geomicrobiological studies on present-day biofilms indicate that microorganisms can significantly influence the water chemistry of microenvironments (e.g., Grözschele and de Beer 2002; Kühl and Jørgensen 1992). The present study also corroborated this view, even in the highly supersaturated tufa creeks. Although experimental temperature of *ex situ* measurements was higher than creek water temperature, results were in general confirmed by comparable *in situ* microprofiles. Upon illumination, pH, O₂ and CO₃²⁻ increased at the tufa biofilm surface, coupled with a strong Ca²⁺ decrease. At dark conditions in turn, pH, O₂ and CO₃²⁻ microprofiles showed a decrease coupled with a minor

Table 2 O₂ and Ca²⁺ fluxes calculated from microprofiles

location	condition	<i>ex situ</i>		<i>in situ</i>
		O ₂ (mol m ⁻² s ⁻¹)	Ca ²⁺ (mol m ⁻² s ⁻¹)	O ₂ (mol m ⁻² s ⁻¹)
WB05	light	2.66 × 10 ⁻⁶	-4.37 × 10 ⁻⁶	—
	dark	-0.82 × 10 ⁻⁶	0.56 × 10 ⁻⁶	—
DB02	light	—	—	3.40 × 10 ⁻⁶

Positive values indicate flux from the tufa biofilm, and negative values indicate flux toward the biofilm.

Ca²⁺ increase (Figs. 4, 5), and hence, net Ca²⁺ loss towards the biofilm occurred (Table 2). Saturation state of calcite increased at the tufa biofilm surface during illumination and decreased under dark conditions, compared to ambient water conditions (Fig. 5). The light–dark cycle of Ca²⁺ profiles at the tufa surface demonstrated that physicochemical CaCO₃ precipitation from the water column alone does not explain tufa formation in karst-water creeks. Instead, the results suggest that tufa biofilms force CaCO₃ precipitation via changing the microenvironmental water chemical by photosynthesis in the light, inhibit precipitation by respiration in the dark, and consequently control CaCO₃ precipitation, even in already highly supersaturated water.

The explanation above implies that observed Ca²⁺ flux towards the biofilm under illumination is caused by direct CaCO₃ precipitation promoted by photosynthetic activity. Instead, Ca²⁺-binding by acidic EPS may be considered as an alternative to explain Ca²⁺ fluxes. As indicated by Alcian Blue staining, the tufa biofilms contain a significant concentration of acidic groups in the EPS matrix (Figs. 2E–H) that can bind Ca²⁺ (Pentecost 1984; Decho 1990, 2000) and thereby would inhibit CaCO₃ precipitation at first (Kawaguchi and Decho 2002a). Decomposition of this EPS by heterotrophic bacteria may then increase Ca²⁺ and alkalinity and cause CaCO₃ precipitation, as suggested by Arp et al. (1998) for soda lake tufa towers and Visscher et al. (1998, 2000) and Reid et al. (2000) for the calcification of recent marine stromatolites.

However, such EPS-mediated mechanism cannot explain the observed Ca²⁺ flux because Ca²⁺ influx occurs only under the illumination and responds to light and dark very quickly (in the order of minute), which is hard to explain by the production of acidic groups. Although pH shifting on tufa biofilms causes reversible Ca²⁺-binding and releasing by the protonation and deprotonation of acidic groups, it cannot account for the observed Ca²⁺ flux, as shown in followings. Dissociation of an acidic group, HA, is expressed as HA ↔ H⁺ + A⁻. The equilibrium constant of this reaction, K_a, is expressed by the relationship:

$$\text{pKa} = \text{pH} + \log [\text{HA}] / [\text{A}^-] = \text{pH} + \log [1 - \alpha] / [\alpha] \quad (2.4)$$

where α denotes the degree of dissociation. Even if the total organic of the biofilm (~693 g

Microenvironmental effects of biofilms and calcium mass balance

Table 3 Estimation of depositional rates and maximum amount of organic components

sampling date	sample ID	dry weight (g)	surface area ($\times 10^{-4} \text{ m}^2$)	inorganic C (wt %)	organic C (wt %)	CaCO ₃ (g m ⁻²)	Max organic contents (g m ⁻²)
May 2006	WB05-06*	0.969	2.82	10.34	2.14	2934	443
	WB05-09	1.311	2.62	10.74	1.14	4514	487
	WB05-10*	1.806	4.34	10.14	2.16	3546	615
	WB05-10	1.167	2.85	10.66	1.31	3670	427
	WB05-14	0.617	1.36	11.35	1.20	4327	210
	WB05-19	0.591	1.42	10.87	1.27	3804	361
	WB05-20	0.605	1.64	10.84	1.07	3362	329
October 2005	DB02-01	0.933	2.76	10.29	1.07	2924	458
	DB02-02	1.054	2.78	10.30	0.95	3281	511
	DB02-03*	1.208	2.89	9.92	1.15	3487	693
October 2006	DB02-02*	1.107	2.61	10.09	1.38	3598	644
	DB02-02	0.809	3.21	10.14	1.05	2148	373
	DB02-03*	0.810	2.98	10.25	1.75	2341	377
	DB02-03	1.072	2.99	10.34	1.43	3116	469

*surface sample.

m⁻²; Table 3) would consist solely of glucuronic acid (pKa is 3.0; Smith et al. 1997), one common acidic EPS component in the biofilms (e.g., Pentecost and Riding 1986), the effect of a pH-rise from 8.08 to 9.02 (as derived from the *ex situ* measurements; Fig. 5) would cause a Ca²⁺ flux of only $-3.04 \times 10^{-10} \text{ mol m}^{-2} \text{ s}^{-1}$ because carboxyl group mostly dissociate in this pH range (see also Braissant et al. 2007). This flux is significantly lower than the measured flux ($-4.37 \times 10^{-6} \text{ mol m}^{-2} \text{ s}^{-1}$; Table 2). Moreover, Ca²⁺ flux caused by acidic groups takes place only during pH rising (duration of several minutes), while measured Ca²⁺ flux continued as long as light was supplied. These facts indicate that EPS-mediated mechanism has negligible role for the observed Ca²⁺ flux. On the other hand, the observed minor Ca²⁺ release from the biofilm in the dark might be explained by decomposition of Ca²⁺-binding EPS, but further investigations are necessary to fully understand this phenomenon.

Although the effect of Ca²⁺-binding by acidic EPS on sustaining CaCO₃ precipitation is minor in the investigated biofilms, it is assumed that acidic EPS probably play an important role in crystal nucleation. As shown by many researchers, different EPS compositions can lead to different crystal types (e.g., Kawaguchi and Decho 2002b; Braissant et al. 2003), and different cyanobacterial species exhibit different calcification fabrics (e.g., Merz 1992; Pentecost and Riding 1986). Therefore, EPS can probably influence the formation of tufa fabrics by providing nucleation sites, as can the cell surfaces of heterotrophic bacteria (e.g., Ferris and Beveridge 1984; Bosak and Newman 2003).

The results discussed above are based on studies in freshwater settings, and when transferring these results to marine biofilm calcification, higher ionic strength that reduces

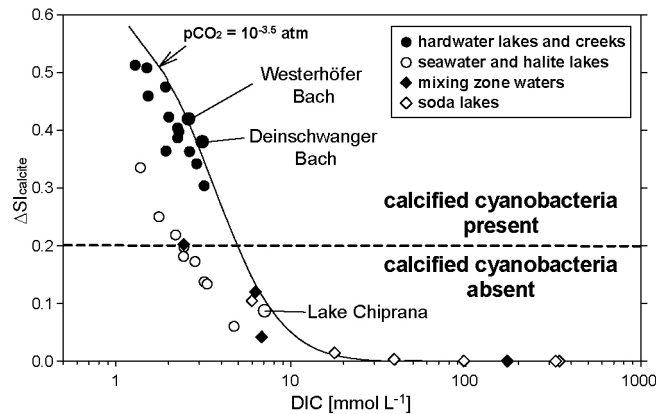


Fig. 6 Computed microenvironmental rise of saturation index ($\Delta SI_{\text{calcite}}$) caused by $200 \mu\text{mol L}^{-1}$ CO_2 assimilation in various DIC conditions. Solid curve indicates the “freshwater curve”, the theoretical change with $p\text{CO}_2$ of $10^{-3.5}$ atm. For details, see Arp et al. (2001a). Calculated values from actual water samples were plotted on the figure, including those from the Westerhöfer and Deinschwanger Creek. Lake Chiprana, the hypersaline lake investigated by Jonkers et al. (2003) and Ludwig et al. (2005), is also plotted.

the ion activities, and the existence of inhibitors such as Mg^{2+} (e.g., Morse 1983) must be taken into account. However, photosynthesis-induced CaCO_3 precipitation theoretically also occurs in seawater environments, as shown by Ludwig et al. (2005), who reported the same mechanism from hypersaline microbial mats, where ion concentration is much higher than in the seawater (Jonkers et al. 2003). Therefore, if the saturation state of macroenvironments is sufficiently high (e.g., 8- to 10-fold) and if the DIC pool is too low to buffer the $\{\text{CO}_3^{2-}\}$ increase (Arp et al. 2001a), photosynthesis can induce CaCO_3 precipitation. Indeed, model calculations by Arp et al. (2001a) predict that the effect of carbonate-buffering in the Westerhöfer and Deinschwanger Creek is sufficiently low to permit the formation of calcified cyanobacterial tubes by photosynthesis-induced calcification (Fig. 6; for details of calculations see Arp et al. 2001a), although they assumed that the photosynthetic effect in tufa systems is largely overridden by CO_2 degassing (Arp et al. 2001a: p. 1702, l. 48–51).

Ca²⁺ mass balance

It is possible to convert estimates of annual CaCO_3 depositional rates (Table 3) into Ca^{2+} fluxes by assuming a 12 h:12 h average annual light–dark cycle. Calculated fluxes are -1.85 to $-2.86 \times 10^{-6} \text{ mol m}^{-2} \text{ s}^{-1}$ in WB05, and they are similar to the net Ca^{2+} influx of *ex situ* measurements ($-3.81 \times 10^{-6} \text{ mol m}^{-2} \text{ s}^{-1}$; Table 2), although their values are slightly lower. This difference may be explained by stronger illumination during *ex situ* measurements in the laboratory, which causes stronger effect of photosynthesis. In addition, the average integral of *in situ* Ca^{2+} flux in the daytime might be lower than the assumption of half-day illumination. A better estimate of the annual Ca^{2+} flux could be obtained by measuring diurnal and seasonal patterns of Ca^{2+} flux and average illumination *in situ* in future

research. Nonetheless, both Ca^{2+} fluxes measured by microelectrodes and calculated from actual tufa deposits are of the same order of magnitude and, therefore, support the contention that annually laminated tufa deposits in the investigated creeks are formed by photosynthesis-induced precipitation.

CaCO_3 precipitation in highly supersaturated settings

Fig. 5 shows that there was no rapid, spontaneous CaCO_3 precipitation on the biofilm free limestone substrate, regardless of the 8-fold supersaturation (Table 1). The potential inorganic precipitation rate of calcite was calculated from water chemistry parameters using the equation of Plummer et al. (1978) as follows:

$$R = -k_1 \{H^+\} - k_2 \{H_2CO_3^*\} - k_3 + k_4 \{Ca^{2+}\}\{HCO_3^-\}$$

$$H_2CO_3^* = H_2CO_3 + CO_{2(aq)} \quad (2.5)$$

This equation was originally provided for dissolution, but it is also possible to apply it to precipitation (Plummer et al. 1979; Reddy et al. 1981), and represents the maximum inorganic precipitation rate of calcite in very turbulent water (Dreybrodt and Buhmann 1991). For the rate constants (k_1 – k_4), the revised values of Buhmann and Dreybrodt (1985) were applied. In the case of the *ex situ* measurements of the biofilm-free limestone substrate (Fig. 5), a Ca^{2+} flux of $-2.39 \times 10^{-6} \text{ mol m}^{-2} \text{ s}^{-1}$ is expected from this equation without CO_2 degassing when water is highly agitated, whereas actual measurements showed no Ca^{2+} flux. This indicates that rapid inorganic precipitation does not occur due to the kinetic barrier under slow flow speed, even if water is 8-fold supersaturated (e.g., Dreybrodt and Buhmann 1991). Even in the relatively fast flowing creek, there was a diffusive boundary layer of $\sim 200 \mu\text{m}$ thick (Fig. 4) which significantly impeded inorganic precipitation (Dreybrodt and Buhmann 1991; Dreybrodt et al. 1992). By contrast, the diffusive boundary layer allows the establishment of chemical gradients, and affects positively for photosynthesis-induced precipitation to stimulate rapid precipitation without high water agitation (Fig. 5).

This fact indicates that photosynthesis is an important mechanism in overcoming the kinetic barrier to promote carbonate precipitation, even in settings already highly supersaturated. As a consequence, macroenvironmental high supersaturation with respect to CaCO_3 minerals does not imply a negligible role of photosynthetic carbon fixation in stromatolite formation. This may apply to non-marine and marine settings including Precambrian and certain periods of Phanerozoic Ocean that are considered having been highly supersaturated with respect to CaCO_3 minerals (Grotzinger 1989, 1990, 1994; Knoll

et al. 1993; Kempe and Kazmierczak 1994).

CONCLUSION

1. *In situ* and *ex situ* microelectrode measurements showed that microbial activities of cyanobacteria-dominated biofilms considerably influenced the water chemistry of tufa surfaces despite of overwhelmingly high supersaturation of the microenvironment. Tufa biofilms stimulated CaCO_3 precipitation by photosynthesis and inhibited it by respiration when photosynthesis was absent. The tufa biofilms, thus, controlled CaCO_3 precipitation.
2. Although the Ca^{2+} -binding of EPS was quantitatively of minor importance with regard to maintaining CaCO_3 precipitation in the tufa biofilms, it probably plays an important role in crystal nucleation.
3. Photosynthesis is an important mechanism in overcoming the kinetic barriers to cause CaCO_3 precipitation in many natural settings, even those that are already highly supersaturated with respect to CaCO_3 .

Acknowledgements

Mr. Dröse and Mr. Satmari (University of Göttingen) introduced sectioning and histological experiments. Ms. Schmidt (University of Göttingen) kindly checked the English of the manuscript. Dr. Kano and Dr. Kawai (Hiroshima University) helped with calculations of inorganic precipitation rates. This project is part of the Research Unit 571 "Geobiology of organo- and biofilms" funded by the German Research Foundation (DFG-FOR 571, AR335/5; publication #17).

REFERENCES

- Allwood AC, Walter MR, Kamber BS, Marshall CP, Burch IW. 2006. Stromatolite reef from the Early Archaean era of Australia. *Nature* 441:714–718.
- Amman R, Krumholz L, Stahl DA. 1990. Fluorescent-oligonucleotide probing of whole cell for determinative, phylogenetic, and environmental studies in microbiology. *J Bacteriol* 172:762–770.
- Arp G, Hofmann J, Reitner J. 1998. Microbial fabric formation in spring mounds ("microbialite") of alkaline salt lakes in the Badan Jaran Sand Sea, PR China. *Palaios* 13:581–592.
- Arp G, Reimer A, Reitner J. 2001a. Photosynthesis-induced biofilm calcification and calcium concentrations in Phanerozoic oceans. *Science* 292:1701–1704.

- Arp G, Wedemeyer N, Reitner J. 2001b. Fluvial tufa formation in a hard-water creek (Deinschwanger Bach, Franconian Alb, Germany). *Facies* 44:1–22.
- Awramik SM. 1984. Ancient stromatolites and microbial mats. In: Cohen Y, Castenholtz RW, Halvorson HO. editors. *Microbial Mats: Stromatolites*. New York: Alan R Liss Inc, p 1–22.
- Awramik SM. 1992. The history and significance of stromatolites. In: Schidlowski M, Golubic S, Kimberley MM, McKirdy DM, Trudinger PA. editors. *Early Organic Evolution: Implications for Mineral and Energy Resources*. Berlin-Heidelberg: Springer-Verlag, p 435–449.
- Awramik SM, Riding R. 1988. Role of algal eukaryotes in subtidal columnar stromatolite formation. *Proc Natl Acad Sci USA* 85:1327–1329.
- Baumgartner LK, Reid, RP, Dupraz C, Decho AW, Buckley DH, Spear JR, Przekop, KM, Visscher PT. 2006. Sulfate reducing bacteria in microbial mats: changing paradigms, new discoveries. *Sediment Geol* 185:131–145.
- Bosak T, Newman DK. 2003. Microbial nucleation of calcium carbonate in the Precambrian. *Geology* 31:577–580.
- Braissant O, Cailleau G, Dupraz C, Verrecchia EP. 2003. Bacterially induced mineralization of calcium carbonate in terrestrial environments: the role of exopolysaccharides and amino acids. *J Sediment Res* 73:485–490.
- Braissant O, Decho AW, Dupraz C, Glunk C, Przekop KM, Visscher PT. 2007. Exopolymeric substances of sulfate-reducing bacteria: interactions with calcium at alkaline pH and implication for formation of carbonate minerals. *Geobiology* 5:401–411.
- Broecker WS, Peng TH. 1974. Gas exchange rates between air and sea. *Tellus* 26:21–35.
- Buhmann D, Dreybrodt W. 1985. The kinetics of calcite dissolution and precipitation in geologically relevant situations of karst areas, 1. Open system. *Chem Geol* 48:189–211.
- Burne RV, Moore LS. 1987. Microbialites: organosedimentary deposits of benthic microbial communities. *Palaios* 2:241–254.
- de Beer D, Köhl M, Stambler N, Vaki L. 2000. A microsensors study of light enhanced Ca^{2+} uptake and photosynthesis in the reef-building hermatypic coral *Favia* sp. *Mar Ecol Prog Ser* 194:75–85.
- Decho AW. 1990. Microbial exopolymer secretions in ocean environments: their role(s) in food webs and marine processes. *Oceanogr Mar Biol Ann Rev* 28:73–154.
- Decho AW. 2000. Microbial biofilms in intertidal systems: an overview. *Cont Shelf Res* 20:1257–1273.
- Decho AW, Visscher PT, Reid RP. 2005. Production and cycling of natural microbial exopolymers (EPS) within a marine stromatolite. *Palaeogeogr Palaeoclimatol Palaeoecol* 219:71–86.
- Dreybrodt W, Buhmann D. 1991. A mass transfer model for dissolution and precipitation of calcite from solutions in turbulent motion. *Chem Geol* 90:107–122.
- Dreybrodt W, Buhmann D, Michaelis J, Usdowski E. 1992. Geochemically controlled calcite precipitation by CO_2 outgassing: field measurements of precipitation rates in comparison to theoretical predictions. *Chem Geol* 97:285–294.
- Dupraz C, Visscher PT. 2005. Microbial lithification in marine stromatolites and hypersaline mats. *Trends Microb* 13:429–438.

- Ferris FG, Beveridge TJ. 1984. Binding of a paramagnetic metal cation to *Escherichia coli* K-12 outer membrane vesicles. *FEMS Microbiol Lett* 24:43–46.
- Ford TD, Pedley HM. 1996. A review of tufa and travertine deposits of the world. *Earth-Sci Rev* 41:117–175.
- Gieseke A, de Beer D. 2004. Use of microelectrodes to measure in situ microbial activities in biofilms, sediments, and microbial mats. In: Kowalchuk GG, de Bruijn FJ, Head IM, Akkermans AD, van Elsas JD. editors. *Molecular Microbial Ecology Manual*. 2nd ed. Berlin-Heidelberg: Springer-Verlag, p 1581–1612.
- Grasshoff K, Erhardt M, Kremling K. 1983. editors. *Methods of Seawater Analysis*. Weinheim: Verlag Chemie, 419 p.
- Grotzinger JP. 1989. Facies and evolution of Precambrian carbonate depositional systems: emergence of the modern platform archetype. In: Crevello PD, Wilson JL, Sarg JF, Read JF. editors. *Controls on Carbonate Platform and Basin Development*. SEPM Spec Publ 44:79–106.
- Grotzinger JP. 1990. Geochemical model for Proterozoic stromatolite decline. In: Knoll AH, Ostrom JH. editors. *Proterozoic Evolution and Environments*. *Am J Sci* 290-A:80–104.
- Grotzinger JP. 1994. Trends in Precambrian carbonate sediments and their implication for understanding evolution. In: Bengtson S. editor. *Early Life on Earth*. Nobel Symposium No 84, New York: Columbia University Press, p 245–258.
- Grotzinger JP, Knoll AH. 1999. Stromatolites in Precambrian carbonates: evolutionary mileposts or environmental dipsticks? *Annu Rev Earth Planet Sci* 27:313–358.
- Grotzinger JP, Rothman DH. 1996. An abiotic model for stromatolite morphogenesis. *Nature* 383:423–425.
- Grözschel S, de Beer D. 2002. Effect of oxygen concentration on photosynthesis and respiration in two hypersaline microbial mats. *Microb Ecol* 44:208–216.
- Hoffmann F, Janussen D, Dröse W, Arp G, Reitner J. 2003. Histological investigation of organisms with hard skeletons: a case study of siliceous sponges. *Biotech Histochem* 78:191–199.
- Jacobson RL, Usdowski E. 1975. Geochemical controls on a calcite precipitating spring. *Contrib Mineral Petrol* 51:65–74.
- Jonkers HM, Ludwig R, de Wit R, Pringault O, Muyzer G, Niemann H, Finke N, de Beer D. 2003. Structural and functional analysis of a microbial mat ecosystem from a unique permanent hypersaline inland lake: 'La Salada de Chiprana' (NE Spain). *FEMS Microbiol Ecol* 44:175–189.
- Kawaguchi T, Decho AW. 2002a. Isolation and biochemical characterization of extracellular polymeric secretions (EPS) from modern soft marine stromatolites (Bahamas) and its inhibitory effect on CaCO₃ precipitation. *Prep Biochem Biotechnol* 32:51–63.
- Kawaguchi T, Decho AW. 2002b. A laboratory investigation of cyanobacterial extracellular polymeric secretions (EPS) in influencing CaCO₃ polymorphism. *J Crystal Growth* 240:230–235.
- Kempe S, Kazmierczak J. 1990. Calcium carbonate supersaturation and the formation of in situ calcified stromatolites. In: Ittekkot VA, Kempe S, Michaelis W, Spitzky A. editors. *Facets of Modern Biogeochemistry*. Berlin-Heidelberg: Springer-Verlag, p 255–278.

- Kempe S, Kazmierczak J. 1994. The role of alkalinity in the evolution of ocean chemistry, organization of living systems, and biocalcification processes. *Bull Inst oceanogr (Monaco) n° spec* 13:61–117.
- Knoll AH, Fairchild IJ, Swett K. 1993. Calcified microbes in Neoproterozoic carbonates: implications for our understanding of the Proterozoic/Cambrian transition. *Palaios* 8:512–525.
- Kühl M, Jørgensen BB. 1992. Microsensor measurements of sulfate reduction and sulfide oxidation in compact microbial communities of aerobic biofilms. *Appl Environ Microbiol* 58:1164–1174.
- Li YH, Gregory S. 1974. Diffusion of ions in sea water and in deep-sea sediments. *Geochim Cosmochim Acta* 38:703–714.
- Ludwig R, Al-Horani F, de Beer D, Jonkers HM. 2005. Photosynthesis-controlled calcification in hypersaline microbial mat. *Limnol Oceanogr* 50:1836–1843.
- Manz W, Arp G, Schumann-Kindel G, Szewzyk U, Reitner J. 2000. Widefield deconvolution epifluorescence microscopy combined with fluorescence in situ hybridization reveals the special arrangement of bacteria in sponge tissue. *J Microbiol Meth* 40:125–134.
- Matsuoka J, Kano A, Oba T, Watanabe T, Sakai S, Seto K. 2001. Seasonal variation of stable isotopic compositions recorded in a laminated tufa, SW Japan. *Earth Planet Sci Lett* 192:31–44.
- Merz MUE. 1992. The biology of carbonate precipitation by cyanobacteria. *Facies* 26:81–102.
- Merz-Preiß M, Riding R. 1999. Cyanobacterial tufa calcification in two freshwater streams: ambient environment, chemical thresholds and biological processes. *Sediment Geol* 126:103–124.
- Morse JW. 1983. The kinetics of calcium carbonate dissolution and precipitation. In: Reeder RJ. editor. *Carbonates: Mineralogy, and Chemistry*. *Rev Mineral Vol 11*, Michigan: Mineralogical Society of America, p 227–264.
- Parkhurst DL, Appelo CAJ. 1999. User's Guide to PHREEQC (version 2)—A Computer Program for Speciation, Batch-Reaction, One-Dimensional Transport, and Inverse Geochemical Calculations. *Water-Resources Investigations Report 99–4259*, Denver: U.S. Geological Survey, 312 p.
- Pentecost A. 1978. Blue-green algae and freshwater carbonate deposits. *Proc Royal Soc London Ser B* 200:43–61.
- Pentecost A. 1984. Association of cyanobacteria with tufa deposits: identity, enumeration, and nature of the sheath material revealed by histochemistry. *Geomicrobiol J* 4:285–298.
- Pentecost A, Riding R. 1986. Calcification of cyanobacteria. In: Leadbeater BSC, Riding R. editors. *Biomineralization in Lower Plants and Animals*. *Systematic Assoc Spec Vol 30*, Oxford: Clarendon Press, p 73–90.
- Plummer LN, Busenberg E. 1982. The solubilities of calcite, aragonite and vaterite in CO₂–H₂O solutions between 0 and 90°C, and an evolution of aqueous model for the system CaCO₃–CO₂–H₂O. *Geochim Cosmochim Acta* 46:1011–1040.
- Plummer LN, Parkhurst DL, Wigley TML. 1979. Critical review of the kinetics of calcite dissolution and precipitation. In: Janne E. editor. *Chemical Modelling in Aqueous Systems: Speciation, Sorption, Solubility and Kinetics*. Washington DC: American Chemical Society, p 537–573.
- Plummer LN, Wigley TML, Parkhurst DL. 1978. The kinetics of calcite dissolution in CO₂–water systems at 5° to

- 60°C and 0.0 to 1.0 atm CO₂. *Am J Sci* 278:179–216.
- Rabus R, Fukui M, Wilkes H, Widdel F. 1996. Degradative capacities and 16S rRNA-targeted whole cell hybridization of sulfate-reducing bacteria in an anaerobic enrichment culture utilizing alkylbenzenes from crude oil. *Appl Environ Microbiol* 62:3605–3613.
- Ramus J. 1977. Alcian Blue: a quantitative aqueous assay for algal acid and sulfated polysaccharides. *J Phycol* 13:345–348.
- Reddy MM, Plumer LN, Busenberg E. 1981. Crystal growth of calcite from calcium bicarbonate solutions at constant pCO₂ and 25°C: a test of the calcite dissolution model. *Geochim Cosmochim Acta* 45:1281–1291.
- Reid RP, Visscher PT, Decho AW, Stolz JF, Bebout BM, Dupraz C, Macintyre IG, Paerl HW, Pinckney JL, Prufert-Bebout L, Stegge TF, Das Marais DJ. 2000. The role of microbes in accretion, lamination and early lithification of modern marine stromatolites. *Nature* 406:989–992.
- Revsbech NP. 1989. An oxygen microsensor with a guard cathode. *Limnol Oceanogr* 34:474–478.
- Riding R. 1982. Cyanophyte calcification and changes in ocean chemistry. *Nature* 299:814–815.
- Riding R. 2000. Microbial carbonates: the geological record of calcified bacterial–algal mats and biofilms. *Sedimentology* 47:179–214.
- Riding R. 2006. Cyanobacterial calcification, carbon dioxide concentrating mechanisms, and Proterozoic–Cambrian changes in atmospheric composition. *Geobiology* 4:299–316.
- Riding R, Liang L. 2005. Geobiology of microbial carbonates: metazoan and seawater saturation state influences on secular trends during the Phanerozoic. *Palaeogeogr Palaeoclimatol Palaeoecol* 219:101–115.
- Romeis B. 1989. *Mikroskopische Technik*. Munich: Urban & Schwarzenberg, 697 p.
- Rosing MT. 1999. ¹³C-depleted carbon microparticles in >3700-Ma sea-floor sedimentary rocks from West Greenland. *Science* 283:674–676.
- Schidlowski M. 1988. A 3,800-million-year isotopic record of life from carbon in sedimentary rocks. *Nature* 333:313–318.
- Scott JE, Quintarelli G, Dellovo MC. 1964. The chemical and histochemical properties of Alcian Blue staining. *Histochemie* 4:73–85.
- Smith RM, Martell AE, Motekaitis RS. 1997. NIST Critically Selected Stability Constants of Metal Complexes Database, Version 4.0. Gaithersburg, MD: National Institute of Standards and Technology.
- Uzdowski E, Hoefs J, Menschel G. 1979. Relationship between ¹³C and ¹⁸O fractionation and changes in major element composition in a recent calcite-depositing spring—a model of chemical variations with inorganic CaCO₃ precipitation. *Earth Planet Sci Lett* 42:267–276.
- Visscher PT, Reid RP, Bebout BM. 2000. Microscale observations of sulfate reduction: correlation of microbial activity with lithified micritic laminae in modern marine stromatolites. *Geology* 28:919–922.
- Visscher PT, Reid RP, Bebout BM, Hoefft SE, Macintyre IG, Thompson JA Jr. 1998. Formation of lithified micritic laminae in modern marine stromatolites (Bahamas): the role of sulfur cycling. *Am Mineral* 83:1482–1493.
- Wallner G, Amann R, Beisker W. 1993. Optimizing fluorescent in situ hybridization with ribosomal-RNA-targeted

Microenvironmental effects of biofilms and calcium mass balance

oligonucleotide probes for flow cytometric identification of microorganisms. *Cytometry* 14:136–143.

Chapter 3

Microbial mediation of stromatolite formation in karst-water creeks

Microbial mediation of stromatolite formation in karst-water creeks

Andrew Bissett, Dirk de Beer, Raphaela Schoon, Fumito Shiraishi, Andreas Reimer, Gernot Arp

Abstract

Epi- and endolithic biofilms were found to control the formation of stromatolites in karst water creeks. We used microsensors to determine the influence of biological processes on chemical conditions within the microenvironment of crystal nucleation sites: the stromatolite surface. Phototrophic members of the biofilms comprised mainly cyanobacteria and diatoms. Oxygen, pH, calcium, and carbonate concentration microprofiles at the stromatolite surface and boundary layer showed a strong diurnal rhythm of calcium carbonate precipitation. During illumination, photosynthesis caused oxygen production, a marked increase in pH and CO_3^{2-} concentrations, and a decrease in Ca^{2+} concentration at the stromatolite surface due to calcium carbonate precipitation. The opposite occurred in the dark, indicating decalcification. Calcite was approximately 16 times oversaturated in the bulk water, photosynthesis induced an increase of the oversaturation to > 27 at the stromatolite surface under illumination, and respiration induced a decrease of the oversaturation to < 10 in the dark. Photosynthetically stimulated calcium carbonate precipitation was confirmed by radioactive isotope ($^{45}\text{Ca}^{2+}$) uptake studies. Over a 24 hour light:dark cycle biofilms were net calcifying. Biotic activity within the stromatolite has a large effect on conditions at its surface, and therefore contributes considerably to the stromatolite precipitation process.

Introduction

Calcareous stromatolites are amongst the oldest known biological formations and provide insights into early-earth environments and climates. For this reason, it is essential that processes governing their formation and dissolution are understood. Presently-forming stromatolites are rare in marine settings, but a common and much investigated feature of karst regions (Grüninger 1965; Merz-Preiss and Riding 1999). Such karst-water creek stromatolites have been termed tufa stromatolites, and defined as macroscopically laminated benthic microbial deposits produced by precipitation of minerals on organic tissue

(Riding 1990). The role of biofilms in the formation of these stromatolites is still debated. Early studies suggested precipitation primarily caused by CO₂ assimilation by cyanobacteria, eukaryotic algae, and plants (Pia 1926; Pia 1933; Wallner 1934). Later hydrochemical investigations, however, concluded that precipitation is largely physicochemically driven by rapid CO₂ degassing from high pCO₂ groundwater (Herman and Lorah 1987; Merz-Preiss and Riding 1999; Usdowski et al. 1979), with only a minor contribution from photosynthetic CO₂ removal. This conclusion was reached when it was observed that calcium and dissolved inorganic carbon (DIC) were lost from water as it moved downstream, but no diurnal pattern was observed in creek-water chemistry. Even in instances where phototrophic communities were observed to affect whole stream inorganic carbon dynamics (Spiro and Pentecost 1991), the development of tufa/travertine deposits was seen as a largely abiotic process. The biofilms in the creeks investigated in the current study were very thin (<100 µm), and indeed whole stream-water chemistry parameters are hardly affected by biological activity. We tested the hypothesis that in these thin biofilms strong shifts in local water chemistry are possible due to photosynthetic and respiratory activity, and that these shifts have highly localised effects on the stromatolite surface where calcium carbonate precipitates.

Precipitation of calcite is initiated when calcium carbonate becomes supersaturated and suitable nucleation sites are present. Karst-waters have a low Mg²⁺:Ca²⁺ ratio (< 2) and therefore low-Mg-calcite is usually the main component in their stromatolite formations (Arp et al. 2001; Irion and Müller 1968). Photosynthesis and respiration can have a large affect on carbonate chemistry. Photosynthesis removes CO₂ and shifts the carbonate equilibrium towards carbonate, thereby increasing Ω . Respiration increases CO₂, and therefore has the opposite effect. Consequently, photosynthesis can lead to calcification, while respiration can lead to calcite dissolution when Ω decreases to values below one. In other aquatic settings, such as hypersaline lakes (Ludwig et al. 2005) and marine sediments (Werner et al. unpubl.) microsensor studies have demonstrated the potential for phototrophic communities to remove large amounts of CO₂ and enhance calcification. For stromatolite forming biofilms in fresh-water settings, this has not yet been investigated, and the view still prevails that the primary mechanism behind stromatolite precipitation is CO₂ degassing (Pentecost 1995).

It is also thought that, in addition to metabolic activity, biofilm components, particularly acid-organic compounds, that can strongly bind Ca²⁺, in extra-cellular polymeric substances (EPS), influence CaCO₃ precipitation. EPS is a common component of biofilms (Decho 1990; Nealson 1997; Neu and Lawrence 1999) and may contribute to precipitation in two ways: (1) suitably arranged acidic EPS groups create a template for precipitation and promote

nucleation upon saturation with Ca^{2+} (organomineralisation), and (2) the decomposition of EPS liberates HCO_3^- and Ca^{2+} and thereby increases calcite oversaturation (Arp et al. 2003; Decho et al. 2005; Dupraz and Visscher 2005; Trichet and Defarge 1995).

Previous studies in the Deinschwanger Creek (see methods) (Arp et al. 2001) were inconclusive as to the exact role of the biofilm in stromatolite formation. Hitherto, diurnal rhythms have not been observed in this creek (Arp et al. 2003), due to resolution limitations of the bulk water analysis methods used. Previous results have not excluded that the phototrophic biofilms diurnally control the local, i.e., on the stromatolite surface, water chemistry. We have, therefore, performed both in situ and ex situ experiments to investigate the role of the biofilm in stromatolite formation in more detail. We used fine scale microsensor and β -imaging techniques to elucidate the influence of biofilm activity on carbonate chemistry and precipitation at the stromatolite surface.

Materials and methods

Creek sites

The Deinschwanger creek is located near Nürenberg, in southern Germany (49°23'N, 11°28'E), and the Westerhöfer near the Harz mountains in northern Germany (51°45'N, 10°5'E). Both sites have been used for previous studies on calcification and are described in more detail in (Arp et al. 2001) and (Usdowski et al. 1979). Both sites show active laminated stromatolite formation of up to 1.8 mm yr⁻¹.

Sampling

Water samples for DIC and calcium measurements were taken from both the creeks and the aquariums during incubation. fifteen mL samples were filtered (0.2 μm) into exetainers (Labco Ltd., Buckinghamshire, England) containing HgCl_2 , sealed without air bubbles, and stored in the dark at 4°C until analysis.

Stromatolite samples for laboratory incubations were taken with a motorized core-drilling device, in October 2005 and 2006 from the Deinschwanger creek and May 2006 from the Westerhöfer creek. Samples were stored in ambient creek water in coolers and transported to the laboratory within 24 h. At the Deinschwanger, samples were collected from two distinct sites. Site 1 comprised a small stromatolite cascade downstream of the spring, in a shaded site in the forest. The stromatolite was laminated and several cm thick. At this site the creek was approximately 1 – 5 cm deep and exhibited a fast flow rate of approximately 0.7 m s⁻¹. Site 2 was a well illuminated section of the lower creek, was approximately 20 cm deep, and had a lower flow rate (approximately 0.05 m s⁻¹) than site 1. Site 2 exhibited thin

(up to 1 mm), fragile carbonate crusts. At the Westerhöfer samples were only taken from one site, which was similar to site 1 from the Deinschwanger. Here the creek was fast flowing and shallow, with laminated stromatolite several cm thick. Ambient pH at all sampling sites was 8.4.

In the laboratory, samples were stored in temperature controlled (10°C), aerated recirculating aquariums (total volume approximately 30 L) containing creek water. Creek water was collected without air bubbles, in 20 L plastic containers, at the same time cores were taken. The water was stored in the dark at 4°C until it was added to the aquarium reservoir. Samples were illuminated by 150 mol quanta m⁻² s⁻¹ on a 12 h light:12 h dark cycle.

Water analyses

Bulk water pH was determined with a MA130 pH electrode (Mettler Toledo, Columbus, Ohio, USA) directly in the creek and in the experimental aquaria. Ca²⁺ was determined by ICP–OES (Perkin Elmer Optima 3300 DV) and DIC by CO₂ Coulometer (UIC Coulometrics, Joliet, USA).

Algal pigment analysis

Triplicate biofilm samples from the Deinschwanger Creek (sites 1 and 2) and single samples from incubation experiments were analysed for algal pigments to assess the change in algal communities induced by experimental conditions. Samples taken freshly from the creek were stored on ice and frozen (–20°C) as soon as possible (<24 h). Samples used for laboratory studies were immediately frozen after the incubations. For analysis, frozen samples were placed in 15 mL centrifuge tubes, in 3 mL of 100% acetone, and sonicated on ice for 10 x 1 minute. Pigments were extracted from the mixture at –20°C, overnight. Samples were then filtered (Acrodisc CR syringe filter, 0.45 µm pore size, PALL, Gellman Laboratory) and diluted with water to a final concentration of 70% acetone. Photo-pigments were separated on a HPLC (2690 Separation module, Waters), equipped with a Eurospher–100 C18, 5 µm Vertex column (Knauer, Berlin, Germany), according to the method of (Wright et al. 1991). Absorption spectra of the separated compounds was measured on a Waters 996 photo diode array detector and pigments quantified and identified by comparison to pigment standards (DHI Waters and Environment, Denmark).

Microelectrode measurements and calculations

Microelectrodes are ideal tools to measure chemical gradients in biotic systems at fine (µm) scale, see (Gieseke and De Beer 2004) for a review of microsensor form, function and

application to microbiological samples. Microelectrode profiles of pH, O₂, and Ca²⁺ concentration gradients were measured in situ at the two creeks. Profiles of these and CO₃²⁻ were also made ex situ, in the laboratory, using biofilm covered stromatolite cores.

Liquid membrane Ca²⁺ and pH sensors (tip 20µm) were prepared and calibrated as described previously (De Beer et al. 2000; De Beer et al. 1997). Liquid membrane CO₃²⁻ sensors were constructed similarly to the other liquid membrane sensors and calibrated as described in de Beer et al. (unpubl.). For carbonate system components pK1 (6.464) and pK2 (10.489) were calculated after (Millero 1979), for fresh water and at 10°C. Fast responding O₂ microsensors (tip 10µm) were prepared as described previously (Revsbech 1989). Biofilms were very thin (50 – 100 µm) and it was difficult distinguish to the biofilm surface from that of the calcium carbonate tufa. Indeed the biofilms were partly endolithic. The glass electrodes could not penetrate the hard mineral surface. All electrodes were, therefore, placed at the stromatolite:biofilm surface while viewing the sample through a dissection microscope. The surface was then set at 0, and all measurements were made above the surface. Negative distances indicate that the sensor is above the stromatolite:water interface, that is, in the overlying water. Sensors were connected to a micromanipulator, which was fixed onto a motorised stage (VT-150, Micos, Eschbach, Germany) and allowed reproducible positioning of the sensor tip with 1 µm precision. The microelectrodes were connected to a picoammeter (O₂ electrode) or a millivoltmeter, and the meter output was collected by a data acquisition device (NI-Daq 6015, National Instruments, Austin, Texas, USA). After positioning at the surface, profiling was done automatically, motor control and data acquisition were performed with a computer and custom written software (µ-Profiler, Dr. L. Polerecky). All profiles were corrected for offset to ion levels in the bulk liquid, as measured by the water analyses. For in situ microelectrode measurements, the micromanipulator was mounted to a heavy stand and placed in the creek, on the downstream side of the measuring position.

Interfacial fluxes (J) were calculated from the concentration profiles using Fick's first law:

$$J = D \times (dc / dx) \quad (3.1)$$

where D is the diffusion coefficient and dc:dx is the interfacial concentration gradient, i.e., the concentration gradient in the mass boundary layer directly adjacent to the stromatolite surface. The diffusion coefficients of O₂ and Ca²⁺ are literature derived values corrected for temperature and type of counter ion (Broeker and Peng 1974; Li and Gregory 1974). Estimated diffusion coefficients of oxygen are, 4°C: 1.28 × 10⁻⁹ m² s⁻¹; 10°C: 1.57 × 10⁻⁹ m² s⁻¹ and 17°C: 1.934 × 10⁻⁹ m² s⁻¹. Diffusion coefficients for Ca²⁺ with HCO₃⁻ as counter ion are,

4°C $0.546 \times 10^{-9} \text{ m}^2 \text{ s}^{-1}$; 10°C: $0.67 \times 10^{-9} \text{ m}^2 \text{ s}^{-1}$ and 17°C: $0.827 \times 10^{-9} \text{ m}^2 \text{ s}^{-1}$.

Calcite saturation is given by the saturation state omega,

$$\Omega = [\text{Ca}^{2+}] \times [\text{CO}_3^{2-}] / K(\text{calcite}) \quad (3.2)$$

where the numerator is the ion concentration product (ion activities were not incorporated) and the denominator the solubility product. $\Omega > 1$ indicates supersaturation, while $\Omega < 1$ indicates undersaturation. The solubility product for calcite was taken from (Plummer and Busenberg 1982).

Incubations with radiotracers

Stromatolite samples from both creeks were subject to radio tracer incubation with $^{45}\text{Ca}^{2+}$. Stromatolite samples were incubated under three experimental conditions: (1) under illumination with $150 \text{ mol quanta m}^{-2} \text{ s}^{-1}$, (2) in the dark, and (3) fixed with formaldehyde (2 %) control, and analysed by both scintillation counting and β -imaging. During each treatment, stromatolite samples were incubated in 400 mL filtered creek water at 20°C, and gently stirred. Prior to addition of the radiotracer, the stromatolite pieces were left for at least 2 h to recover from the transfer. Radioactive tracer, $^{45}\text{Ca}^{2+}$ as CaCl_2 , (Amersham Pharmacia Biotech, UK) was added to each beaker to a final activity of 3 kBq mL^{-1} (specific activities were 74.0 MBq mL^{-1}) in all the experiments. Samples were incubated with tracer for 1, 3, 6, and 24 h.

After the incubation, the samples were fixed in 2 % formaldehyde for 2 hours. The fixed stromatolite samples were then washed 4 times for 5 min in 200 mL filtered creek water. Samples were then left to air dry overnight.

Samples for scintillation counting were weighed and dissolved in 10 mL of 12 N HCl. Two mL of dissolved sample was then added to 3 mL of Ultima gold scintillation cocktail (Perkin-Elmer, Massachusetts, USA) and radioactivity determined using a Packard TR 2500 liquid scintillation counter operating in efficiency tracing mode to correct for quench.

Samples for β -imaging were immersed in Epothin resin (Buehler, Düsseldorf, Germany), cut into approximately 4 mm cross sections with a diamond band saw (Proxon MBS 240E, Niersbach, Germany) and polished flat with a Buehler Beta polishing system. β -imaging auto-radiographs of the stromatolite samples were acquired in a Micro-Imager (Laniece et al. 1998). The resin fixation and polishing process occasionally produced artifacts in the data obtained by the β -imager. These artifacts were caused by air-bubbles in the resin, which filled with radioactive dust when the samples were cut and polished. They were easily recognizable as a circular “hotspot” that coincided with an air-bubble induced hole. These artifacts were removed from the analysis with Photoshop CS (Adobe Systems Inc.).

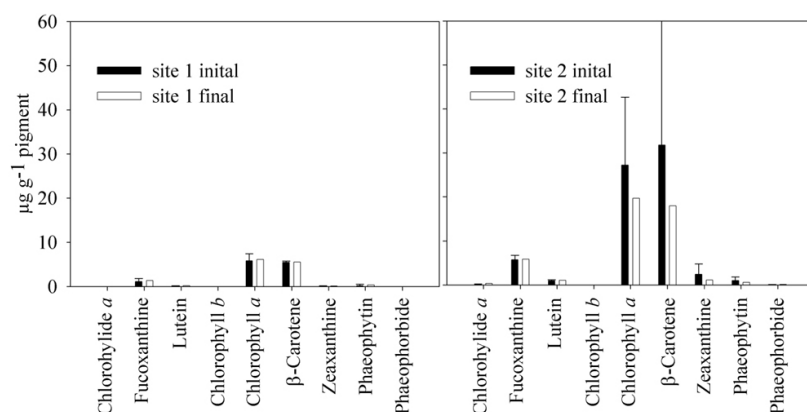


Fig. 1 Algal pigments in tufa samples from the Deinschwanger Creek (sites 1 and 2) prior to and following incubation. (Initial samples $n = 3$, final samples $n = 1$)

Results

Sample description and pigment analysis

Stromatolite biofilms in both the Deinschwanger and Westerhöfer Creeks were green-brown and composed of cyanobacteria, diatoms, and associated non-phototrophic bacteria. Pigment composition was analysed only for samples from the Deinschwanger creek, site 1 (small tributary on northern valley side) and site 2 (lower end section, near end of stromatolite deposition).

Samples from site 1 comprised thick stromatolite cores, whose top was covered by an approximately 50–100 µm thick green and brown biofilm, while those at site 2 comprised an equally thick brown colored biofilm covering a 1 mm thick, fragile carbonate crust. The appearance of the samples did not change markedly during the study, but biofilm thickness sometimes increased slightly. Pigment composition did not change markedly during incubation (Fig. 1). The pigment concentrations and compositions in samples at the end of incubations were similar to those from the creek, showing that the algal community remained stable during incubations. Pigment concentrations were higher at site 2. The composition of the pigments was similar at both sites. Pigments were dominated by chlorophyll a and β-carotene. Smaller amounts of fucoxanthene, zeaxanthine, phaeophytin and chlorohylide a were also seen in both sites. Fucoxanthene and zeaxanthine and phaeophytin indicate the presence of cyanobacteria and diatoms in these biofilms.

In situ measurements

In situ profiling was complicated by the heterogeneous substrate topography, debris flowing down the river, and difficult visualisation of the hard substratum by poor light

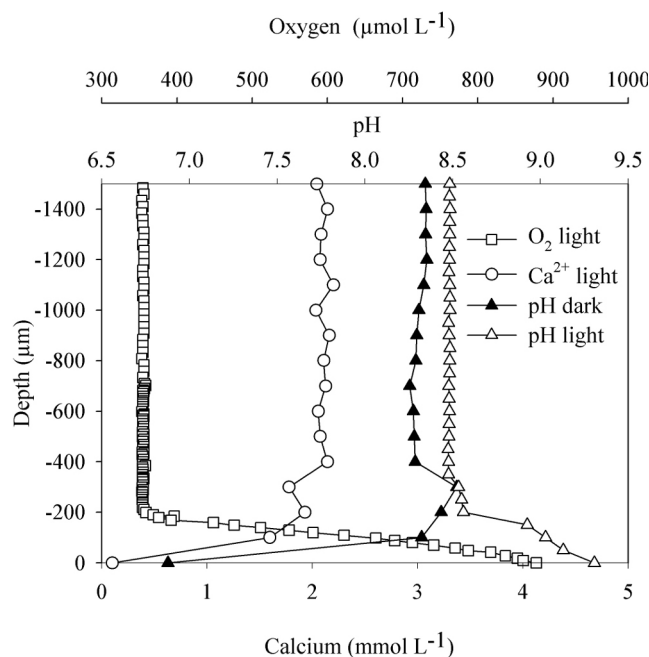


Fig. 2 In situ concentration profiles of Ca^{2+} , pH, and O_2 at Deinschwanger Creek.

conditions. Consequently, in situ microprofiling was often interrupted by breaking of microsensors. In situ concentration gradient profiling was successfully carried out for O_2 , pH and Ca^{2+} in both the Deinschwanger and Westerhöfer Creek, although not all species could be profiled both in the day and night at both sites (Figs. 2 and 3). The data clearly indicate a day:night change in chemical conditions on the stromatolite surface. Flux's calculated from profiles are given in Table 1. Photosynthesis occurred at the stromatolite surface of both creeks in daylight and caused a flux of O_2 from the biofilm to the water column, an increase in pH at the stromatolite surface and a concomitant decrease in Ca^{2+} ion concentration. The night profiles showed the opposite. In the Westerhöfer a decrease in O_2 concentration occurs with respiration and an increase in Ca^{2+} concentration is evident. At the Deinschwanger only a pH profile was obtained at night, which shows a decrease in pH at the stromatolite surface, indicating respiratory activity. The efflux of Ca^{2+} in the dark is lower than its influx in the light thus, during a 12:12 h photoperiod, there is a net flux of $1.2 \times 10^{-5} \text{ mol Ca}^{2+} \text{ m}^2 \text{ s}^{-1}$ towards the stromatolite surface over a full 24 h cycle.

Table 1 In situ fluxes ($\text{mol m}^2 \text{ s}^{-1}$) of oxygen and calcium in the Deinschwanger and Westerhöfer Creek. A negative flux indicates a flux from the water column towards the tufa surface.

	<i>Deinschwanger Creek</i>		<i>Westerhöfer Creek</i>	
	Oxygen	Calcium	Oxygen	Calcium
Day	5.6×10^{-6}	-2.0×10^{-5}	1.0×10^{-6}	-1.3×10^{-5}
Night			-9.1×10^{-7}	7.3×10^{-6}

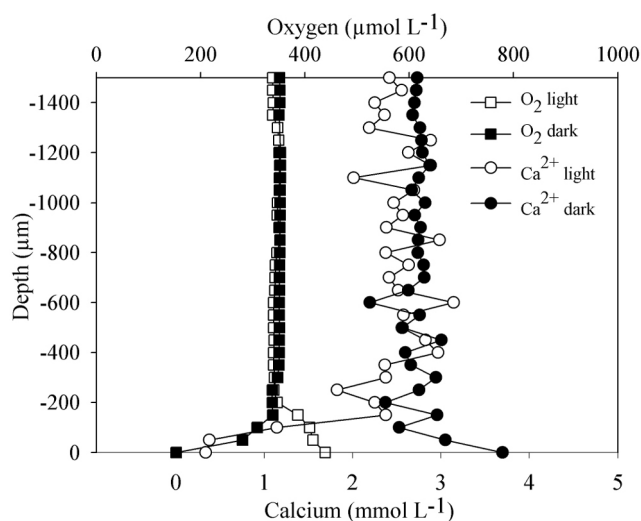


Fig. 3 In situ concentration profiles of Ca^{2+} and O_2 at Westerhöfer Creek.

Ex situ measurements

The in situ measurements were complemented with a detailed ex situ study. In samples from both creeks, under illumination O_2 and pH increased due to photosynthesis, coincident to a decrease in Ca^{2+} . The opposite occurred under dark conditions (Figs. 4 and 5). Respiration resulted in O_2 consumption and a decrease in pH. The Ca^{2+} profile also changed with this change in metabolism, such that Ca^{2+} uptake (CaCO_3 precipitation) ceased and its release from the tufa (apparent CaCO_3 dissolution) occurred. The carbonate concentration increased at the stromatolite surface during light conditions, and decreased in the dark (Fig. 5). Fluxes calculated from the profiles are shown in Table 2. The fluxes of both O_2 and Ca^{2+} were similar during in situ measurements and the laboratory incubations. Accurate quantitative comparisons are difficult because of the heterogeneity of the samples.

Carbonate profiles, measured by carbonate microsensor in several samples from the

Table 2 Ex situ fluxes ($\text{mol m}^{-2} \text{s}^{-1}$) of oxygen, calcium, and carbonate in the Deinschwanger and Westerhöfer Creek. Numbers in parentheses identify site (1) or (2). A negative flux indicates a flux towards the tufa surface.

	<i>Deinschwanger creek</i>		<i>Westerhöfer Creek</i>		
	Oxygen	Calcium	Oxygen	Calcium	Carbonate
Light	4.37×10^{-6} (1)	-1.30×10^{-6} (1)	3.24×10^{-6}	-3.42×10^{-6}	2.39×10^{-7}
	1.62×10^{-6} (2)	-8.88×10^{-7} (2)			
Dark	-3.75×10^{-7} (1)	1.16×10^{-7} (1)	-2.47×10^{-7}		-1.44×10^{-7}
	-4.3×10^{-7} (2)	0 (2)			

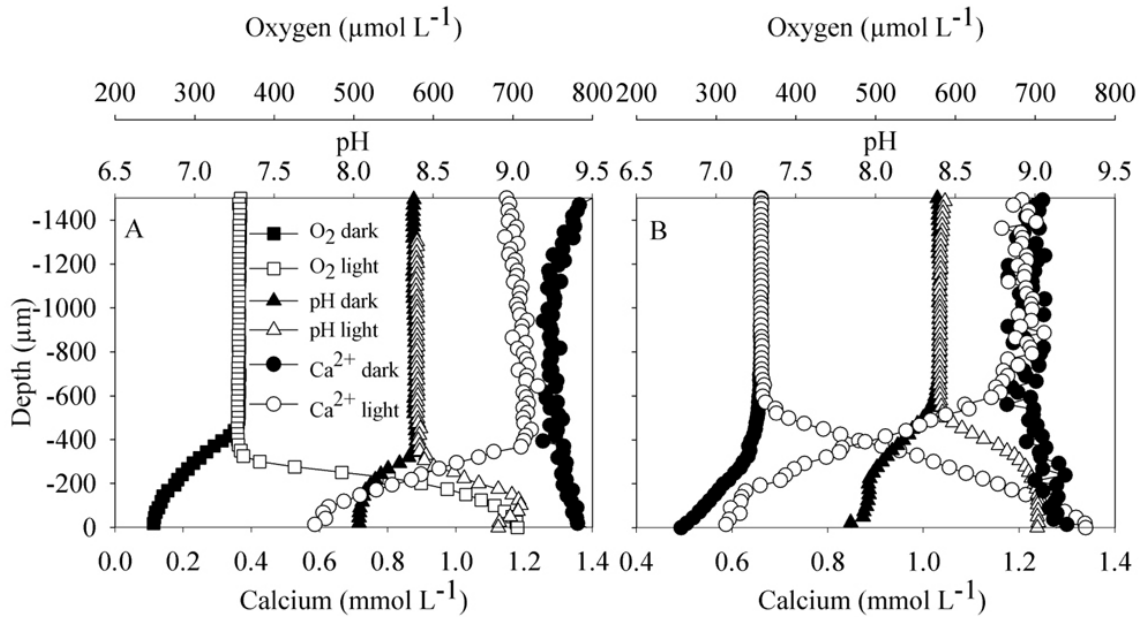


Fig. 4 Ex situ concentration profiles Ca^{2+} , pH, and O_2 from Deinschwanger Creek tufa biofilm samples. (A) Site 1. (B) Site 2.

Westerhöfer Creek, agreed well with carbonate profiles modeled from the bulk water DIC concentrations and pH microprofiles using the CO_2 system equations (Zeebe and Wolf-Gladrow 2001) (data not shown). Subsequently, bulk water DIC and pH microprofiles were used to predict the CO_3^{2-} concentration and Ω profiles for tufa samples (Fig. 6). These calculations revealed an increase in CO_3^{2-} in light, which caused Ω to become > 20 . The opposite was seen in the dark, with CO_3^{2-} and Ω becoming < 10 .

Water flow had a small effect on the photosynthesis rates. Increasing the flow rate from 0.009 L s^{-1} to 0.035 L s^{-1} caused the diffusive boundary layer (DBL) to decrease in thickness from approximately $600 \mu\text{m}$ to $200 \mu\text{m}$ and the areal rate of O_2 production to increase from 1.93×10^{-6} to $2.47 \times 10^{-6} \text{ mol m}^{-2} \text{ s}^{-1}$. The height of the DBL indicates the range over which diffusion determines chemical gradients. The smaller the DBL the faster chemicals can move between the overlying water and the sediment surface. Flow rates in situ were very fast, and the DBL probably slightly less than that in our ex situ experiments. This, however, does not change the interpretation of the clear diurnal calcium dynamics observed.

Radiotracer incubations

Scintillation counts of whole samples showed that calcium was incorporated under all conditions, but rates of incorporation in the light were approximately twice as high as in the dark and controls (Fig. 7). Dark rates equaled control rates, indicating that in the dark the

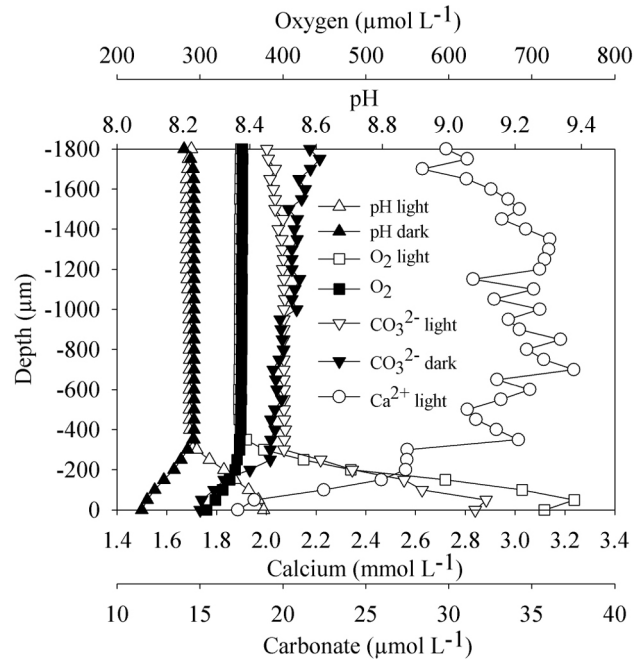


Fig. 5 Ex situ concentration profiles Ca^{2+} , pH, O_2 , and CO_3^{2-} from Westerhöfer Creek tufa biofilm samples.

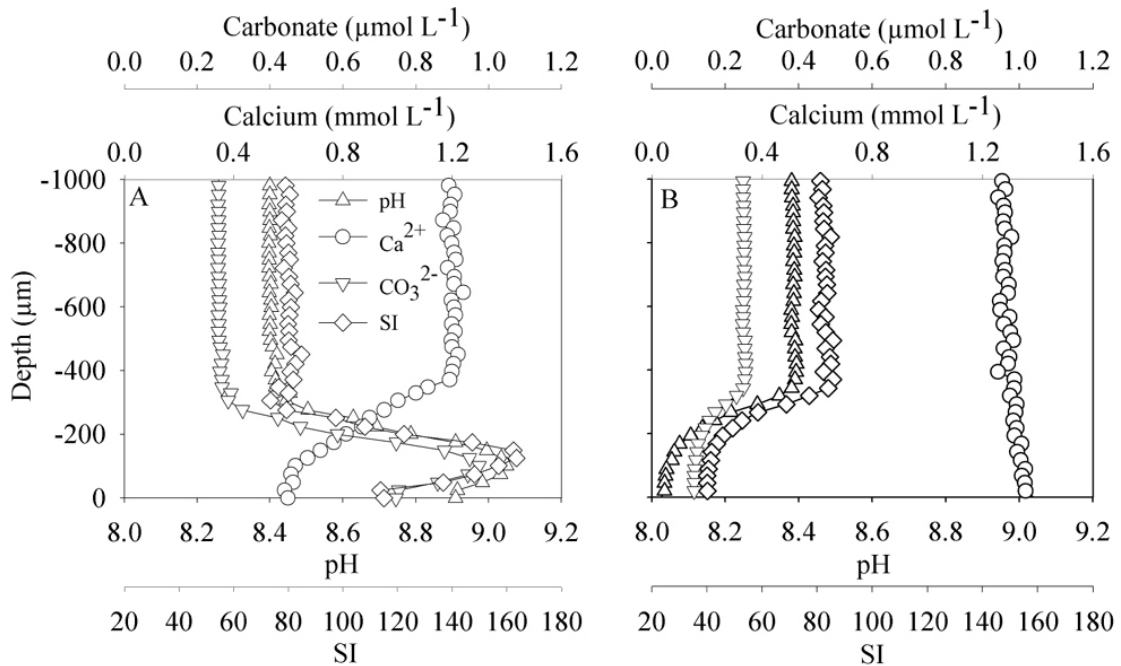


Fig. 6 Measured microprofiles of pH and Ca^{2+} in the (A) light and (B) dark and predicted CO_3^{2-} and calcite saturation Ω calculated from the measured pH profiles and bulk water DIC concentrations. Samples from the Deinschwanger Creek, site 1.

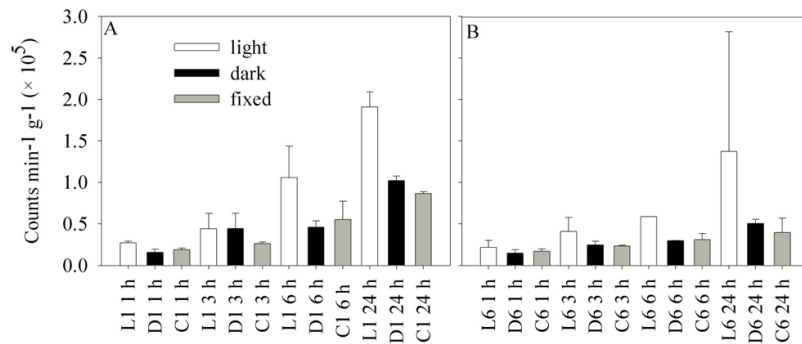


Fig. 7 $^{45}\text{Ca}^{2+}$ uptake of tufa samples from the Deinschwanger Creek. (A) Site 1 and (B) site 2. Open bars represent light incubations, black bars dark incubations, and gray bars formaldehyde fixed controls. X-axis labels refer to Light (L), Dark (D) and Control (C) incubations as well as incubations time (h). (mean \pm SE, $n = 2$)

calcium uptake was mainly isotopic exchange. The β -imaging (Fig. 8) confirmed that uptake of $^{45}\text{Ca}^{2+}$ was stimulated by light, and that Ca^{2+} uptake preferentially occurred at the stromatolite surface. Indeed, $^{45}\text{Ca}^{2+}$ uptake appears to occur most strongly in the middle of the biofilm, but can be seen throughout the whole biofilm (photosynthetic zone), not only at the biofilm:overlying water interface. In the dark and control samples radioactive signals were detected throughout the whole sample.

Discussion

There has been a long controversy regarding whether stromatolites in karst-water creeks are formed by biological removal of CO_2 , so by photosynthesis, or by CO_2 degassing. It is, however, conceivable that both processes occur simultaneously in the creek: in the water-column the carbonate system is driven by abiotic forces, as suggested previously, while stromatolite formation is driven by metabolic processes. We propose that the most dominant calcification process in the creek does not result in stromatolite formation, but occurs in the water column and the precipitated calcium carbonate is washed from the spring area as suspended crystals. This calcification process is driven by CO_2 degassing and manifests itself as a downstream calcium loss from the water column, and a downstream pH increase, with no diurnal pattern to the calcium loss, stream pH or saturation-state parameters. This physical process was well documented in similar systems and also in the creeks of this study (Merz-Preiss and Riding 1999; Usdowski et al. 1979).

Parallel to this physicochemical process, a biologically controlled calcification results in stromatolite formation. Local CO_2 fixation by photosynthesis leads to calcification in the top 100 μm of the stromatolite surface. Interestingly, apparent decalcification is observed during the night, due to respiration, so locally the biological processes can counter the massive

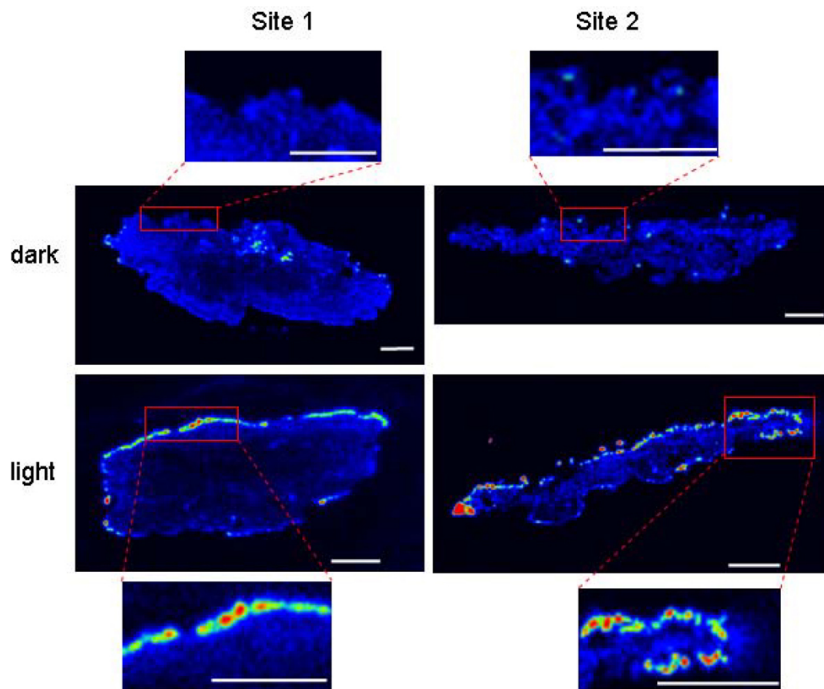


Fig. 8 8-images of light and dark incubated tufa samples from the Deinschwanger Creek after 24 hours. The original biofilm surface is at the top of each sample. Scale bar = 3 mm.

physical process of out-gassing. The biological processes exert no significant influence over the whole stream carbonate system, so does not induce diurnal rhythms in pH and Ca^{2+} concentrations in the water column. Indeed a rough, conservative calculation can be made regarding the relative contributions of the two processes. Assuming about 100 m^2 of stromatolite area, a flow rate of 2 L s^{-1} , Ca^{2+} flux estimated from actual tufa deposits (about 4 mm thick annual lamination, unpublished data) and Ca^{2+} loss from the bulk water of 0.4 mmol L^{-1} , stromatolite precipitation accounts for less than 15 % of the creek's calcium loss. The biological processes are only measurable at the stromatolite surface with high-resolution methods, such as microsensors. The biological effects on the water column pH or Ca^{2+} concentrations are lost in the overwhelming background of the larger CO_2 degassing driven process. However, locally the effects of biological processes are highly significant. The biological precipitation process, which results in stromatolite growth, manifests itself as precipitation at the stromatolite surface and exhibits a clear diurnal rhythm, synchronous with biofilm photosynthetic and respiration processes. The present microsensor pH, O_2 and Ca^{2+} profiles clearly demonstrate this diurnal pattern and therefore a decisive biological control on the microenvironment and Ca^{2+} removal for stromatolite formation.

It is also argued that biofilms merely act as nucleation site for calcification or concentrate calcium by binding to EPS (Dupraz and Visscher 2005). With this in mind, two possible

scenarios will be discussed in view of the observed Ca^{2+} microprofiles and radiotracer data, (1) Ca^{2+} -uptake at newly produced EPS without precipitation and later Ca^{2+} release due to pH decrease or EPS decomposition causing precipitation in a second step, or (2) CaCO_3 precipitation caused by photosynthetic CO_2 removal.

The first scenario does not explain our radiotracer data: EPS is produced mainly under illumination and decomposed in the dark (Decho and Lopez 1993; Epstein 1997; Staats et al. 2000). If release of Ca^{2+} from EPS were driving supersaturation under these conditions, CaCO_3 would be precipitated in the dark. All samples were illuminated immediately before the tracer experiment. If release of Ca^{2+} bound to EPS was initiating precipitation, $^{45}\text{Ca}^{2+}$ uptake should have been seen in both the light and dark treatments. In the light as the tracer was bound to EPS, and in the dark as previously bound Ca^{2+} was released, leading to CaCO_3 supersaturation and precipitation. This was not the case; $^{45}\text{Ca}^{2+}$ uptake was observed only in the light. We do not exclude that pH changes induced by photosynthesis:respiration cycles make EPS more amenable to Ca^{2+} binding in the light and release in the dark (Gregor et al. 1996). Such a scenario would show Ca^{2+} uptake during the day, due to binding to EPS, and release in the night, as EPS groups become unfavourable to binding. Under such a case of binding and release the Ca^{2+} is not precipitated, but merely removed from and returned to the water-phase. As EPS can have only a limited number of binding sites, the uptake and release would be transient, occurring during the pH transitions upon illumination or darkening. No such behaviour of Ca^{2+} microprofiles was observed: typical light and dark profiles were stable for 12 hours. The Ca^{2+} taken up during the day is also clearly precipitated as CaCO_3 .

Thus the second scenario, that biofilm photosynthetic activity changes conditions at the stromatolite:water interface (the site of precipitation), by removal of CO_2 , to such an extent that rapid CaCO_3 precipitation is the most probable.

As reported in (Arp et al. 2001) the stromatolite biofilms were dominated by cyanobacteria and diatoms. The pigment data show that the community, is stable when removed from the creek to the laboratory, and is thus an appropriate model for ex situ experimental investigations. Water chemistry parameters also varied somewhat between our in situ and ex situ measurements. The Ca^{2+} and DIC concentrations decreased as the incubations continued. Particulate deposits were observed on the base of the recirculating incubation system, but a light:dark pattern to calcium loss was only observed at the stromatolite surface. The loss of Ca^{2+} and DIC may be seen in the relatively low bulk water Ω observed during the light in our ex situ measurements (Fig. 6). Despite these variations, and although the resultant rates may differ somewhat between the in- and ex situ measurements, general patterns are the same. The differences in rates (that seem generally higher in in situ

measurements) might be an effect of the different analytical set-ups (lab vs. creek) or due to the natural variation caused by mat patchiness. The level of replication used for the in situ measurements is necessarily small, thus quantitative interpretation of the microsensor observations to whole creek systems must be done with caution. The general agreement among the processes indicated and patterns observed between the different measurements, however, make it appropriate to discuss in general terms the overall processes occurring in the mats, based on both our in situ and ex situ observations.

The apparent, slight, Ca^{2+} flux to the water phase in the dark period, despite an Ω value always greater than 1, may be explained by dissolution that occurred below the stromatolite surface, in the endolithic part of the biofilm, which the microsensors could not reach. Heterotrophic activity probably continues below this zone and creates an environment conducive to stromatolite dissolution. As the stromatolite dissolves in the dark, Ca^{2+} diffuses upward, past the stromatolite surface, and is recorded by microsensors as Ca^{2+} flux from the stromatolite.

The importance of photosynthesis, not merely the presence of the biofilm and its potential nucleation sites, was also shown by the incubation of samples with the radioactive tracer $^{45}\text{Ca}^{2+}$. Incorporation rates of the tracer were highest in the photosynthesising sample and β -imaging showed the tracer to be specifically incorporated in the biofilm covered surfaces. The incorporation can be seen at or just below the surface of the light incubated samples (Fig. 8). The region just below the surface is within the biofilm and would be the zone of highest pH. The incorporation seen occasionally at the base of the samples was not an artifact. The samples were incubated in aquariums for several weeks and the biofilms had colonised parts of the underneath and sides of the samples. Thus, both the light stimulated uptake rates and the distribution of tracer incorporation are compatible with photosynthetically driven calcification.

It is interesting that not only was the calcium flux toward the stromatolite surface higher in the in situ measurements, but also the rate of photosynthesis. This agrees with lab results on flow rates, which suggest photosynthesis should be lower in the slower flow rates of the laboratory.

Because replication in this study was low, the exact rates determined herein need to be taken with some caution, but the diurnal pattern and net precipitation (rather than net dissolution) over a light:dark cycle observed here was remarkably persistent over all samples.

While further studies are needed to elucidate the exact mechanism and rates of nucleation and precipitation in these stromatolite creek systems, the biological activity of their phototrophic communities appears to be much more important than previously thought.

Despite not driving the total stream, carbonate system dynamics, the biofilm has a strong influence over the state of the carbonate system at the sites of nucleation. We have demonstrated this, for the first time, by observing a strong diurnal pattern in Ca^{2+} and CO_3^{2-} concentration profiles and Ω : a pattern that coincides with the photosynthetic activity of the biofilm.

Acknowledgements

We thank the microsensor technicians at the Max Planck Institute for Marine Microbiology, Bremen, for assistance with microsensor construction, and Lubos Polerecky for the microprofiling software. We thank Hakhyun Nam (Kwangwoon University, Korea) for supplying the carbonate ionophore. This project is part of the Research Unit "Geobiology of organo- and biofilms" funded by the German Research Foundation (DFG-FOR 571, publication no. 23).

References

- Arp, G., A. Reimer, and J. Reitner. 2003. Microbialite Formation in Seawater of Increased Alkalinity, Satonda Crater Lake, Indonesia. *Journal of Sedimentary Research* 73: 105–127.
- Arp, G., N. Wedemeyer, and J. Reitner. 2001. Fluvial tufa formation in a hard-water creek (Deinschwanger Bach, Franconian Alb, Germany). *FACIES* 44: 1–22.
- Broecker, W. S., and T. H. Peng. 1974. Gas exchange rates between air and sea. *Tellus* 26: 21–35.
- de Beer, D., M. Kühl, N. Stambler, and L. Vaki. 2000. A microsensor study of light enhanced Ca^{2+} uptake and photosynthesis in the reef-building hermatypic coral *Favia* sp. *Marine Ecology - Progress Series* 194: 175–185.
- de Beer, D., A. Schramm, C. M. Santegoeds, and M. Kühl. 1997. A nitrite microsensor for profiling environmental biofilms. *Applied and Environmental Microbiology* 63: 973–977.
- Decho, A. W. 1990. Microbial exopolymer secretions in ocean environments - their role(s) in food webs and marine processes. *Oceanography and Marine Biology Annual Reviews* 28: 73–153.
- Decho, A. W., and G. R. Lopez. 1993. Exopolymer microenvironments of microbial flora: multiple and interactive effects on trophic relationships. *Limnology and Oceanography* 38: 1633–1645.
- Decho, A. W., P. T. Visscher, and R. P. Reid. 2005. Production and cycling of natural microbial exopolymers (EPS) within a marine stromatolite. *Palaeogeography, Palaeoclimatology, Palaeoecology* 219: 71–86.
- Dupraz, C., and P. T. Visscher. 2005. Microbial lithification in marine stromatolites and hypersaline mats. *Trends in Microbiology* 13: 429–438.
- Epstein, S. S. 1997. Microbial food webs in marine sediments. 1. Trophic interactions and grazing rates in two tidal flat communities. *Microbial Ecology* 34: 188–198.

- Gieseke, A., and D. De Beer. 2004. Use of microelectrodes to measure in situ microbial activities in biofilms, sediments, and microbial mats, p. 1581–1612. In G. A. Kowalchuk, F. J. de Bruijn, I. M. Head, A. D. Akkermans and J. D. van Elsas [eds.], *Molecular Microbial Ecology Manual*. Kluwer Academic Publishers.
- Gregor, J. E., E. Fenton, G. Brokenshire, P. Van Den Brink, and B. O'Sullivan. 1996. Interactions of calcium and aluminium ions with alginate. *Water Research* 30: 1319–1324.
- Grüniger, W. 1965. Rezenten Kalktuffbildung im Bereich der Uracher Wasserfälle. - *Abhandlungen zur Karst- und Höhlenkunde. Reihe E Botanik* 2: 1–113.
- Herman, J. S., and M. M. Lorah. 1987. CO₂ outgassing and calcite precipitation in Falling Spring Creek, Virginia, U.S.A. *Chemical Geology* 62: 251–262.
- Irion, G., and G. Müller. 1968. Minerology, petrology and chemical composition of some calcareous tufa from the Schwäbische Alb, Germany., p. 157–171. In G. Müller and G. M. Friedman [eds.], *Recent developments in carbonate sedimentology in central Europe*. Springer.
- Laniece, P., Y. Charon, A. Cardona, L. Pinot, S. Maitrejean, R. Matrippolito, B. Sandkamp, and L. Valentin. 1998. A new high resolution radioimager for the quantitative analysis of radiolabelled molecules in tissue section. *Journal of Neuroscience Methods* 86: 1–5.
- Li, Y., and S. Gregory. 1974. Diffusion of ions in seawater and in deep-sea sediments. *Geochimica et Cosmochimica Acta* 38: 703–714.
- Ludwig, R., F. A. Al-Horani, D. de Beer, and H. Jonkers. 2005. Photosynthesis controlled calcification in a hypersaline microbial mat. *Limnology and Oceanography* 50: 1836–1843.
- Merz-Preiss, M., and R. Riding. 1999. Cyanobacterial tufa calcification in two freshwater streams: ambient environment, chemical thresholds and biological processes. *Sedimentary Geology* 126: 103–124.
- Millero, F. J. 1979. The thermodynamics of the carbonate system in seawater. *Geochimica et Cosmochimica Acta* 43: 1651–1661.
- Nealson, K. H. 1997. Sediment bacteria: who's there, what are they doing and what's new? *Annual Rev. Earth Planet. Sci.* 25: 403–434.
- Neu, T. R., and J. R. Lawrence. 1999. In situ characterization of extracellular polymeric substances (EPS) in biofilm systems, p. 21–47. In J. Wingender, T. R. Neu and H.-C. Flemming [eds.], *Microbial extracellular polymeric substances*. Springer Verlag.
- Pentecost, A. 1995. Geochemistry of carbon dioxide in six travertine-depositing waters of Italy. *Journal of Hydrology* 167: 263–278.
- Pia, J. 1926. *Pflanzen als Gesteinsbildner*. Borntraeger.
- . 1933. *Die rezenten Kalksteine*. Ergänzungsband.
- Plummer, L. N., and E. Busenberg. 1982. The solubilities of calcite, aragonite and vaterite in CO₂-H₂O solutions between 0 and 90°C, and an evolution of aqueous model for the system CaCO₃-CO₂-H₂O. *Geochim Cosmochim Acta* 46: 1011–1040.
- Revsbech, N. P. 1989. An oxygen microsensor with a guard cathode. *Limnology and Oceanography* 34: 474–478.

- Riding, R. 1990. *Calcareous algae and stromatolites*. Springer-Verlag.
- Spiro, B., and A. Pentecost. 1991. One day in the life of a stream - a diurnal inorganic carbon mass balance for a travertine-depositing stream (Waterfall Beck, Yorkshire). *Geomicrobiology Journal* 9: 1–11.
- Staats, N., L. J. Stal, B. de Winder, and L. R. Mur. 2000. Oxygenic photosynthesis as driving process in exopolysaccharide production of benthic diatoms. *Marine Ecology-Progress Series* 193: 261–269.
- Trichet, J., and C. Defarge. 1995. Non-biologically supported organomineralization. *Bulletin de l'Institut océanographique* 14: 203–236.
- Uzdowski, E., J. Hoefs, and G. Menschel. 1979. Relationship between ^{13}C and ^{18}O fractionation and changes in major element composition in a recent calcite-depositing spring -- A model of chemical variations with inorganic CaCO_3 precipitation. *Earth and Planetary Science Letters* 42: 267–276.
- Wallner, J. 1934. Über die Beteiligung kalkablagernder Pflanzen bei der Bildung südbayerischer Tuffe. *Bibliotheca Botanica* 110: 1–30.
- Wright, S. W., S. W. Jeffrey, R. F. C. Mantoura, C. A. Llewellyn, T. Bjornland, D. Repeta, and N. Welschmeyer. 1991. Improved HPLC method for the analysis of chlorophylls and carotenoids from marine-phytoplankton. *Marine Ecology-Progress Series* 77: 183–196.
- Zeebe, R. E., and D. Wolf-Gladrow. 2001. *CO₂ in seawater: Equilibrium, Kinetics, Isotopes*, 1st ed. Elsevier.

Chapter 4

The affect of changing pH and temperature on calcium carbonate precipitation in cyanobacterial biofilms

The affect of changing pH and temperature on calcium carbonate precipitation in cyanobacterial biofilms

Andrew Bissett, Andreas Reimer, Dirk de Beer, Fumito Shiraishi, Gernot Arp

Abstract

Ex situ microelectrode experiments, using cyanobacterial biofilms from karst-water creeks, were conducted under varying pH and temperature and constant alkalinity to investigate the affect of changing environmental parameters on cyanobacterial photosynthesis-induced calcification. Contrary to previous assumptions, the highest photosynthesis-induced rise in pH was observed at comparatively low pH conditions (7.8). This may be due to a high pCO₂ gradient from outside to into the cyanobacterial cell, thereby facilitating photosynthetic CO₂ assimilation. In turn, comparatively high pH conditions (8.9), and hence low pCO₂ gradient, are less favourable for cyanobacterial calcification under illumination, but maintain a minor Ca²⁺ flux into the biofilms under dark conditions due to the increased background calcite supersaturation.

A temperature increase from 4 to 17°C increased biological activity, as indicated by O₂ fluxes, although the effect on pH was non-linear. In summary, a rise in pCO₂ and minor decrease in pH may have been more favourable for the formation of cyanobacterial tubular microfossils in the fossil record, given constant alkalinity, while temperature effects appear evident, but of secondary importance to calcification within the experimental range 4 and 17°C.

Introduction

Calcifying biofilms have contributed significantly to the formation of carbonate sediments throughout earth-history (Burne and Moore, 1987; Riding, 1991; Riding, 1999). These sediments are known as microbialites and, if macroscopically laminated, stromatolites. Their temporal and geographic distributions have been used to infer the impacts of metazoan evolution (Walter and Heys, 1985; Awramik, 1971) and changes in ocean chemistry (Riding, 1992; Grotzinger and Kasting, 1993; Arp et al., 2001). Many stromatolites are formed in the photic zone of shallow-water environments by thin cyanobacterial biofilms, rather than by thick microbial mats, which tend to produce more irregular fabrics.

The principal mechanisms involved in stromatolite formation are (1) heterogeneous crystal nucleation at acidic extra-cellular polymeric substances, and (2) increases in the $\text{Ca}^{2+} \times \text{CO}_3^{2-}$ ion activity product (IAP), which may be induced by microbial activity (e.g., photosynthesis, sulphate reduction) and/or external physicochemical factors (e.g., evaporation, CO_2 -degassing). Lamination of microbialite deposits may result from a number of factors, including, seasonally induced changes to calcification process induced by changes in biofilm composition and calcium carbonate mineral supersaturation. Some calcifying biofilms exhibit fabrics containing cyanobacterial CaCO_3 tubes, such as *Girvanella* or *Cayeuxia*, that can be preserved as microfossils. These cyanobacterial tubes have been attributed to photosynthesis-induced pH microgradients under conditions of low DIC and consequently low, bulk-phase, pH buffering (Arp et al., 2001). Specifically, the impact of a given amount of C removal on changes in CaCO_3 supersaturation should, theoretically, increase with decreasing DIC concentration and initial pH. Other factors that have been discussed in this context are temperature and CaCO_3 mineral supersaturation (Kempe and Kazmierczak, 1990; Riding, 1992).

Despite the importance of understanding these processes to paleoenvironmental interpretations, experimental studies on calcification in cyanobacterial communities are rare (e.g., Merz, 1992; Dittrich et al., 2003), and the specific relationship between various environmental factors, such as temperature and pH conditions, on photosynthesis-induced calcification of cyanobacterial biofilms have not, thus far, been investigated. Temperature changes may alter the rate of abiotic degassing and the rate of biological processes, and hence precipitation. Changes to bulk water pH will alter the bulk water CaCO_3 saturation state, but may not have such a great affect at the stromatolite surface, if biological processes are maintained. In this study, the results of ex situ microelectrode experimental studies, using cyanobacterial biofilms from karst-water creeks, are presented and discussed with respect to possible implications for interpretation paleonevironmental conditions.

Methods

Samples and sample collection

Samples were collected from the Deinschwanger Bach, as described in Bissett et al. (2008). The Deinschwanger Bach lies near Nürnberg (49°23'N, 11°28'E), in southern Germany and has been used for previous studies on cyanobacterial biofilm calcification. It is described in more detail in Arp et al. (2001) and shows active laminar stromatolite formation up to 1.8 mm/year.

Samples were collected from two distinct sites for pH manipulation experiments. Site 1

comprised a small stromatolite cascade 65 m downstream of a side spring. At this site the creek was approximately 1–5 cm deep and exhibited a fast flow rate (approx. 40 cm s⁻¹). Stromatolite at Site 1 was laminated and several cm thick. Site 2 was a well illuminated section of the lower creek, approx 20 cm deep, and had a lower flow rate (approx. 10 cm s⁻¹) than Site 1. Site 2 exhibited thin (up to 1 mm), fragile carbonate crusts. Samples from Site 2 only were used for temperature manipulation experiments. Samples were removed from the creek with a motorized core-drilling device (modified Stihl chainsaw) and stored in ambient creek water in coolers until return to the laboratory, within 24 hours. Creek water for the experiments was collected without air bubbles in 20 l plastic containers and stored at 4°C in the dark until use.

Laboratory setup

Once in the laboratory, samples were stored in temperature controlled, aerated, recirculating aquariums (total volume approx. 30 L) containing creek water. Samples were removed to flow cells connected to the same recirculating water supply for ambient and temperature manipulated measurements, and to a separate reservoir of creek water for pH manipulated experiments. pH was manipulated by the addition of CO₂, in bottled “mineral water”, to lower pH, or by aerating the reservoir with CO₂ free air (air scrubbed in NaOH), to raise it. During pH adjustments, pH was monitored continuously with a MA130 ion detector (Mettler Toledo, Columbus, Ohio, USA) and CO₂ addition or removal rates adjusted to maintain the desired pH.

Microelectrode measurements comprised three sets of measurements. The first were measurements of O₂, pH and Ca²⁺ concentration profiles on samples held at ambient creek conditions (temp. 10°C, pH 8.4). The second comprised measurements of concentration gradients of the same ions on the same samples under conditions of elevated (8.9) and lowered (7.8) pH. The final set of measurements (the same ions as above) involved temperature manipulations on samples from the Deinschwanger Bach, collected 12 months later. In this set of measurements temperature was raised from the ambient 10°C to 17°C and lowered to 4°C.

Microelectrode measurements and calculations

Liquid membrane Ca²⁺ and pH sensors were prepared and calibrated as described previously (de Beer et al., 2000; de Beer et al., 1997). Fast responding O₂ microsensors were also prepared as described previously (Revsbech, 1989). All electrodes were placed at the stromatolite surface, manually, while viewing the sample through a dissection microscope. The stromatolite surface was then set at 0, and all measurements made above the surface.

Negative distances indicate that the sensor is above the stromatolite/water interface. Profiling was automated after electrodes were positioned at the stromatolite surface. Sensors were connected to a micromanipulator, which was fixed to a motorized stage (VT-150, Micos, Eschbach, Germany) and allowed reproducible positioning of the sensor tip with 1 μm precision. The microelectrodes were connected to a picoammeter (O_2 electrode) or a millivoltmeter, and the meter output was collected by a data acquisition device (NIDaq 6015, national Instruments, Austin, Texas, USA). After positioning at the surface, profiling was performed automatically. Motor control and data acquisition were performed with a computer and custom written software (μ -Profiler, Dr. L. Polerecky). All profiles were corrected for offset to ion levels in the bulk liquid: oxygen concentrations in the bulk liquid were determined from literature values at experimental temperatures (salinity = 0 ppt), pH as described above, Ca^{2+} by ICP-OES (Perkin Elmer Optima 3300 DV) and DIC by CO_2 Coulometer (UIC Coulometrics, Joliet, USA).

Interfacial fluxes (J) were calculated from the concentration profiles using Fick's first law:

$$J = D \times (dc/dx) \quad (4.1)$$

where D is the diffusion coefficient and dc/dx is the interfacial concentration gradient, i.e., the concentration gradient in the mass boundary layer directly adjacent to the stromatolite surface.

Calcite saturation is given by the saturation state omega (Ω),

$$\Omega = \{ \text{Ca}^{2+} \} \times \{ \text{CO}_3^{2-} \} / K_{(\text{Calcite})} \quad (4.2)$$

where the numerator is the IAP and the denominator the solubility product. $K_{(\text{Calcite})}$ is given by Plummer and Busenberg (1982). Carbonate concentrations were determined from bulk water DIC and pH microprofiles. For the calculation of $\Omega_{(\text{Calcite})}$, activities were estimated by applying the activity coefficients of experimental water delivered from PHREEQC (0.686 for Ca^{2+} and CO_3^{2-}).

Diffusion coefficients

The diffusion coefficients of O_2 and Ca^{2+} are literature derived values corrected for temperature and type of counter ion (Li and Gregory, 1974; Broecker and Peng, 1974). Diffusion coefficients of oxygen are, 4°C: $1.28 \times 10^{-9} \text{ m}^2 \text{ s}^{-1}$; 10°C: $1.57 \times 10^{-9} \text{ m}^2 \text{ s}^{-1}$ and 17°C $1.934 \times 10^{-9} \text{ m}^2 \text{ s}^{-1}$. Diffusion coefficients for Ca^{2+} with HCO_3^- as counter ion are 4 °C: $0.546 \times 10^{-9} \text{ m}^2 \text{ s}^{-1}$; 10°C: $0.67 \times 10^{-9} \text{ m}^2 \text{ s}^{-1}$ and 17°C: $0.827 \times 10^{-9} \text{ m}^2 \text{ s}^{-1}$.

Results

pH Manipulations

Concentration profiles of O₂, pH, and Ca²⁺ were successfully measured on all samples (Fig. 1) at experimentally manipulated pH's. It should be noted that slight discrepancies in the observed height of the diffusive boundary layer (DBL) and bulk water concentrations of chemical species measured are evident in the results presented. The profiles presented are averages of two positions on each sample and these variations indicate both the heterogeneity within the samples and also the difficulty in aligning the various sensors to exactly the same position on each sample. The profiles do, however, show a strong, consistent pattern.

In all samples photosynthesis increased O₂ concentration at the stromatolite surface in light incubations, causing a concomitant increase in pH and a decrease in Ca²⁺ ion concentration. In dark incubations, respiration resulted in a decrease in O₂ concentration and often a small decrease in pH and increase in Ca²⁺ concentration. In the high (8.9) pH treatment, however, a decrease in calcium ion concentration was seen in both light and dark incubations.

Flux rates of O₂ and Ca²⁺ and pH changes (Δ pH) achieved are presented in Table 1. In all treatments pH's approached the same values in both light and dark incubations, although there were some small differences, largely between sites.

At both sites pH increased towards the biofilm surface under illumination, with larger Δ pH values in the low pH treatment (7.8) than in the high pH treatment (8.9). Only the high pH (8.9) treatment at Site 2 showed a moderately high Δ pH value, deviating from this general trend. In the dark, a decrease in pH towards the biofilm surface was observed for both sites, with increasing Δ pH values from the low pH (7.8) to the high pH treatment (8.9). The highest fluxes of O₂ from the biofilm were seen in the samples at ambient pH (8.4) at both sites, as were the highest O₂ fluxes to the biofilm surface during dark incubations.

The flux of Ca²⁺ was somewhat more complicated. Calcium flux was always towards the biofilm surface in light conditions, but the magnitude of the fluxes varied between the treatments. At Site 1 the flux was highest in the high pH treatment and lowest in the low pH treatment. The converse was true at Site 2. The actual fluxes, though, were reasonably similar. Dark fluxes were much lower than those seen in the light, and except in the high (8.9) pH treatment, were all away from the biofilm surface. The flux towards the biofilm surface at Site 2 was, however, very small. The data clearly show a biologically controlled, diurnal pattern to calcium precipitation.

Effects of pH and temperature on biofilm calcification

Site 1				
Experimental pH	7.8	8.4	8.9	
Initial pH actually achieved	7.8	8.4	8.9	
O ₂ flux light (mol m ⁻² s ⁻¹)	1.7×10 ⁻⁶ ±7.1×10 ⁻⁸	4.4×10 ⁻⁶ ±1.4×10 ⁻⁶	1.1×10 ⁻⁶	
O ₂ flux dark (mol m ⁻² s ⁻¹)	-2.4×10 ⁻⁷ ±2.3×10 ⁻⁹	-3.8×10 ⁻⁷ ±1.4×10 ⁻⁷	-1.4×10 ⁻⁷	
Ca ²⁺ flux light (mol m ⁻² s ⁻¹)	-1.2×10 ⁻⁶	-1.3×10 ⁻⁶	-1.4×10 ⁻⁶	
Ca ²⁺ flux dark (mol m ⁻² s ⁻¹)	0	1.2×10 ⁻⁷	-5.1×10 ⁻⁷	
Δ pH light	+0.86	+0.54	+0.07	
Δ pH dark	-0.04	-0.36	-0.66	

Site 2				
Initial pH actually achieved	7.6	8.4	8.9	
O ₂ flux light (mol m ⁻² s ⁻¹)	8.0×10 ⁻⁷	1.6×10 ⁻⁶	6.4×10 ⁻⁷	
O ₂ flux dark (mol m ⁻² s ⁻¹)	-1.5×10 ⁻⁷	-4.3×10 ⁻⁷	-2.4×10 ⁻⁷	
Ca ²⁺ flux light (mol m ⁻² s ⁻¹)	-1.1×10 ⁻⁶	-8.9×10 ⁻⁷	-7.9×10 ⁻⁷	
Ca ²⁺ flux dark (mol m ⁻² s ⁻¹)	3.3×10 ⁻⁷	0	-1.7×10 ⁻⁹	
Δ pH light	+1.75	+0.62	+0.67	
Δ pH dark	+0.20	-0.48	-0.85	

Table 1 Fluxes of oxygen and calcium and pH changes at biofilm surfaces measured in samples from the Deinschwanger Bach. For fluxes, positive values indicate flux from the biofilm to the water column, negative

Calcite saturation state microprofiles (Fig. 2), calculated from bulk water DIC, pH and Ca²⁺ microprofiles, demonstrate the degree to which Ω_{Calcite} is controlled by the carbonate system. Ω_{Calcite} profiles mirrored pH profiles and indicated that the waters were supersaturated with respect to calcite under all experimental conditions.

At both sites illumination caused a photosynthetically induced increase in Ω_{Calcite} . In turn, a clear decrease in Ω_{Calcite} is evident at both sites without illumination. The high pH (8.9) treatment for Site 1 showed no significant Ω_{Calcite} change under illumination, but a strong decrease in the dark. For Site 2, a similar decrease of Ω_{Calcite} under dark conditions was calculated, while under illuminated conditions the rise in Ω_{Calcite} reflects the pH increase.

Temperature Manipulations

The second experiment comprised manipulations of temperature, in order to investigate its affects on calcification processes. In light of the heterogeneity in each sample indicated by

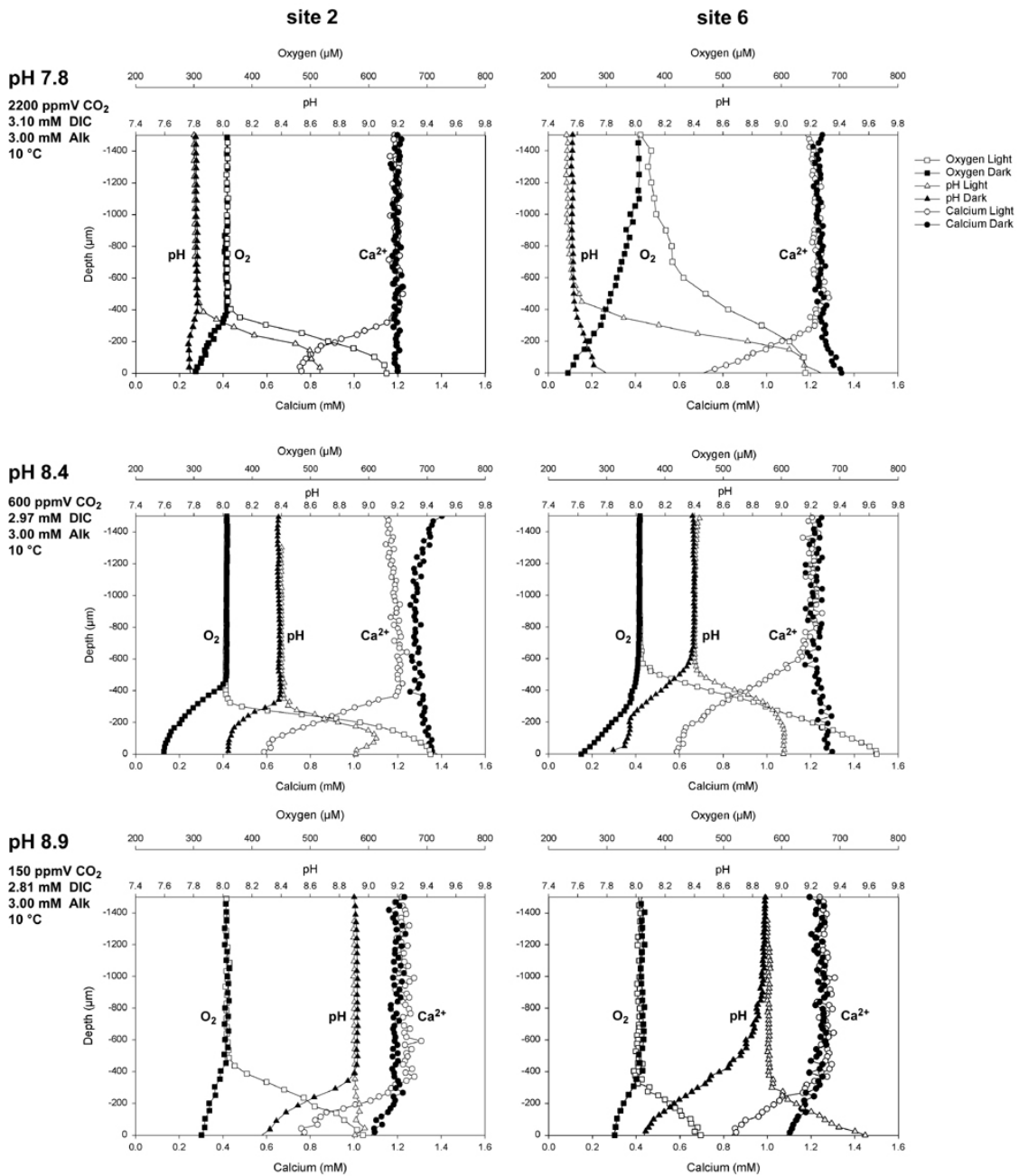


Fig. 1 pH, O₂ and Ca²⁺ profiles in the light and dark at three experimental pH's

the pH experiment concentration profiles in the temperature experiments were performed at the same place on each sample, and only samples from Site 2 were considered. Temperatures tested were 4°C, 10°C (ambient) and 17°C. Measured profiles are presented in Fig. 3.

In all treatments pH's approached the same values in both light and dark incubations, although there were some small differences (Table 2). pH's increased markedly under light

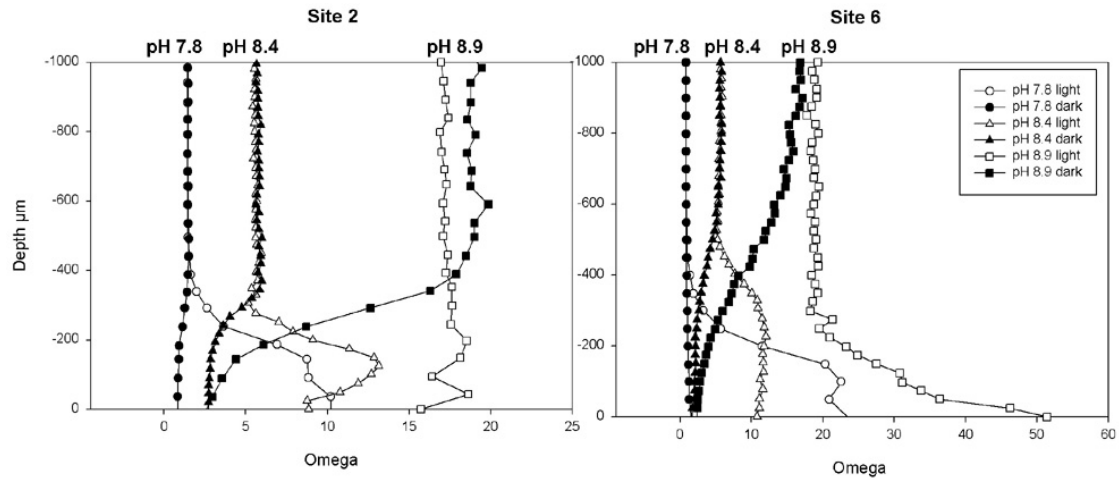


Fig. 2 Omega values at each experimental pH.

conditions from 8.4 to approximately 9.5 (maximum 9.7). Under dark conditions, the pH decreased slightly from 8.4 to approximately 8.1 at 10°C and 17°C, while no pH decrease was observed at 4°C.

Oxygen fluxes both away from and toward the sediment increased with temperature in the light and dark respectively. Calcium flux was always towards the stromatolite biofilm surface in light conditions, and increased with increasing temperature. Dark fluxes were much lower than those seen in the light conditions, were always away from the stromatolite biofilm surface and also increased with increasing temperature. Under dark conditions no calcium flux was observed from or to the stromatolite biofilm surface at 4°C.

Discussion

The investigated biofilm community, rich in filamentous cyanobacteria, flourishes in its natural setting (hardwater creeks) under a wide range of pH and temperature conditions:

Table 2 Fluxes of oxygen and calcium and pH changes at biofilm surfaces measured in samples from Deinschwanger Bach at different temperatures. NA indicates no profile obtained.

Experimental Temp.	4°C	10°C	17°C
O ₂ flux light (mol m ⁻² s ⁻¹)	2.8×10 ⁻⁶	3.0×10 ⁻⁶	1.0×10 ⁻⁵
O ₂ flux dark (mol m ⁻² s ⁻¹)	3.7×10 ⁻⁷	NA	1.0×10 ⁻⁶
Ca ²⁺ flux light (mol m ⁻² s ⁻¹)	2.0×10 ⁻⁶	3.5×10 ⁻⁶	4.1×10 ⁻⁶
Ca ²⁺ flux dark (mol m ⁻² s ⁻¹)	0	2.0×10 ⁻⁷	2.9×10 ⁻⁷
Δ pH light	1.3	1.0	1.3
Δ pH dark	0.0	-0.3	-0.3

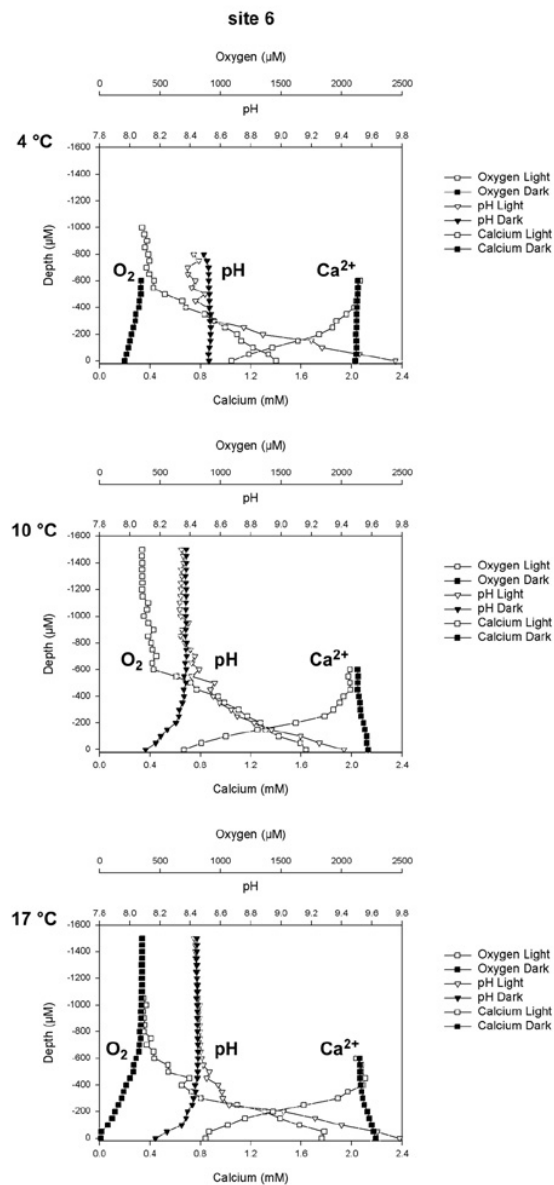


Fig. 3 pH, O₂ and Ca²⁺ at each experimental temperature

The pH ranges from 7.6 (a short distance downstream of the spring) to 8.5 (lower creek sections and end of the carbonate deposition zone), with maximum values up to 9.3 within the biofilm microenvironment (Bissett et al., 2008). The cyanobacterial community composition is reasonably constant over this zone, with only the immediate spring environment (pH 7.3–7.4) exhibiting distinct communities. In situ temperatures vary seasonally between 5°C and 13°C.

Experimental manipulations of pH and temperature were conducted at conditions of constant alkalinity (3.0 mM), but slightly varying DIC (2.8 to 3.1 mM); pH was manipulated

by the addition of CO₂. pH and temperature manipulations will be considered separately.

pH experiments

Under illumination Δ pH was always positive, but its magnitude decreased with decreasing pCO₂ (2200 to 150 ppm V), despite the observation of similar O₂ production rates. In the dark the opposite was seen. That is, Δ pH was always negative and increased with decreasing pCO₂ (2200 to 150 ppm V), again despite the observation of similar O₂ consumption rates. Under both light and dark conditions the maximum O₂ fluxes were observed at bulk water pH 8.4. The direction of Δ pH changes was as expected, i.e. light induced photosynthesis increased pH, while in the dark respiration lead to its decrease. The different magnitude of Δ pH, however, has several possible explanations.

The first is that the observed Δ pH was related to the physiological optima of the mat community. If this were the case it would be expected that the highest Δ pH should correlate with the highest O₂ fluxes. This was not the case. O₂ fluxes at all pH treatments were reasonably similar, with the maximum actually occurring at the in situ pH of 8.4.

The second explanation for the Δ pH values observed is the possibility of different pH buffering at the various initial pH's. Under this model the highest Δ pH's should correlate with the lowest buffering at pHa = 6.34 and pKb = 10.36. This, however is not the case. In fact + Δ pH and - Δ pH show opposite trends for increasing pH (Fig. 1) and, further, within the experimental pH range (7.8–8.9), which is near the half equivalence point of 8.1, changes in pH buffering are very minor.

The final, and most likely, possible explanation for the observed results is the induced changes to the pCO₂ gradient between the bulk phase and the microorganisms. In the low pH (high pCO₂) treatment the assimilation of CO₂ during photosynthesis is facilitated, thus a greater Δ pH is observed in the light, but the dissipation of CO₂ under reparative conditions is hampered, thus lowering Δ pH in the dark. The opposite is observed in the high pH (low pCO₂) treatment, less CO₂ is available for assimilation, reducing Δ pH in the light, but its dissipation is easier, increasing Δ pH in the dark. Although we did not assess other biogeochemical processes in the present study, the non-linearity of the results (e.g., the exceptional increase in pH seen at site 2 under the high pH treatment) may be possibly explained by their contribution (e.g., nitrate/ammonia assimilation; Soetaert et al., 2007).

Temperature experiments

Temperature manipulations were all conducted at pH 8.4 and temperature 10°C in situ conditions at the time of sampling. Temperature was clearly shown to affect biological activity, with O₂ fluxes increasing with increasing temperature, both in the light and in the

dark. Ca^{2+} fluxes (indicating calcium carbonate precipitation and dissolution) also increased with increasing temperature, indicating the control of photosynthesis and respiration over calcification in this system (Table 2; Fig. 3). The pH changes at the experimental temperatures are a little more difficult to interpret. In the dark a larger decrease in pH was seen at higher temperature: consistent with the idea that increasing temperature leads to increases biological activity (within the experimental temperature range). In the light, however, the pH at all temperatures increased to approximately the same value in all treatments (9.5), despite higher photosynthetic rates at higher temperatures. We have observed this upper pH value of approx. 9.5 in stromatolite biofilms from this creek and from the Westerhöfer Bach (Bissett et al., 2008) many times before (data not shown), and the value seems to be some upper limit for these systems. The explanation for this upper limit may be a buffering effect from the calcification process, allowing the pH to reach a steady state despite varying photosynthetic rates. Despite this apparent pH “ceiling” it is evident that temperature affects biological activity, which in turn controls calcification in the system under investigation.

It is evident, then, that both temperature and pH affect calcification processes. Temperature alters biological activity, which in turn affects rates of calcite deposition and dissolution in systems where calcification is biologically controlled. The net effect of temperature changes, however, may be small. Although temperature increase leads to an increase in photosynthesis and an increase in calcification the concomitant increase in dark respiration rates also increases dissolution, thereby maintaining similar net diel precipitation rates. The abundance of cyanobacterial microfossils and related stromatolites in Earth History, therefore, appears not to be significantly affected by temperature variations within the investigated range (4°C to 17°C), but may be visible at higher temperatures (20–35°C; Riding 1992; Wallmann 2001; Fig. 8). Indeed, a rough correlation between cyanobacterial calcification episodes and paleotemperature curves from oxygen isotopes has been recognized by Riding (1992). Although the initially proposed absolute temperatures, with values to more than 60°C, for the early Paleozoic (Karhu and Epstein, 1986) reflect a long-term decrease of seawater $\delta^{18}\text{O}$ (Veizer et al., 1997), the superimposed fluctuations are still considered to reflect seawater temperature changes (Wallmann, 2001).

pH changes also lead to interesting implications for the paleogeological interpretation of calcification. It appears that under high pCO_2 conditions cyanobacterial calcification may be facilitated by high CO_2 availability and pH 7–8. Therefore, as long as calcite saturation remains > 1 , the presence of calcareous, tubular, microfossils may be related to low pH conditions (7.8–8.4). This is contradictory to ideas that increasing pCO_2 should reduce the potential of photosynthesis-induced calcification in cyanobacterial biofilms by lowering bulk

phase pH and hence CaCO₃ mineral supersaturation (Kempe and Kazmierczak, 1990; Riding and Liang, 2005).

Conclusions

Bulk water temperature and pH both affect calcification processes in stromatolite formation. Temperature changes induce changes to metabolic processes which govern precipitation, but since temperature changes affect both precipitation and dissolution processes, the net effect of temperature changes may not be pronounced.

pCO₂ induced pH changes affect calcification by altering the ease with which CO₂ can be consumed and dissipated: Within the experimental pH range (7.8–8.9), cyanobacterial calcification was facilitated under illumination: at low pH conditions, probably because of a higher pCO₂ gradient from outside to into the cell, thereby facilitating CO₂ assimilation and photosynthesis. Thus, calcification occurs at, and may even be facilitated by, low pH, high pCO₂ conditions. In turn, high pH conditions of 8.9 and, hence, low pCO₂ gradients, reduce light-driven cyanobacterial CO₂ assimilation and calcification, while a photosynthesis-independent, minor Ca²⁺ loss occurs under dark conditions.

Acknowledgements

We thank the microsensor technicians at the MPI, Bremen, for assistance with microsensor construction, and Lubos Polerecky for the microprofiling software. We thank Prof. Hakhyun Nam (Kwangwoon University, Korea) for supplying the carbonate ionophore. This project is part of the Research Unit "Geobiology of organo- and biofilms", funded by the German Research Foundation (DFG–FOR 571, publication # 23).

References

- Arp G, Reimer A, Reitner J. 2001. Photosynthesis-induced biofilm calcification and calcium concentrations in Phanerozoic oceans. *Science* 292:1701–1704.
- Arp G, Wedemeyer N, Reitner J. 2001b. Fluvial tufa formation in a hard-water creek (Deinschwanger Bach, Franconian Alb, Germany). *Facies* 44:1–22.
- Awramik, S.M., 1971. Precambrian columnar stromatolite diversity: reflection of metazoan appearance. *Science* 174, 82–827.
- Bissett, A., de Beer, D., Schoon, R., Shiraishi, F., Reimer, A., Arp, G., 2008. Microbial mediation of stromatolite formation in karst-water creeks. *Limnol. Oceanogr.* in press.

- Broecker WS, Peng TH. 1974. Gas exchange rates between air and sea. *Tellus* 26:21–35.
- Burne RV, Moore LS. 1987. Microbialites: organosedimentary deposits of benthic microbial communities. *Palaios* 2:241–254.
- de Beer, D., Schramm, A., Santegoeds, C.M., Kühl, M., 1997. A nitrite microsensor for profiling environmental biofilms. *Appl. Environ. Microbiol.* 63, 973–977.
- de Beer D, Kühl M, Stambler N, Vaki L. 2000. A microsensor study of light enhanced Ca^{2+} uptake and photosynthesis in the reef-building hermatypic coral *Favia* sp. *Mar Ecol Prog Ser* 194:75–85.
- Dittrich, M., Mueller, B., Mavrocordatos, D., Wehrli, B., 2003. Induced calcite precipitation by cyanobacterium *synechococcus*. *Acta Hydrochim. Hydrobiol.* 31, 162–169.
- Grotzinger, J.P., Kasting, J.F., 1993. New constraints on Precambrian ocean composition. *J. Geol.* 101, 235–243.
- Karhu, J. Epstein, S., 1986. The implication of the oxygen isotope records in coexisting cherts and phosphates. *Geochim. Cosmochim. Acta*, 50, 1745–1756.
- Kempe S, Kazmierczak J. 1990. Calcium carbonate supersaturation and the formation of in situ calcified stromatolites. In: Ittekkot VA, Kempe S, Michaelis W, Spitzy A. editors. *Facets of Modern Biogeochemistry*. Berlin-Heidelberg: Springer-Verlag, p 255–278.
- Li YH, Gregory S. 1974. Diffusion of ions in sea water and in deep-sea sediments. *Geochim Cosmochim Acta* 38:703–714.
- Merz MUE. 1992. The biology of carbonate precipitation by cyanobacteria. *Facies* 26:81–102.
- Plummer LN, Busenberg E. 1982. The solubilities of calcite, aragonite and vaterite in CO_2 - H_2O solutions between 0 and 90°C, and an evolution of aqueous model for the system CaCO_3 - CO_2 - H_2O . *Geochim Cosmochim Acta* 46:1011–1040.
- Revsbech NP. 1989. An oxygen microsensor with a guard cathode. *Limnol Oceanogr* 34:474–478.
- Riding, R., 1991. Calcified cyanobacteria. In: Riding, R. (Ed.), *Calcareous algae and stromatolites*. 55–87.
- Riding, R., 1992. Temporal variation in calcification in marine cyanobacteria. *J. Geol. Soc. London* 149, 979–989.
- Riding, R., 1999. The term stromatolite: towards an essential definition. *Lethaia* 32, 321–330.
- Riding R, Liang L. 2005. Geobiology of microbial carbonates: metazoan and seawater saturation state influences on secular trends during the Phanerozoic. *Palaeogeogr Palaeoclimatol Palaeoecol* 219:101–115.
- Soetaert, K., Hofmann, A.F., Middelburg, J.J., Meysman, F.J.R., Greenwood, J., 2007. The effect of biogeochemical processes on pH. *Marine Chemistry* 105, 30–51.
- Veizer, J., Buhl, D., Diener, A., Ebner, S., Podlaha, O.G., Bruckschen, P., Jasper, T., Korte, C., Schaaf, M., Ala, D. and Azmy, K., 1997. Strontium isotope stratigraphy: potential resolution and event correlation. *Paleogeogr., Paleoclimatol., Paleoecol.* 132, 65–77.
- Wallmann, K., 2001. Controls on the cretaceous and cenozoic evolution of seawater composition, atmospheric CO_2 and climate. *Geochim. Cosmochim. Acta* 65, 3005–3025.
- Walter, M.R., Heys, G.R., 1985. Links between the rise of the Metazoa and the decline of Stromatolites. *Precambrian Res.* 29, 149–174.

Chapter 5

Microbial effects on biofilm calcification, ambient water chemistry and stable isotope records in a highly supersaturated setting (Westerhöfer Bach, Germany)

Microbial effects on biofilm calcification, ambient water chemistry and stable isotope records in a highly supersaturated setting (Westerhöfer Bach, Germany)

Fumito Shiraishi, Andreas Reimer, Andrew Bissett, Dirk de Beer, Gernot Arp

Abstract

Cyanobacteria-dominated biofilms in a CO₂-degassing karst-water creek (Westerhöfer Bach, Germany) were investigated with regard to the effects of microbial activity on CaCO₃ precipitation, water chemistry of micro- and macroenvironment, stable isotopic records, and tufa fabric formation. *Ex situ* microelectrode measurements of pH, O₂, Ca²⁺ and CO₃²⁻ revealed that annually laminated calcified biofilms composed mainly of filamentous cyanobacteria (tufa stromatolites) strongly induced CaCO₃ precipitation by photosynthesis under illumination, but inhibited precipitation by respiration in the dark. In contrast, endolithic cyanobacterial biofilms and mosses did not cause photosynthesis-induced precipitation under experimental conditions. No spontaneous precipitation occurred on bare limestone substrates, despite high calcite supersaturation of the ambient water. Mass balance calculations suggest that biofilm photosynthesis was responsible for 10-20% of Ca²⁺ loss in the creek, while remaining Ca²⁺ loss derived from physicochemical precipitation on branches, leaves and fine-grained calcite particles. Neither analysis of bulk water chemistry nor oxygen and carbon stable isotopic records of the tufa stromatolites did confirm photosynthetic effects, despite the evident photosynthesis-induced calcite precipitation. Oxygen stable isotopic values reflected the seasonal change in water temperature and carbon stable isotope values probably recorded carbon isotopic composition of dissolved inorganic carbon in the creek water. Annual lamination and fabric formation of the tufa stromatolites is suggested to vary with photosynthesis-induced calcite precipitation rates that are affected by temperature dependency of diffusion coefficients. Photosynthesis-induced precipitation resulted in encrusted cyanobacterial sheaths, reflecting syntaxial overgrowth of microcrystalline cyanobacterial tubes by microspar, instead of microcrystalline sheath impregnation, that was previously suggested as an indicator of photosynthesis-induced precipitation. Therefore, sheath impregnation or encrustation by CaCO₃ cannot be used to distinguish photosynthesis-induced from physicochemically-induced CaCO₃ precipitation.

1. Introduction

Freshwater carbonates of karst-water creeks and lakes, commonly called "tufa" (Ford and Pedley, 1996), provide an important high-resolution archive of the Quaternary palaeoclimate (e.g., Andrews and Brasier, 2005; Andrews, 2006). Particularly, annually laminated porous tufa deposits (tufa stromatolites; Riding, 2000) in karst creeks provide accurate information on seasonal changes of water temperature, hydrochemistry, and rainfall events (e.g., Matsuoka et al., 2001; Ihlenfeld et al., 2003; Kano et al., 2004, 2007). In addition, tufa stromatolites are considered potential analogues of ancient marine stromatolites (Shiraishi et al., in press; Bissett et al., in press) because they resemble many fossil marine stromatolites mainly formed by *in situ* precipitation, contrary to present-day marine stromatolites mainly forming by particle agglutination (e.g., Awramik, 1984). Therefore, tufa stromatolites also provide essential information on the mechanisms of microbial calcification, which may help to understand the palaeoenvironment and palaeoecology of the Phanerozoic and Precambrian earth (e.g., Riding, 1982, 2006; Grotzinger and Knoll, 1999; Arp et al., 2001a).

The depositional process of tufa is still a matter of controversy because physicochemical CO₂-degassing and photosynthesis, can both shift the carbonate equilibrium to cause calcite precipitation, occur simultaneously in tufa-forming creeks. Although it has been assumed for decades that both organic and inorganic mechanisms are involved in tufa precipitation (e.g., Golubic, 1973; Ford and Pedley, 1996), it has been difficult to evaluate the exact role of microorganisms because of technical limitations. Previous studies based on bulk water chemistry analysis demonstrated that calcite supersaturation of creek water is primarily attained by physicochemical CO₂-degassing (e.g., Jacobson and Usdowski, 1975), and microbial effect is negligible on tufa formation. In addition, it is thought that a significant effect of photosynthesis should result in diurnal cycles of pCO₂, pH, δ¹³C and calcite saturation state, but such diurnal cycles were rarely detected (e.g., Usdowski et al., 1979; Dandurand et al., 1982; Merz-Preiß and Riding, 1999). Moreover, there has been no clear signal of photosynthesis detected in carbon stable isotopic records of tufa stromatolites (e.g., Matsuoka et al., 2001). Therefore, many researchers are nowadays convinced that inorganic precipitation is the major process in fluvial tufa deposition, whereas microbial effects are thought to be restricted to low pCO₂ and/or slow flowing settings such as stagnant pools and lakes (e.g., Andrews et al., 1997; Merz-Preiß and Riding, 1999; Pedley, 2000; Arp et al., 2001b; Chen et al., 2004).

However, studies based on microelectrode measurements recently revealed that

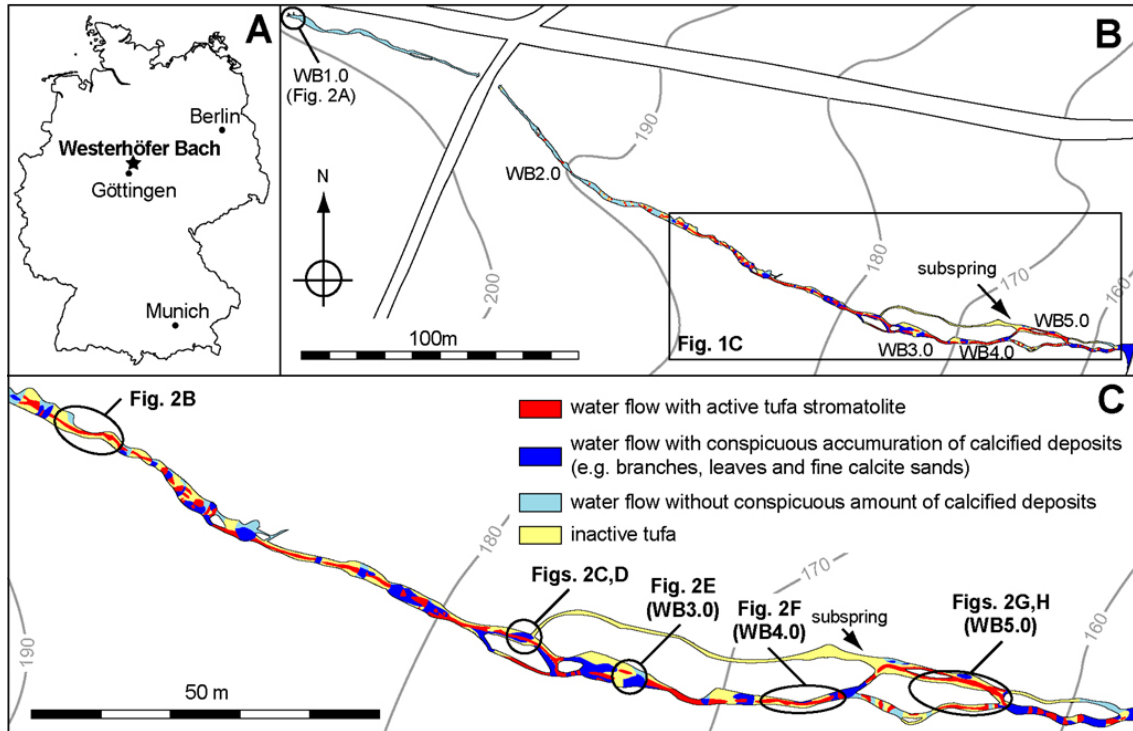


Fig. 1 (A) Location of the Westerhöfer Bach. (B) Map of the Westerhöfer Bach. (C) Detail of (B) showing the distribution of active tufa stromatolites, inactive tufa, calcified deposits, and areas without conspicuous amounts of calcified particles in the middle and lower creek section.

photosynthesis induces CaCO_3 precipitation on the surface of tufa stromatolites under illumination, whereas respiration inhibits precipitation in the dark, even in a highly supersaturated fast-flowing environment (Shiraishi et al., in press; Bissett et al., in press).

The aim of this work was to resolve these discrepancies and elucidate the process of tufa deposition by quantifying the effects of photosynthesis. Firstly, we evaluated the metabolic effects of several types of tufa biofilms by geomicrobiological methods including pH, O_2 , Ca^{2+} and CO_3^{2-} microelectrodes and the detection of heterotrophic bacteria and EPS (extracellular polymeric substances) that potentially affect biofilm calcification. Secondly, analysis of bulk water chemistry including 21 h monitoring and stable isotope analysis of water and tufa deposits was conducted to evaluate the microbial metabolic effects on the bulk water chemistry and deposits.

2. Study area and environmental settings

The investigated tufa-forming karst-water creek, the Westerhöfer Bach, is located west of the Harz Mountains, Central Germany ($51^\circ 45' \text{N}$, $10^\circ 5' \text{E}$; Fig. 1A). The creek water recharges from the limestone-dominated upper Muschelkalk Group (Anisian-Ladinian), which is

underlain by the middle Muschelkalk Group (Anisian) that is composed of dolomite with gypsum lenses (Jacobson and Usdowski, 1975). The initial 330 m section of the creek, where active tufa formation occurs, was selected for this study. Here, the width of the creek is 1-2 m and water flows ESE (Fig. 1B). There is one main spring, and lateral seepage influx is negligible except for one recognizable subspring that enters the creek 288 m downstream from the main spring. At the spring site, water flows gently over limestone gravels colonized by non-calcifying biofilms (Fig. 2A), mainly composed of endolithic cyanobacteria. Continuous tufa deposition starts approximately 150 m downstream from the spring where water flow becomes turbulent (Figs. 1B, C, 2B). Tufa stromatolites usually develop in the center of the flow path. Their biofilm communities are mainly composed of filamentous cyanobacteria accompanied by diatoms, green algae and a number of heterotrophic bacteria (Shiraishi et al., in press). At both sides of the main flow path and in stagnant pools of the middle and lower creek section, conspicuous amounts of calcified particles and fragments, such as branches, leaves, and fine-grained calcite sands accumulate, and sometimes oncoids are recognized (Figs. 2C, D). Mosses mostly colonize the low flowing middle to lower creek and inactive tufa deposits, although some occur in the fast flowing reaches. In the lower section, the creek branches off and rejoins at several places. A tufa cascade about 2 m in height develops at 250 m downstream (Fig. 2E). After this cascade, water flows through a narrow channel (Fig. 2F) and then over widely developing tufa stromatolites in the lowermost part of the creek (Figs. 2G, H). Typically, tufa stromatolites exhibit green colour during summer (Fig. 2G), while brownish biofilms develop in the marginal part of the flow path during autumn (Fig. 2H).

Five sampling sites (WB1.0-WB5.0; Fig. 1B) were chosen for main investigations, and some complementary sites along the creek were also included for hydrochemical analysis. The difference in altitude from the spring site (WB1.0) to the site 300 m downstream (WB5.0) is approximately 40 m. Previous investigations of the creek have been performed by Jacobson and Usdowski (1975), Usdowski et al. (1979), and Dreybrodt et al. (1992) with regard to hydrochemistry, oxygen and carbon stable isotopes, and by Shiraishi et al. (in press) and Bissett et al. (in press) with regard to microbial metabolic effects on tufa deposition.

3. Methods

3.1. Microelectrode measurements, biofilm sectioning and staining

Microelectrode measurements of pH, O₂, Ca²⁺ and CO₃²⁻ were conducted in the laboratory to evaluate the microbiological effects at the tufa surface, the site of calcite precipitation. In

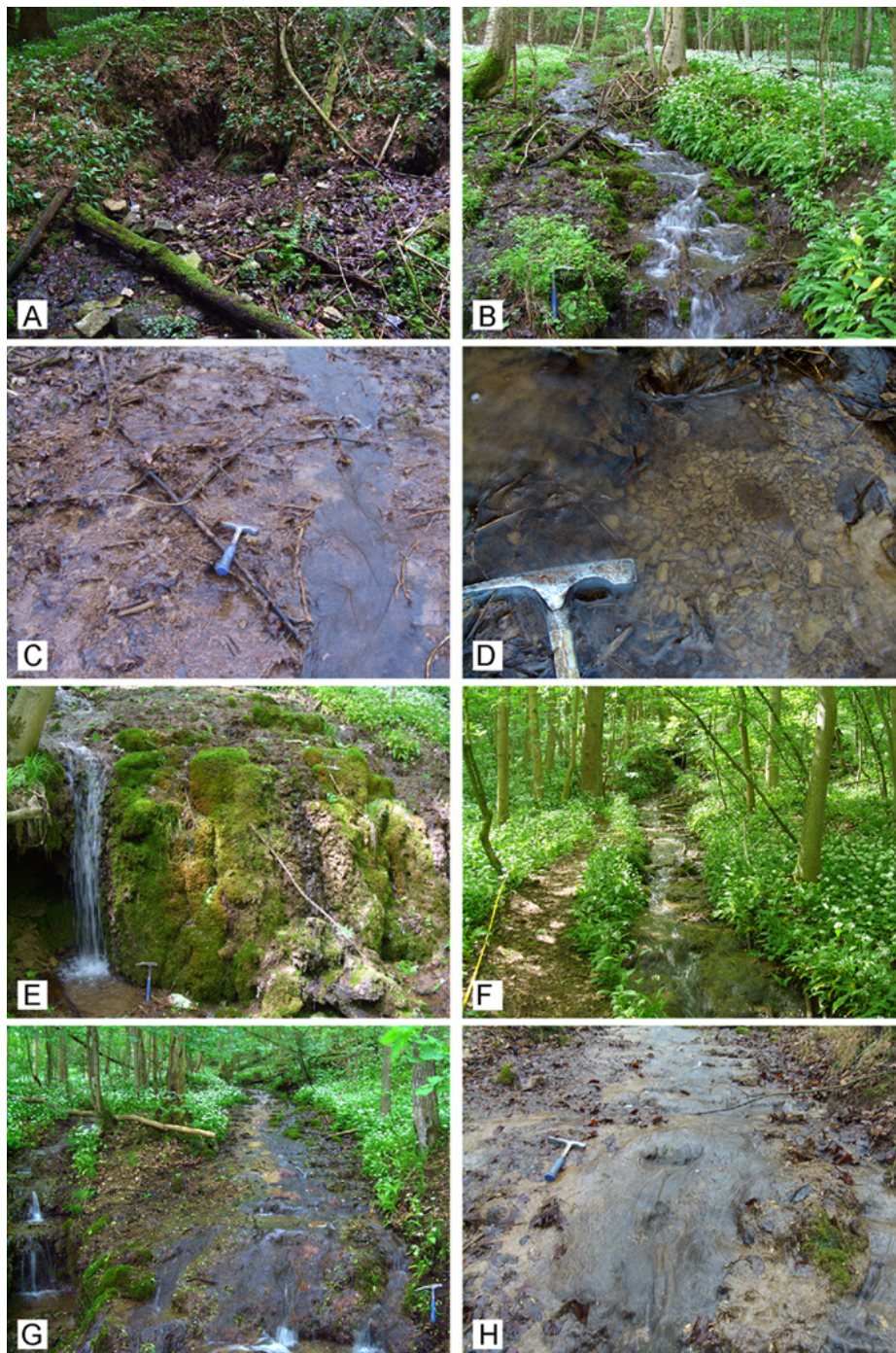


Fig. 2 Field views of the Westerhöfer Bach. (A) Spring site (WB1.0) with water seeping over the limestone pebbles covered by endolithic biofilms. (B) Sampling site WB2.2, the starting point of active tufa deposition. (C) Sampling site WB2.8 of the middle creek section with tufa stromatolites restricted to the central flow path. Note that oncoids and calcified plant remains accumulate at both sides of fast-flowing path. (D) Close-up view of calcified deposits consisting of leaves, branches and fine-grained calcite sands. (E) Tufa cascade at sampling site WB3.0. Note that most parts of the cascade are inactive and covered by mosses. (F) Sampling site WB4.0 with creek water flowing through a stromatolite-covered narrow channel. (G) Lowermost creek section with broad development of tufa stromatolites at sampling site WB 5.0 (May 2006). (H) Almost same view of (G) in October 2006. Note that green biofilms develop in the center of the creek, whereas brown biofilms are restricted to marginal parts.

this study, the following five substrates were used: tufa stromatolite from the center of the flow path colonized by a green-coloured biofilm (WB5.0; Fig. 2H), tufa stromatolite from the margin of the flow path colonized by a brown-coloured biofilm (WB5.0; Fig. 2H), moss from the center of the flow path (WB5.0; Fig. 2G), a limestone pebble with an endolithic biofilm from a pool at the spring site (WB1.0; Fig. 2A) and a biofilm free limestone pebble from the spring site (WB1.0; Fig. 2A). The substrates were collected three days before measurements (October 2006), and statically incubated in creek water at 10°C under a light:dark cycle of 12:12 h. With respect to moss, non-calcified leaf surfaces were measured.

O₂ microelectrodes (tip diameter of 10 µm) were prepared according to Revsbech (1989). pH, Ca²⁺ and CO₃²⁻ were measured with ion-specific liquid ion-exchange (LIX) membrane glass microelectrodes with tip diameter of 10 µm (de Beer et al., 2000; Gieseke and de Beer, 2004). Microelectrode positions were controlled by a motorized micromanipulator (VT-150, Micos, Eschbach). Microelectrodes were connected to a picoamperemeter (for O₂) or millivoltmeter (for LIX microelectrodes), and output was collected by a data acquisition box (NI DAQPad-6015, National Instruments, Austin). Micromanipulator control and data acquisition were performed with a computer and custom written software (µ-Profiler, Dr. L. Polerecky). The measurements were conducted at room temperature, which was stable at ~25°C throughout the measurements, in recirculating aquariums filled with spring water (WB1.0). Water was retained throughout whole measurements. As a nature of microelectrode measurement, it takes quite long time to obtain good quality of profiles, and the whole measurements of five substrates in this study took four days. Therefore, water chemistry of experimental water (pH, Ca²⁺ and alkalinity) was monitored throughout the measurements, as described below. All measurements were conducted under both light and dark conditions. Light was supplied by a fiber-optic lamp (KL 1500, Schott) at 500 µE m⁻² s⁻¹. Microelectrodes tips were set to the biofilm surface using a dissection microscope (SV6, Zeiss).

In this study, representative microprofiles were obtained for each microelectrode and biofilm. Therefore, measured points were not always exactly the same between different microelectrodes, while measured points for light and dark profiles of same microelectrodes were the same.

Fluxes of dissolved components were calculated from measured microprofiles applying Fick's first law,

$$J = -D \times dC / dz \quad (5.1)$$

where D denotes the diffusion coefficient (m² s⁻¹), dC is the concentration difference of the

given component (mol m^{-3}), and dz is the diffusion distance (m). The diffusion coefficients at 25°C are delivered from literatures: Ca^{2+} is $7.93 \times 10^{-10} \text{ m}^2 \text{ s}^{-1}$ (Li and Gregory, 1974), O_2 is $2.35 \times 10^{-9} \text{ m}^2 \text{ s}^{-1}$ (Broecker and Peng, 1974).

Following microelectrode measurements, biofilms were immediately fixed with PBS (phosphate buffered saline) buffered 3.7% formaldehyde, and kept cool and dark for two days. Samples were then transferred to 50% ethanol in PBS, and stored at 10°C in the dark until further processing. Samples were divided into several pieces and embedded in either resin or paraffin. Resin embedded samples were used for hard-part sections, while paraffin embedded samples were decalcified and used for FISH (fluorescence *in situ* hybridization) and EPS staining with Alcian Blue, as described by Shiraishi et al. (in press). For FISH, the 16S rRNA targeted oligonucleotide probe EUB338 (Amman et al., 1990) labeled with Cy3 was applied. These sections were also used for analyzing the populations of major phototrophs (filamentous cyanobacteria and diatom) in green- and brown-coloured biofilms. Resin-embedded sections were used for analyzing the population of filamentous cyanobacteria, and their surface areas in the microscopic view field ($200 \times 200 \mu\text{m}$) was measured by Scion Image (Scion Corporation). Alcian Blue-stained paraffin sections were used for diatoms, and their cell number was counted in the microscopic view field ($214 \times 172 \mu\text{m}$). For both analyses, four sections were prepared, and three points of biofilm surface were chosen from each section. In addition to the samples used for microelectrode measurements, hard-part sections of calcified leaves, branches and oncoids collected from the creek were also prepared, in order to check the involvement of microbial communities in the calcification of these substrates. EPS stained sections were observed by epifluorescence microscopy (Zeiss Axioplan). Other sections were observed under a Zeiss 510 Meta confocal laser scanning microscope (CLSM).

3.2. Water chemistry analysis

Three sampling campaigns for water chemistry analysis were conducted in May and October 2006, and January 2007. The pH of creek water was measured in the field using a portable pH meter (WTW GmbH) equipped with a Schott pH-electrode calibrated against standard buffers (pH 7.010 and 10.010; HANNA instruments). Water samples for titration of total alkalinity were collected in glass bottles, and for determination of main anion (Cl^- , SO_4^{2-} and NO_3^-) and cation concentrations (Ca^{2+} , Mg^{2+} , Na^+ and K^+) in plastic bottles. Samples for cation analysis were filtered in the field through $0.8 \mu\text{m}$ ϕ membrane filters (Millipore) and fixed by adding $50 \mu\text{l}$ concentrated methane sulfonic acid to 50 ml sample water. Samples were stored cool and dark until laboratory measurements. Within 48 h after sampling, alkalinity was determined by acid-base titration using a hand-held titrator and

1.6 N H₂SO₄ cartridges (Hach Corporation). Cation and anion concentrations were measured by ion chromatography with suppressed conductivity detection (Dionex). Additionally, dissolved silica concentration was measured by photometric methods according to Grasshoff et al. (1983).

Ion activities and partial pressure of CO₂ (pCO₂) were calculated with the computer program PHREEQC (Parkhurst and Appelo, 1999). The saturation of calcite is given as follows,

$$\Omega_{(\text{calcite})} = \{\text{Ca}^{2+}\} \times \{\text{CO}_3^{2-}\} / K_{\text{sp}(\text{calcite})} \quad (5.2)$$

where brackets denote the activities of ions and $K_{\text{sp}(\text{calcite})}$ is given by Plummer and Busenberg (1982). For the calculation of $\Omega_{(\text{calcite})}$ from microelectrode profiles of Ca²⁺ and CO₃²⁻ concentrations, {Ca²⁺} and {CO₃²⁻} were estimated by applying the activity coefficients of experimental water delivered from PHREEQC (0.62 for Ca²⁺ and 0.66 for CO₃²⁻).

Inorganic precipitation rate for calcite was calculated using the equation of Plummer et al. (1978),

$$R = -k_1 \{\text{H}^+\} - k_2 \{\text{H}_2\text{CO}_3^*\} - k_3 + k_4 \{\text{Ca}^{2+}\}\{\text{HCO}_3^-\}$$

$$\text{H}_2\text{CO}_3^* = \text{H}_2\text{CO}_3 + \text{CO}_{2(\text{aq})} \quad (5.3)$$

Although this empirical equation was originally provided for calcite dissolution, it is also applicable to precipitation (Plummer et al., 1979; Reddy et al., 1981). It provides the maximum rate of inorganic precipitation in turbulent water (Dreybrodt and Buhmann, 1991). The revised rate constants delivered by Buhmann and Dreybrodt (1985) were applied.

In addition to sampling along the creek profile, a continuous sampling for 21 h was conducted in October 2006 to evaluate the effect of microbial metabolism on bulk water chemistry. During this sampling, light intensity, air and water temperatures and water chemistry were monitored every hour at the spring site (WB1.0) and the lower creek site (WB5.0).

Flow rate measurements and detailed sediment mappings were conducted to calculate the creek mass balance. The flow rates at the lower creek site (WB5.0) was measured by collecting water in plastic bags for given times (5-10 sec.), which is an accurate method to measure the flow rate in this narrow and shallow creek (the deviation from the average values of three times measurements was less than 0.1 L s⁻¹). A detailed sediment map was constructed, and the image processing software Scion Image (Scion Corporation) was used to

measure the surface area of tufa stromatolites and calcified particles between WB1.0 and WB5.0.

3.3. Carbon and oxygen stable isotope measurements

To investigate the effect of microbial metabolism on carbon and oxygen stable isotopes, water and sediment samples were collected in October 2006. Water samples were collected in 250 ml glass bottles at the five main sampling sites. The bottles were first thoroughly rinsed with creek water, filled without air bubbles, sterilized by adding 2-3 drops of a HgCl₂ solution, and kept cool and dark. Isotope measurements were conducted at the Centrum voor Isotopen Onderzoek, University of Groningen, the Netherlands. Here, the water was treated under vacuum with 85% H₃PO₄, and carbon isotope ratios were measured after drying of the released CO₂. For oxygen, water samples were degassed under vacuum. After equilibrium exchange (24 h) at 25°C, a fraction of the CO₂ was sampled for oxygen isotope ratio measurements. Both carbon and oxygen isotopes were determined with a VG Micromass SIRA II mass spectrometer, and reported against V-PDB. Analytical precision was about ± 0.1‰ for both isotopes.

Sediment samples for stable isotope analysis were collected by scraping the tufa stromatolite surface (about 0.5 mm) with a knife at four of the major sampling sites (WB2.0 to 5.0). These samples were dehydrated in ethanol, and dried (~50°C) for 24 h. Additionally, one resin embedded sample was prepared for analysing isotopic depth profiles. The sample taken from the lower creek section (WB4.0) was embedded in resin as described above, and vertically sectioned. Sample powders for isotope analysis were obtained with a microsampling device (MicroMill, Merchantek) with vertical intervals of approximately 0.5 mm. Stable isotope analyses of tufa samples were conducted at the Institute of Geology, University of Erlangen, Germany. Here, samples were dissolved in purified H₃PO₄ at 75°C, and released CO₂ measured by a mass spectrometer ThermoFinnigan 252. Both carbon and oxygen isotope ratio were reported against V-PDB. Analytical precision was ± 0.02‰.

4. Results

4.1. General fabric of calcified crusts and related microorganisms.

Fig. 3 shows the general view of calcite crusts in the Westerhöfer Bach. The biofilms comprised mainly filamentous cyanobacteria (morphotype of “*Phormidium incrustatum*”, see e.g. Freytet and Placiat 1996), which covered the tufa stromatolite surface and also locally colonized calcified branches and mosses. The cyanobacterial filaments were surrounded by calcite microspar crystals and exhibited “encrusted sheaths” (Pentecost and

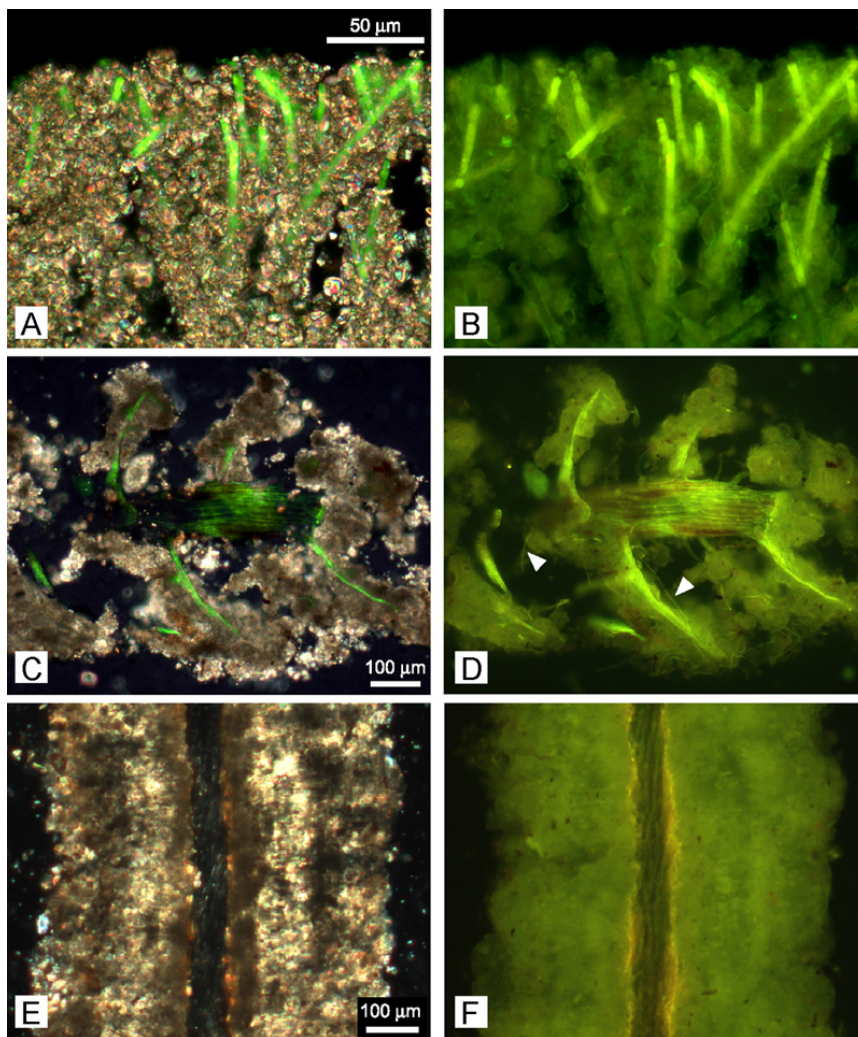


Fig. 3 Microfabrics of tufa deposits of the Westerhöfer Bach. (A, B) Vertical section of tufa stromatolite top showing filamentous cyanobacteria enclosed in microspar tubes. (C, D) Section of calcite veneered moss stem. Some filamentous cyanobacteria are present (e.g., arrows). (E, F) Vertical section of calcite-veneered tree leaf. There is almost no phototrophic microorganism in the crust. A, C and E are overlay images of cross polar and epifluorescence images (ex. 546 nm, em. 580 nm). B, D and F are epifluorescence images.

Riding, 1986; Merz-Preiß and Riding, 1999), thereby forming calcite tubes (Figs. 3A, B). Mosses were locally calcified especially in the older parts, whereas the younger leaves were usually free from calcification. The heavily calcified old parts of mosses were commonly colonized by other phototrophic microorganisms such as filamentous cyanobacteria and diatoms (Figs. 3C, D). In contrast to these biofilms, the relatively young calcite crusts of leaves, branches and oncoids were almost free of phototrophic biofilms (Figs. 3E, F).

4.2. Biofilm compositions and microprofiles

An overview of the biofilm substrates used for microelectrode measurements is given in Fig. 4A. The green-coloured tufa stromatolite was densely colonized by filamentous

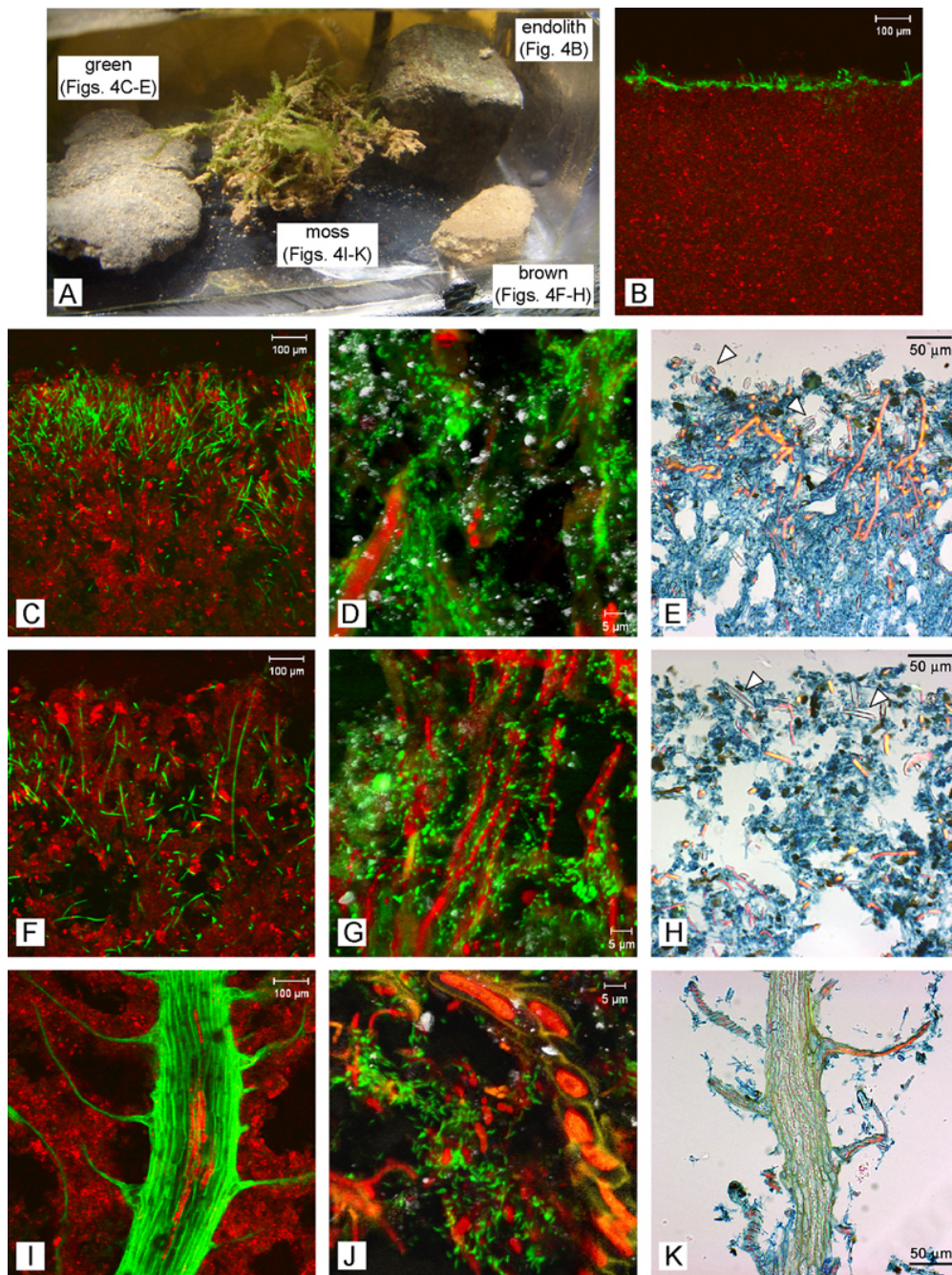


Fig. 4 Biofilm compositions of the substrates used for the microelectrode measurements. (A) The overview of biofilm substrates in the aquariums used for *ex situ* measurements. (B) Endolithic biofilm. (C)-(E) Green-coloured tufa stromatolite biofilm. (F)-(H) Brown-coloured tufa stromatolite biofilm. (I)-(K) Moss leaves and stems. The images B, C, F and I were taken by CLSM, with reflected light (carbonate crystals) shown in red and autofluorescence shown in green. Exited by 488, 543, 633 nm lasers, and processed by emission fingerprinting. CLSM images D, G and J show the results of FISH using oligonucleotide probe EUB338 (green), with autofluorescence (red) from autotrophs and reflected light (white) from debris such as clay minerals. Exited by 543 and 633 nm lasers, and processed by emission fingerprinting. E, H and K show overlays of transmitted light and epifluorescence (ex. 485, em. 535) views of paraffin sections stained by Alcian Blue. Blue stained areas are EPS rich in acidic groups, and bright orange represents Nuclear Fast Red-stained cells. Diatoms are indicated by arrows.

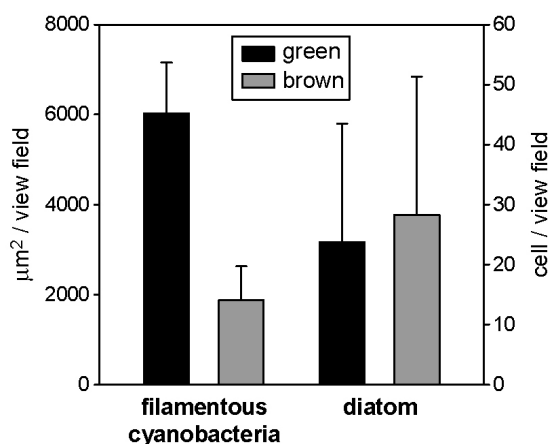


Fig. 5 Population of filamentous cyanobacteria and diatom in green- and brown-coloured biofilms. Population of cyanobacteria was indicated by the surface area in the microscopic view field ($200 \times 200 \mu\text{m}$). Autofluorescence of cyanobacteria was extracted by emission finger printing with CLSM. Population of diatom was indicated by cell number counted in the microscopic view field ($214 \times 172 \mu\text{m}$). Three points from four sections each were measured for both components.

cyanobacteria (morphotype “*Phormidium incrustatum*”; Fig. 4C), accompanied by a number of diatoms and heterotrophic bacteria, as demonstrated by FISH (Figs. 4D, E). All were surrounded by an acidic EPS matrix (Fig. 4E). On the other hand, the brown-coloured tufa stromatolite exhibited a sparse distribution of filamentous cyanobacteria (Fig. 4F) and acidic EPS matrix (Fig. 4H). There were a number of diatoms and heterotrophic bacteria, like in green-coloured tufa stromatolite (Figs. 4E, G). There was no significant difference in the diatom populations between the green-coloured and brown-coloured tufa stromatolites, while former contained higher number of filamentous cyanobacteria (Fig. 5). The older moss stems and leaves were fringed by calcite (Fig. 4I), while the surfaces of moss leaves and stems exhibited only minor amounts of acidic EPS (Fig. 4K). Cyanobacteria, diatoms and heterotrophic bacteria were locally present at the bottom part of the stems (Figs. 4J, K). Endolithic biofilms colonized the surface of limestone pebbles (about $50\text{-}100 \mu\text{m}$; Fig. 4B).

Microprofiles of pH, O_2 , Ca^{2+} and CO_3^{2-} under light and dark conditions were measured at the surface of the five substrates investigated (Fig. 6). Ca^{2+} fluxes calculated from these microprofiles are shown in Table 1. Microprofiles showed a distinct light-dark cycle in the diffusive boundary layer for the green-coloured tufa stromatolite (for the concept of diffusive boundary layer, see e.g., Jørgensen and Revsbech, 1985). Under illumination, pH, O_2 and CO_3^{2-} increased from the water column to the biofilm surface, and Ca^{2+} decreased. Consequently, the saturation state of calcite calculated from Ca^{2+} and CO_3^{2-} microprofiles showed a strong increase from 8.8-fold in the water column ($\sim 500 \mu\text{m}$ above from the substrate) to 27.7-fold at the biofilm surface. The opposite occurred in the dark; pH, O_2 and

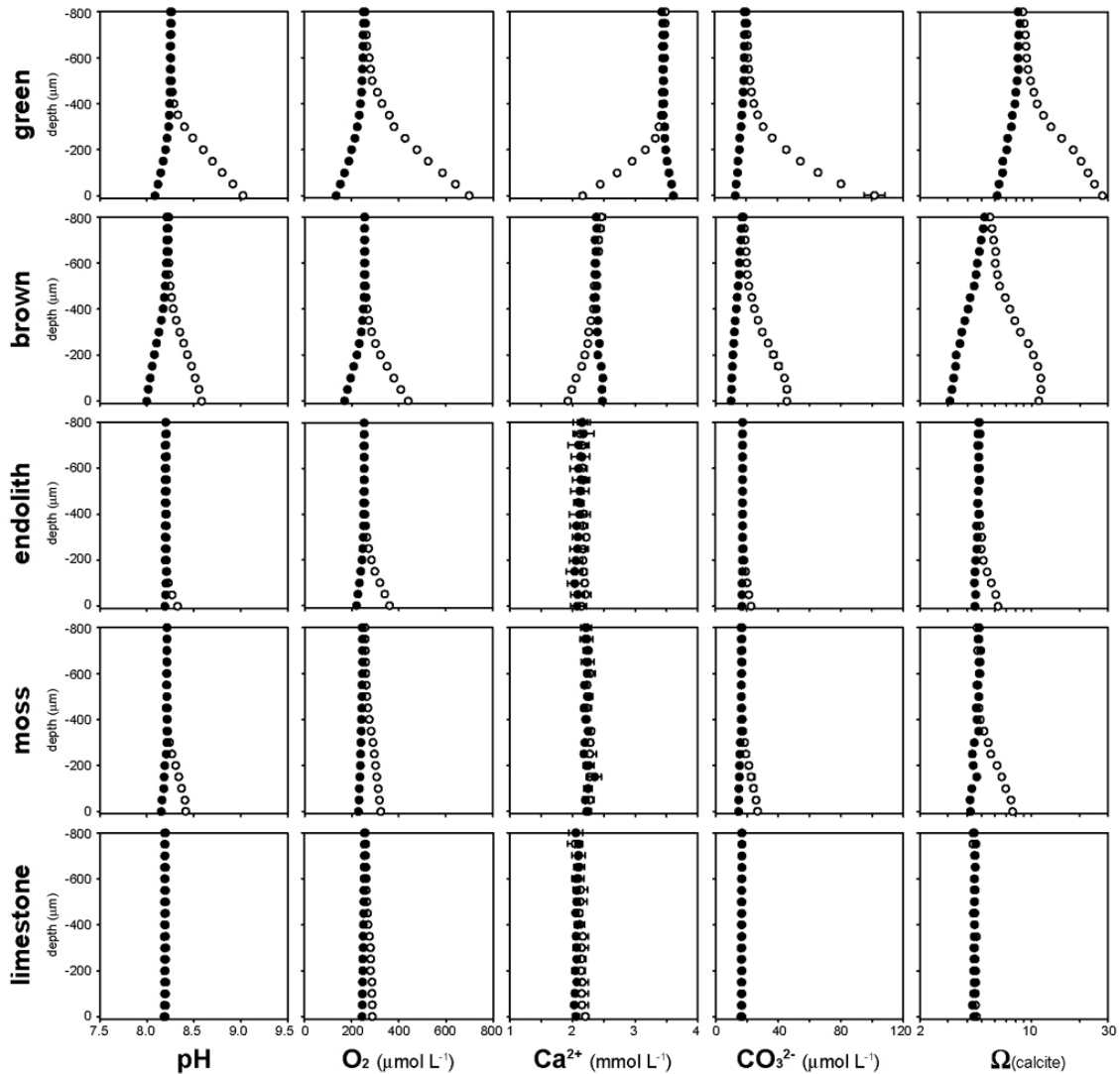


Fig. 6 Microelectrode profiles of pH, O_2 , Ca^{2+} , CO_3^{2-} and calculated calcite saturation for measurements at five substrates. Open circles indicate profiles obtained under light conditions, and filled circles indicate profiles obtained under dark conditions.

CO_3^{2-} decreased to the surface, and Ca^{2+} slightly increased. Accordingly, calcite supersaturation decreased from 8.2-fold to 6.0-fold. This light-dark cycle resulted in the net precipitation of calcite (Table 1; Shiraishi et al., in press). The brown-coloured tufa stromatolite showed similar cycles although the absolute fluctuations were smaller than that detected at the green-coloured tufa stromatolite. Calcite saturation at the biofilm surface increased from 5.4-fold to 11.0-fold under light conditions, and decreased to 3.0-fold in the dark. Again, a net precipitation was observed, although the amount of calcite precipitated was considerably smaller than in the green-coloured tufa stromatolite (Table 1). pH, O_2 and CO_3^{2-} microprofiles above endolithic biofilm and moss leaf showed a cycle similar to tufa stromatolites accounting for a change of saturation states (increase from 4.6-fold to

Table 1 Ca²⁺ fluxes of five substrates during the light and dark incubations.

	green	brown	endolith	moss	limestone
	(×10 ⁻⁶ mol m ⁻² s ⁻¹)				
light	-4.37	-1.06	-0.09	-0.04	0.26
dark	0.56	0.29	0.07	0.02	0.02
net	-3.81	-0.77	-0.02	-0.02	-0.24

Negative values indicate fluxes toward the substrates, and positive values the opposite. Note that, calculation for irregular Ca²⁺ microprofiles of endolith, moss and limestone substrates is not significant.

6.1-fold in the light, and decrease to 4.4-fold in the dark for endolithic biofilm surface; increase from 4.5-fold to 7.6-fold in the light, and decrease to 4.1-fold in the dark for moss leaf surface). However, these two biofilm types did not cause a detectable Ca²⁺ flux toward the biofilm surface (Fig. 6; Table 1). Compared to the biofilm substrates, the bare limestone substrate showed almost no changes in all microprofiles except for a slight change in O₂, which was possibly caused by minor colonies of phototrophs present.

Although chemistry of experimental water changed through the measurements because of CO₂ degassing and CaCO₃ precipitating, it was relatively stable after the second day (Table 2).

4.3. The change of water chemistry through the creek and day

Water chemistry along the course of the creek is shown in Table 3, and the profiles of major parameters are summarized in Fig. 7.

In general, the initially high pCO₂ (~10 matm) of the spring water decreased rapidly downstream (~1 matm) because of CO₂-degassing, but did not attain equilibrium with the atmosphere. This pCO₂ decrease was coupled with a pH increase from 7.4 to 8.3. While the concentrations of ions such as Na⁺, K⁺, Mg²⁺ and Cl⁻ kept very constant throughout the creek, Ca²⁺ concentrations and alkalinity began noticeably to decrease at a distance of about 150 m from the spring. Both Ca²⁺ and alkalinity further declined in the turbulent flowing creek section upstream of the tufa cascade at 250 m, followed by a sudden enhanced decrease below the cascade. The profiles of calculated calcite saturation state (Ω) and maximum

Table 2 Hydrochemistry of experimental water through the microelectrode measurements.

	measurement			pH	Ca ²⁺	Alk
	(day / electrode / sample)				(mmol L ⁻¹)	(meq L ⁻¹)
creek water				7.4	3.52	5.76
experiment	1st day	Ca ²⁺	green	—	3.47	—
	2nd day	Ca ²⁺	rest	8.2	2.07	—
	3rd day	pH	all	8.3	—	—
		O ₂	all	—	—	—
4th day	CO ₃ ²⁻	all	8.3	1.97	2.38	

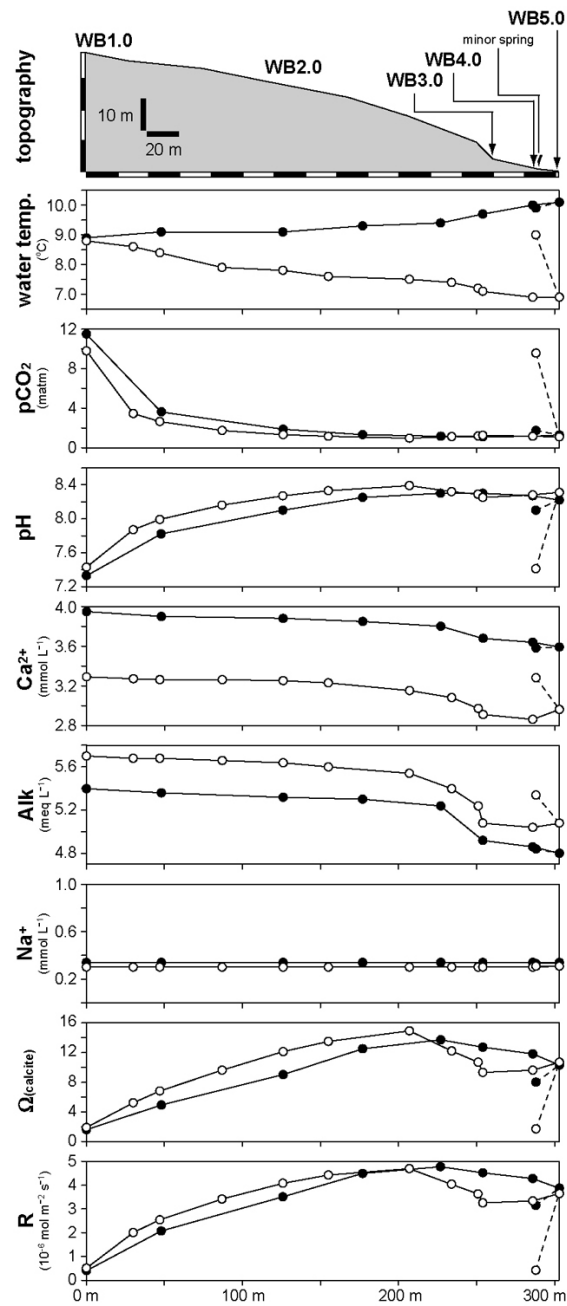


Fig. 7 Water chemistry along the course of the creek. Open circles indicate the data of May 2006, filled circles indicate data of January 2007.

inorganic precipitation rate (R) were concordant to that of pH. Both parameters increased downstream, and attained a maximum about 20-30 m before the tufa cascade, followed by a decrease. Seasonal hydrochemical fluctuations were recorded in May 2006 and January 2007 (Fig. 7; Table 3). Water temperature increased downstream in springtime, and decreased in wintertime, reflecting seasonal changes of air temperature. During springtime

Table 3 Hydrochemistry data of the Westerhöfer Bach for three sampling campaigns.

date	sampling site	distance (m)	Temp. (°C)	pH	Ca ²⁺ (mmol L ⁻¹)	Mg ²⁺ (mmol L ⁻¹)	Na ⁺ (mmol L ⁻¹)	K ⁺ (mmol L ⁻¹)	Si (mmol L ⁻¹)	Alk (meq L ⁻¹)	Cl ⁻ (mmol L ⁻¹)	SO ₄ ²⁻ (mmol L ⁻¹)	NO ₃ ⁻ (mmol L ⁻¹)	pCO ₂ (µatm)	R (10 ⁶ mol m ⁻² s ⁻¹)	Ω _(calcite)
May 2006	WB1.0	0	8.9	7.33	3.95	1.72	0.34	0.05	0.16	5.40	0.30	2.94	0.09	11481	0.40	1.6
	WB1.4	48	9.1	7.82	3.90	1.72	0.34	0.05	0.16	5.36	0.30	2.95	0.09	3630	2.07	4.9
	WB2.0	126	9.1	8.10	3.88	1.71	0.34	0.05	0.16	5.32	0.29	2.93	0.09	1862	3.51	9.0
	WB2.4	177	9.3	8.25	3.85	1.71	0.34	0.05	0.16	5.30	0.30	2.92	0.09	1318	4.49	12.5
	WB2.8	227	9.4	8.30	3.80	1.72	0.34	0.05	0.16	5.24	0.29	2.91	0.09	1148	4.77	13.7
	WB3.0	254	9.7	8.30	3.68	1.71	0.34	0.05	0.16	4.92	0.29	2.90	0.09	1096	4.52	12.7
	WB4.0	286	10.0	8.27	3.64	1.70	0.34	0.05	0.16	4.86	0.29	2.89	0.09	1148	4.27	11.8
	WB4.0(sub)	288	9.9	8.10	3.58	1.67	0.33	0.05	0.16	4.84	0.29	2.81	0.08	1738	3.15	8.0
WB5.0	303	10.1	8.22	3.59	1.71	0.34	0.05	0.16	4.80	0.29	2.87	0.08	1288	3.87	10.3	
Oct. 2006	WB1.0	0	9.4	7.60	3.49	1.65	0.36	0.05	0.17	5.84	0.39	2.21	0.09	6760	1.13	3.0
	WB2.0	126	9.1	8.13	3.48	1.65	0.35	0.05	0.16	5.80	0.37	2.17	0.09	1905	3.55	9.9
	WB3.0	254	8.6	8.35	3.23	1.64	0.36	0.05	0.17	5.40	0.37	2.16	0.09	1047	4.48	13.8
	WB4.0	286	8.7	8.25	3.18	1.64	0.34	0.05	0.17	5.28	0.37	2.18	0.09	1318	3.71	10.7
	WB5.0	303	8.7	8.22	3.16	1.64	0.33	0.05	0.17	5.28	0.36	2.16	0.09	1412	3.51	10.0
Jan. 2007	WB1.0	0	8.8	7.43	3.29	1.53	0.30	0.05	0.17	5.70	0.29	1.92	0.17	9772	0.51	1.9
	WB1.2	30	8.6	7.87	3.27	1.47	0.30	0.05	0.16	5.68	0.29	1.84	0.16	3467	2.00	5.2
	WB1.4	47	8.4	7.99	3.26	1.45	0.30	0.05	0.16	5.68	0.29	1.82	0.16	2630	2.54	6.8
	WB1.8	87	7.9	8.16	3.26	1.45	0.30	0.05	0.16	5.66	0.29	1.83	0.16	1738	3.41	9.6
	WB2.0	126	7.8	8.27	3.25	1.46	0.30	0.05	0.16	5.64	0.29	1.82	0.17	1318	4.08	12.1
	WB2.2	155	7.6	8.33	3.23	1.47	0.30	0.05	0.16	5.60	0.29	1.82	0.16	1148	4.42	13.5
	WB2.6	207	7.5	8.39	3.15	1.44	0.30	0.05	0.16	5.54	0.29	1.81	0.16	977	4.70	14.9
	WB2.8	234	7.4	8.32	3.08	1.44	0.30	0.05	0.16	5.40	0.29	1.81	0.16	1122	4.04	12.2
	WB2.9	251	7.2	8.29	2.97	1.45	0.30	0.05	0.16	5.24	0.29	1.80	0.16	1175	3.63	10.7
	WB3.0	254	7.1	8.25	2.91	1.46	0.30	0.05	0.16	5.08	0.29	1.80	0.16	1259	3.25	9.3
	WB4.0	286	6.9	8.28	2.86	1.45	0.30	0.05	0.16	5.04	0.29	1.80	0.16	1148	3.33	9.6
	WB4.0(sub)	288	9.0	7.41	3.28	1.49	0.31	0.04	0.16	5.34	0.29	2.04	0.12	9550	0.42	1.7
	WB5.0	303	6.9	8.31	2.96	1.45	0.31	0.05	0.16	5.08	0.29	1.85	0.16	1094	3.64	10.7

the chemistry of the minor subspring between WB4.0 and WB5.0 was similar to that of the lower creek section waters, but during wintertime it resembled that of the main spring. In any case, this minor inflow had only little influence on the chemistry of the main creek water because the recharging amount was relatively small.

The results of the 21 h monitoring at the spring site (WB1.0) and the lower creek site (WB5.0) are shown in Table 4, and summarized in Fig. 8. At the spring site, all parameters, except for light intensity and air temperature, were almost constant through time. Minor fluctuations in pH and water temperature at the beginning of monitoring reflected a technical trouble on pH meter. At the lower creek site (WB5.0), light intensity tended to be higher than at the spring site due to less shading from trees. Water temperature increased during the day with air temperature, and Ca²⁺ and alkalinity were always lower than at the spring site. There was no clear diurnal change on pH, alkalinity and Ca²⁺, although both Ca²⁺ and alkalinity slightly decreased during the course of the monitoring (Table 4). Flow rates remained almost constant through time (Table 5), although slight fluctuations were observed during 21 h monitoring.

The coverage areas of active tufa stromatolites and calcified particles and fragments measured from the detail map (Fig. 1) are shown in Table 6. Active tufa stromatolites covered about 25% of the creek floor.

Microbial effects on bulk water chemistry, stable isotopes and fabrics

Table 4 Hydrochemistry data of 21 h-monitoring at sampling site WB1.0 (spring site) and WB5.0 (lower creek site).

sampling site	time	light (Lux)	air temp. (°C)	water temp. (°C)	pH	Ca ²⁺ (mmol L ⁻¹)	Mg ²⁺ (mmol L ⁻¹)	Na ⁺ (mmol L ⁻¹)	K ⁺ (mmol L ⁻¹)	Si (mmol L ⁻¹)	Alk (meq L ⁻¹)	Cl ⁻ (mmol L ⁻¹)	SO ₄ ²⁻ (mmol L ⁻¹)	NO ₃ ⁻ (mmol L ⁻¹)
WB1.0	0:00	0	9.5	9.0	7.52	3.52	1.51	0.31	0.05	0.16	5.68	0.29	2.30	0.07
	1:00	0	9.0	9.0	7.52	3.51	1.52	0.31	0.05	0.16	5.70	0.29	2.31	0.07
	2:00	0	9.0	9.2	7.46	3.51	1.53	0.31	0.05	0.16	5.64	0.29	2.31	0.07
	3:00	0	8.8	10.2	7.41	3.52	1.52	0.31	0.05	0.16	5.68	0.29	2.30	0.07
	4:00	0	8.8	10.2	7.54	3.51	1.54	0.31	0.05	0.16	5.64	0.29	2.31	0.07
	5:00	0	8.8	10.3	7.55	3.50	1.54	0.31	0.05	0.16	5.66	0.29	2.31	0.07
	6:00	0	9.1	10.4	7.50	3.50	1.54	0.31	0.05	0.16	5.66	0.29	2.31	0.07
	7:00	0	9.5	10.3	7.46	3.50	1.54	0.31	0.05	0.16	5.66	0.29	2.31	0.07
	8:00	27	10.0	10.1	7.53	3.51	1.55	0.31	0.05	0.16	5.64	0.29	2.30	0.07
	9:00	155	10.0	10.1	7.51	3.52	1.54	0.31	0.05	0.16	5.66	0.29	2.30	0.07
	10:00	435	11.0	10.2	7.51	3.52	1.55	0.31	0.04	0.16	5.64	0.29	2.29	0.07
	11:00	730	11.2	10.1	7.49	3.53	1.56	0.31	0.04	0.16	5.64	0.29	2.31	0.07
	12:00	483	12.0	10.0	7.46	3.51	1.54	0.31	0.04	0.16	5.68	0.29	2.30	0.07
	13:00	770	12.2	10.2	7.48	3.53	1.55	0.31	0.04	0.16	5.68	0.29	2.30	0.07
	14:00	905	13.0	10.2	7.46	3.52	1.55	0.31	0.04	0.16	5.68	0.29	2.30	0.07
	15:00	530	13.2	10.2	7.43	3.52	1.56	0.31	0.04	0.16	5.72	0.29	2.30	0.07
	16:00	335	14.2	10.0	7.42	3.51	1.54	0.31	0.04	0.16	5.68	0.29	2.29	0.07
	17:00	150	14.0	10.3	7.44	3.49	1.54	0.31	0.04	0.16	5.66	0.29	2.30	0.07
	18:00	23	13.0	10.3	7.43	3.51	1.55	0.31	0.05	0.16	5.72	0.29	2.29	0.07
	19:00	0	13.0	10.2	7.41	3.52	1.55	0.31	0.05	0.16	5.72	0.29	2.29	0.07
	20:00	0	13.0	10.3	7.42	3.51	1.56	0.31	0.04	0.16	5.68	0.29	2.29	0.07
21:00	0	13.0	10.2	7.40	3.50	1.55	0.31	0.04	0.16	5.76	0.29	2.30	0.07	
WB5.0	0:00	0		9.3	8.27	3.17	1.52	0.31	0.05	0.17	4.88	0.29	2.29	0.07
	1:00	0		9.2	8.27	3.16	1.52	0.31	0.05	0.17	4.92	0.29	2.30	0.07
	2:00	0		10.1	8.16	3.17	1.52	0.31	0.05	0.17	4.90	0.29	2.30	0.07
	3:00	0		10.5	8.18	3.16	1.51	0.31	0.05	0.17	4.88	0.29	2.31	0.07
	4:00	0		10.4	8.26	3.16	1.51	0.31	0.05	0.17	4.88	0.29	2.31	0.07
	5:00	0		10.3	8.20	3.16	1.51	0.31	0.05	0.17	4.90	0.29	2.31	0.07
	6:00	0		10.4	8.21	3.16	1.50	0.31	0.05	0.17	4.88	0.29	2.31	0.07
	7:00	0		10.4	8.22	3.16	1.51	0.31	0.05	0.17	4.92	0.29	2.31	0.07
	8:00	86		10.1	8.28	3.16	1.52	0.31	0.05	0.17	4.92	0.29	2.30	0.07
	9:00	218		10.3	8.28	3.16	1.52	0.31	0.05	0.17	4.92	0.29	2.30	0.07
	10:00	707		10.5	8.18	3.16	1.54	0.31	0.05	0.17	4.86	0.29	2.30	0.07
	11:00	1240		10.6	8.23	3.15	1.51	0.31	0.05	0.17	4.86	0.29	2.31	0.07
	12:00	782		10.9	8.17	3.15	1.52	0.31	0.05	0.17	4.80	0.29	2.31	0.07
	13:00	656		10.4	8.18	3.15	1.52	0.31	0.05	0.17	4.84	0.29	2.30	0.07
	14:00	1010		10.5	8.19	3.14	1.53	0.31	0.05	0.17	4.86	0.29	2.30	0.07
	15:00	544		10.7	8.16	3.15	1.52	0.31	0.05	0.17	4.80	0.29	2.31	0.07
	16:00	625		10.9	8.17	3.14	1.51	0.31	0.05	0.17	4.76	0.29	2.31	0.07
	17:00	120		10.9	8.16	3.14	1.52	0.31	0.05	0.17	4.82	0.29	2.30	0.07
	18:00	18		11.0	8.12	3.14	1.54	0.31	0.05	0.17	4.80	0.29	2.29	0.07
	19:00	0		10.8	8.18	3.13	1.54	0.31	0.05	0.17	4.78	0.29	2.31	0.07
	20:00	0		10.6	8.10	3.13	1.52	0.31	0.05	0.17	4.76	0.29	2.30	0.07
21:00	0		10.6	8.12	3.13	1.52	0.31	0.05	0.17	4.82	0.29	2.29	0.07	

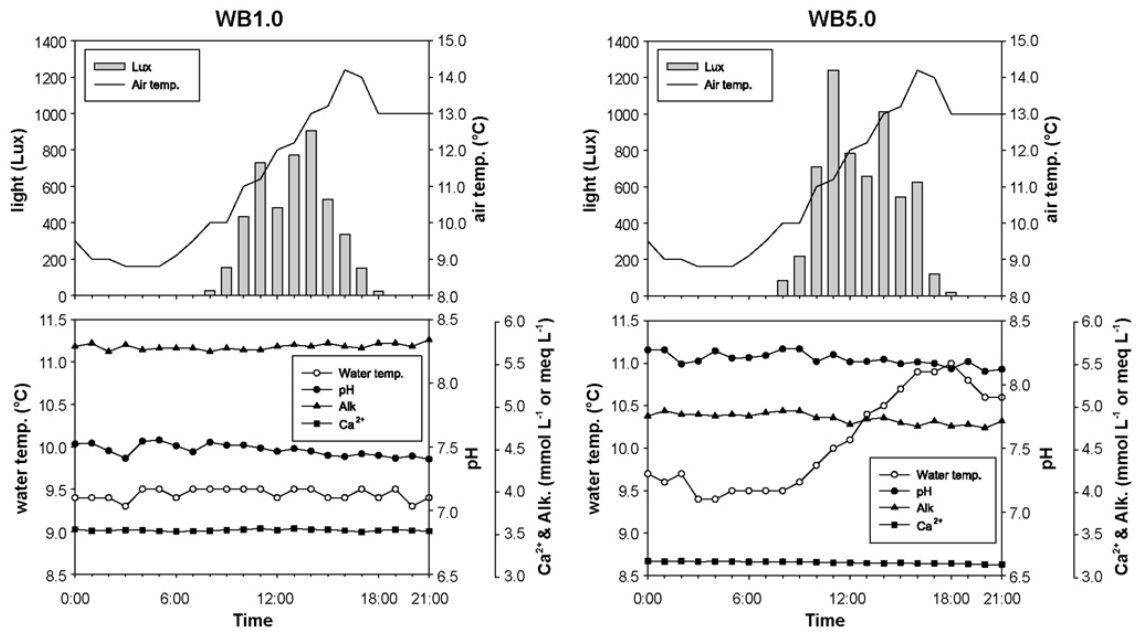


Fig. 8 21 h-monitoring of light intensity, air and water temperatures, pH, Ca²⁺ and alkalinity at sampling site WB1.0 (spring site) and WB5.0 (lower creek site).

Table 5 Water flow rates at sampling site WB5.0 (lower creek site) for three sampling campaigns.

	18/10/2006 17:00	19/10/2006 8:00	10/11/2006	30/01/2007
WB5.0 (L s ⁻¹)	2.1	2.3	2.0	2.0

Note that flow rates were almost comparable for all sampling campaigns.

Table 6 Coverage area of creek floor, active tufa stromatolites and calcified particles between sampling sites WB1.0 and WB5.0 measured from the detail creek map in Fig. 1.

	creek floor	active tufa stromatolites	calcified particles and fragments
area (m ²)	365	94	78

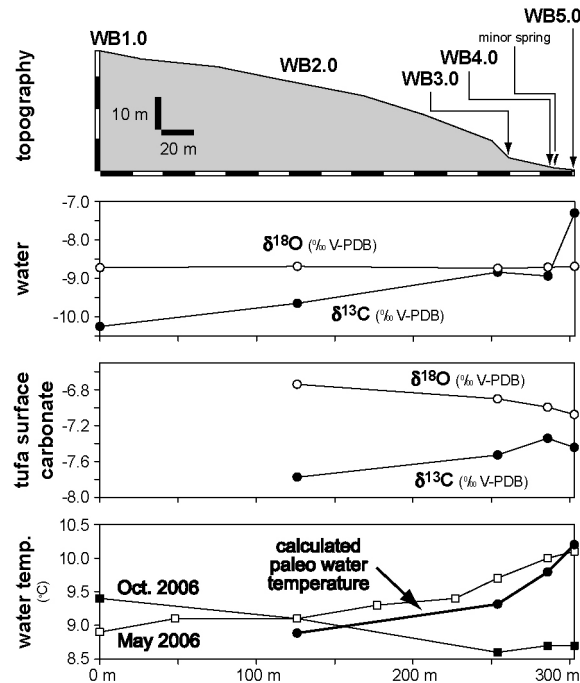


Fig. 9 Oxygen and carbon stable isotope profiles of bulk water and calcite from tufa stromatolite surfaces along the course of the creek. Palaeo water temperature calculated from $\delta^{18}\text{O}$ of calcite, and measured water temperatures are also shown.

4.4. Carbon and oxygen stable isotopes of water and tufa deposits

Carbon and oxygen stable isotopes of water and tufa stromatolite surfaces are shown in Table 7 and Fig. 9. $\delta^{18}\text{O}$ of water was constant along the creek at $\sim -8.7\text{‰}$, while $\delta^{13}\text{C}$ increased from -10.25‰ to -7.3‰ downstream.

$\delta^{13}\text{C}$ of calcite of the tufa stromatolite surfaces increased from -7.77‰ to -7.44‰ downstream, similar to that of water. $\delta^{18}\text{O}$ of tufa stromatolite surfaces decreased from -6.74‰ to -7.08‰ downstream.

$\delta^{13}\text{C}$ and $\delta^{18}\text{O}$ depth profiles of tufa stromatolite from the lower creek section (WB4.0) are shown in Table 8 and Fig. 10. Both showed similar, sine curved cycles although there was a small phase difference. $\delta^{13}\text{C}$ displayed an amplitude of approximately 1.0 to 1.8‰, while

Table 7 $\delta^{13}\text{C}$ and $\delta^{18}\text{O}$ of water and calcite of tufa stromatolite surfaces.

sampling site	water		tufa	
	$\delta^{13}\text{C}$ (‰ V-PDB)	$\delta^{18}\text{O}$ (‰ V-PDB)	$\delta^{13}\text{C}$ (‰ V-PDB)	$\delta^{18}\text{O}$ (‰ V-PDB)
WB1.0	-10.25	-8.72	—	—
WB2.0	-9.65	-8.69	-7.77	-6.74
WB3.0	-8.84	-8.74	-7.53	-6.90
WB4.0	-8.94	-8.71	-7.34	-6.99
WB5.0	-7.30	-8.69	-7.44	-7.08

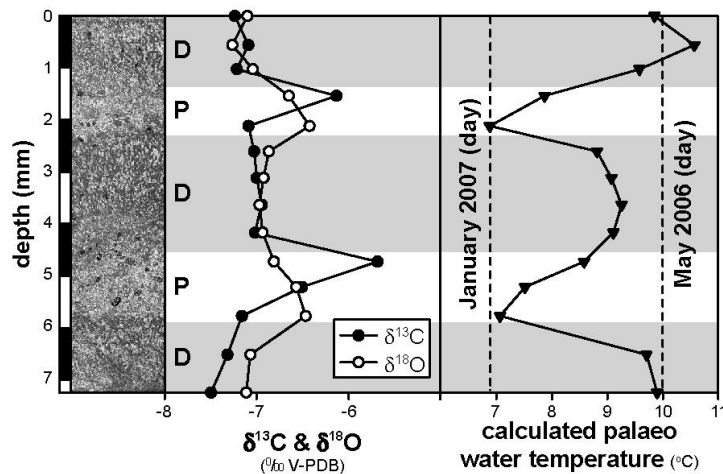


Fig. 10 $\delta^{13}\text{C}$ and $\delta^{18}\text{O}$ depth profiles of the top 7 mm of a tufa stromatolite from sampling site WB4.0 (lower creek section), and calculated palaeo water temperatures. Left hand side shows a cross polar view of the thin section analysed, with dense layers appearing darker (D) and porous layer appearing lighter (P).

$\delta^{18}\text{O}$ amplitude was approximately 0.6 to 0.7‰. Both $\delta^{13}\text{C}$ and $\delta^{18}\text{O}$ values tended to be lower in the dense layers, and higher in the porous layers.

5. Discussion

5.1. Biofilm composition and influence of microbial activities on CaCO_3 precipitation

Microbial biofilms of all substrates investigated by microelectrodes were capable of photosynthesis, but they differed in their impact on CaCO_3 precipitation (Fig. 6). Only the green and brown-coloured tufa stromatolite biofilms could induce CaCO_3 precipitation by

Table 8 $\delta^{13}\text{C}$ and $\delta^{18}\text{O}$ depth profiles of the top 7 mm of a tufa stromatolite from sampling site WB4.0 (lower creek section), and calculated palaeo water temperatures.

depth (mm)	$\delta^{13}\text{C}$ (‰ V-PDB)	$\delta^{18}\text{O}$ (‰ V-PDB)	calculated paleo water temperature (°C)
0.0	-7.23	-7.10	9.84
0.5	-7.08	-7.26	10.56
1.0	-7.21	-7.03	9.57
1.5	-6.13	-6.65	7.86
2.1	-7.08	-6.42	6.87
2.6	-7.02	-6.86	8.81
3.1	-6.99	-6.92	9.06
3.6	-6.94	-6.96	9.25
4.1	-7.01	-6.93	9.10
4.7	-5.68	-6.81	8.57
5.2	-6.50	-6.57	7.50
5.7	-7.16	-6.46	7.05
6.5	-7.31	-7.06	9.70
7.2	-7.49	-7.11	9.89

photosynthesis. Although differences in bulk water Ca^{2+} concentrations at the time of measurements necessitate a degree of caution in interpreting the profiles, the pH, O_2 and CO_3^{2-} microprofiles all indicated that green-coloured tufa stromatolite had a stronger photosynthetic effect on the carbonate system at the tufa surface. The major difference of phototroph composition between these two biofilms was the higher abundance of filamentous cyanobacteria in green-coloured tufa stromatolite, while there were qualitatively no significant differences on the diatom populations (Fig. 5). Although acidic EPS and numbers of heterotrophs present (Fig. 4), pH-dependent binding and release of Ca^{2+} by acidic groups of EPS, as well as the activity of heterotrophic bacteria, are quantitatively not important for maintaining precipitation in the tufa biofilms (Shiraishi et al., in press). Therefore, photosynthetic CO_2 assimilation by filamentous cyanobacteria is thought to be directly responsible for CaCO_3 precipitation.

In contrast to tufa stromatolite biofilms, the endolithic biofilms and moss leaves did not cause Ca^{2+} flux towards the substrate, and therefore apparent CaCO_3 precipitation, under experimental conditions (Fig. 6). pH, O_2 and CO_3^{2-} microprofiles of the endolithic biofilm and moss leaf clearly showed lower photosynthetic rates, thereby lower the effect on supersaturation, than the tufa stromatolite (Fig. 6). Consequently, it is assumed that the photosynthesis by endolithic biofilms and moss has a lower impact on the carbonate equilibrium and that this impact is too low to overcome the kinetic barrier for CaCO_3 precipitation.

Endolithic biofilms are usually found in the upper stream where saturation state is much lower than that of the experimental conditions, and their photosynthetic effects in the creek must even be smaller than in the measurements of this study. Moss leaves in the creek, however, become calcite-veneered with time, especially in the middle to lower creek section where calcite supersaturation is high. Their calcification may start with a trapping of cyanobacteria, diatoms and/or EPS from the water column. Then, EPS itself or small calcite particles trapped by EPS provide the nucleation sites, as suggested by Emeis et al. (1987) and Turner and Jones (2005). Furthermore, protrusions such as the tips of moss leaves attain lesser diffusive boundary layers (Skelland, 1974), and this may also increase the likelihood of precipitation. Subsequently, mosses become more and more colonized by cyanobacteria (Figs. 3C, D), which then cause further calcification by enhanced photosynthetic CO_2 assimilation. In contrast to the four biofilm substrates, the uncolonized limestone substrate did not show any spontaneous precipitation (Fig. 6) despite an ambient 4-fold calcite supersaturation.

The observations substantiate the view that photosynthesis is an effective mechanism to overcome the kinetic barrier of calcite precipitation without high water turbulence

(Shiraishi et al., in press). Although the results discussed above were obtained under slow flow conditions in the laboratory, and there were three days interval between the sampling and measurements which might caused alteration of biofilm composition, comparable results of photosynthesis-induced CaCO_3 precipitation, obtained *in situ*, have been reported previously (Shiraishi et al., in press; Bissett et al., in press).

5.2. Influence of photosynthesis on creek water chemistry

As demonstrated previously (Fig. 6; Shiraishi et al., in press; Bissett et al., in press), microbial metabolism controls CaCO_3 precipitation in tufa stromatolites, even in CO_2 -degassing, highly supersaturated conditions that preferentially cause physicochemical precipitation. However, the bulk water chemistry along the course of the investigated creek all displayed characteristics of physicochemical precipitation: a strong pCO_2 decrease concurrent with an increase in calcite supersaturation, followed by a decrease in Ca^{2+} and alkalinity (Fig. 7) due to calcite precipitation, and no diurnal pattern (Fig 8). This has also been observed in previous studies (e.g., Usdowski et al., 1979; Dandurand et al., 1982; Dreybrodt et al., 1992; Merz-Preiß and Riding, 1999).

Although initially it appears that the bulk water chemistry and microelectrode data are incompatible, discrepancies are explained by mass balance estimations. Assuming that CaCO_3 precipitation on the tufa stromatolites is exclusively governed by microbial photosynthesis, the amount of Ca^{2+} decreasing throughout the creek by photosynthesis-induced CaCO_3 precipitation, $\Delta\text{Ca}^{2+}_{\text{PS}}$ (mol L^{-1}), is calculated as following:

$$\Delta\text{Ca}^{2+}_{\text{PS}} = J_{\text{Ca}} \times S / F \quad (5.4)$$

where J_{Ca} is the photosynthesis-induced Ca^{2+} flux in unit area and time ($\text{mol m}^{-2} \text{s}^{-1}$), S is the total surface area of tufa stromatolites over which this occurs (m^2) and F is water flow (L s^{-1}). For J_{Ca} , the annual average of Ca^{2+} flux determined by actual tufa stromatolites at site WB5.0 was used ($1.85\text{-}2.86 \times 10^{-6} \text{ mol m}^{-2} \text{ s}^{-1}$; Shiraishi et al., in press). The surface area of tufa stromatolites (S) amounted to 94 m^2 (Table 6), and water flow F at site WB5.0 was $\sim 2.0 \text{ L s}^{-1}$ (Table 5). Based on these values, a $\Delta\text{Ca}^{2+}_{\text{PS}}$ of 0.086 to $0.134 \text{ mmol L}^{-1}$ is calculated, i.e., a value that is almost within the analytical error of the bulk water chemistry analyses conducted. This indicates that the effect of photosynthesis-induced CaCO_3 precipitation is diluted, and not detectable by conventional bulk water chemistry analysis. The situation would be different when water flow rates in the creek are lower. Then, $\Delta\text{Ca}^{2+}_{\text{PS}}$ will be larger as indicated by Eq. (5.4), and the effects of photosynthesis-induced CaCO_3 precipitation would be traceable by bulk water chemistry analysis.

In turn, if total Ca^{2+} loss throughout the creek is assumed to precipitate only at tufa stromatolites, the Ca^{2+} flux at the tufa surface would be $7.45 \times 10^{-6} \text{ mol m}^{-2} \text{ s}^{-1}$ (used Ca^{2+} loss of 0.35 mmol L^{-1} , and calculated by Eq. 5.4) and, hence, the annual deposition would be $23684 \text{ g m}^{-2} \text{ y}^{-1}$. These values highly exceed both the measured annual calcite deposition of $2934\text{-}4514 \text{ g m}^{-2} \text{ y}^{-1}$ at tufa stromatolites (Shiraishi et al., in press) and the maximum inorganic precipitation rate of the creek water of $4.53 \times 10^{-6} \text{ mol m}^{-2} \text{ s}^{-1}$ (estimated by Eq. 5.3; Table 3), further supporting the view that only a minor percentage of Ca^{2+} loss in the creek can be explained by tufa stromatolite biofilm calcification.

In any case, the major Ca^{2+} loss, which is removed from the creek water independent of photosynthesis, remains to be explained. The possibility of progressive dilution of the creek water appears unlikely since conservative ion (Na^+ , K^+ and Cl^-) concentrations remained constant along the course of the creek. Although acidic EPS can bind Ca^{2+} (Kawaguchi and Decho, 2002), the possibility of such mechanisms for explaining the Ca^{2+} decrease through the creek is refuted by following mass balance calculations. As an approximation, the amount of CO_2 assimilated can be derived from the O_2 production, as demonstrated by the sum reaction of photosynthesis:



Although cyanobacteria also use HCO_3^- as a carbon source under low CO_2 conditions (e.g., Badger and Price, 1994), and consequently in high pH environments like tufa creeks, the ratio between CH_2O and O_2 does not change. Assuming e.g. the production of glucuronic acid as an example, the production rate of this EPS monomer should be two times higher than divalent Ca^{2+} flux in order to bind it. If the entire assimilated carbon is used for producing glucuronic acid, production of glucuronic acid through the creek per day (mol day^{-1}) is calculated as followings,

$$\text{Glucuronic acid (production)} = J_{\text{O}_2} \times S \times T / C_{\text{gluc}} \quad (5.6)$$

where J_{O_2} is oxygen flux delivered from O_2 microprofile of green biofilm ($2.66 \times 10^{-6} \text{ mol m}^{-2} \text{ s}^{-1}$; Fig. 6), S is the total surface area of tufa stromatolites (94 m^2 ; Table 6), T is duration of photosynthesis per day ($4.32 \times 10^4 \text{ s}$), C_{gluc} is the number of carbon atom in glucuronic acid molecule. With values above, production of glucuronic acid through the creek is estimated as $1.80 \text{ mol day}^{-1}$. On the other hand, required amount of glucuronic acid to bind observed Ca^{2+} decrease in the creek per day is calculated as followings,

$$\text{Glucronic acid (required)} = \Delta\text{Ca}^{2+}_{\text{total}} \times \text{EC}_{\text{Ca}} \times F \times T \quad (5.7)$$

where $\Delta\text{Ca}^{2+}_{\text{total}}$ is total Ca^{2+} loss through the creek ($\sim 0.35 \times 10^{-3} \text{ mol L}^{-1}$; Table 1), EC_{Ca} is electric charge of Ca^{2+} , F is flow rate ($\sim 2.0 \text{ L s}^{-1}$; Table 5), T is one day ($8.64 \times 10^4 \text{ s}$). With these values, the required amount of glucronic acid is estimated as $120.96 \text{ mol day}^{-1}$ that is significantly larger than the estimated production. Of course, actual production of acidic EPS must be much lower than the calculated value because such organic molecules comprise only part of the EPS, and organisms must produce other carbohydrate compounds to survive. Therefore, the role of Ca^{2+} binding by acidic EPS has negligible role on the Ca^{2+} decrease through the creek water. The major Ca^{2+} loss in the investigated creek section is thought to be removed physicochemically e.g., at tree branches, leaves and fine-grained calcite sands, which are almost free of phototrophic biofilm colonization (Figs. 3E, F). This is supported by high inorganic precipitation rate in the middle and lower creek where Ca^{2+} decrease is evident (Fig. 7). From the discussions above, it can be concluded that the photosynthetic effect is diluted by high water supply, and has a relatively small impact on bulk water chemistry. The different interpretations emphasizing either "inorganic", physicochemical precipitation or "biological", microbially-controlled precipitation, in tufa systems is only a discrepancy at first glance. The present study revealed that physicochemically-forced precipitation is responsible for the major Ca^{2+} loss in the tufa creek system, while the concurrent biofilm photosynthesis drives tufa stromatolite formation. As derived from the mass balance estimation above, metabolic processes are thought to be responsible for approximately 10-20% of Ca^{2+} loss in the Westerhöfer Bach.

5.3. Influence of photosynthesis on carbon and oxygen stable isotopes

The $\delta^{18}\text{O}$ of the creek water was almost stable along the course of the creek (Fig. 9), an observation that coincides with previous studies on temperate tufa creeks with limited evaporation (e.g., Usdowski et al., 1979; Chafetz et al., 1991; Matsuoka et al., 2001). On the other hand, the $\delta^{18}\text{O}$ values of tufa surface calcite decreased downstream (Fig. 9). If calcite was precipitated under isotopic equilibrium with regard to oxygen, water temperature at the time of precipitation can be calculated by the following empirical equation (Erez and Luz, 1983),

$$T(^{\circ}\text{C}) = 17.0 - 4.52 (\delta^{18}\text{O}_{\text{C}} - \delta^{18}\text{O}_{\text{W}}) + 0.03 (\delta^{18}\text{O}_{\text{C}} - \delta^{18}\text{O}_{\text{W}})^2 \quad (5.8)$$

where $\delta^{18}\text{O}_{\text{C}}$ and $\delta^{18}\text{O}_{\text{W}}$ are the oxygen isotope composition of calcite and water respectively (vs. V-PDB). The calculated temperatures increase downstream, which is the opposite of the

water temperature gradient measured on the day of sampling (October 2006; Fig. 9). However, the calculated trend in temperatures fits well with the water temperatures of May, which obviously reflects the fact that the tufa surface analysed mainly formed in spring and summer. This reflects the fact that the samples for isotope measurements were collected by scalping ~0.5 mm of deposit surfaces which contains palaeo-temperature information of last several month. Although the calculated temperatures are slightly lower than the temperature measured in May, and of course, profiles of water temperatures in summer are thought to be higher than that of May, differences are attributed to an averaging effect of sampling (Matsuoka et al., 2001). These results indicate that the $\delta^{18}\text{O}$ of the Westerhöfer Bach water was almost stable throughout the year and calcite precipitated near isotopic equilibrium with regard to oxygen. This has also been observed in other temperate tufa creeks (e.g., Chafetz et al., 1991; Matsuoka et al., 2001). This is strongly supported by the depth profile of $\delta^{18}\text{O}$ obtained from tufa stromatolites. Calculated palaeo-water-temperatures from this profile (assuming constant $\delta^{18}\text{O}$ of water) exhibit a sine curve between 7.0 to 10.5°C, which is in accordance with the actual seasonal change of water temperature at the sampling site (WB4.0; Fig. 10). Although actual water temperature fluctuation is thought to be somewhat larger, the smaller amplitude of calculated palaeo-water-temperatures are also explained by an averaging effect. Calcite precipitation at oxygen isotopic equilibrium as presented above is contrary to the findings of previous investigations of the Westerhöfer Bach by Usdowski et al. (1979), but it has been reported from many other tufa forming creeks (e.g., Chafetz et al., 1991; Matsuoka et al., 2001; Ihlenfeld et al., 2003; Kano et al., 2007).

The interpretation of $\delta^{13}\text{C}$ values is more complicated because they are affected by several factors, i.e., CO_2 -degassing, photosynthesis and seasonal fluctuations of $\delta^{13}\text{C}$ in the spring water. The $\delta^{13}\text{C}$ values of the creek water increased downstream (Fig. 9), as a result of preferential ^{12}C loss during CO_2 -degassing (e.g., Usdowski et al., 1979; Dandurand et al., 1982; Michaelis et al., 1985; Matsuoka et al., 2001). The $\delta^{13}\text{C}$ values of tufa surface calcite showed a similar trend, and are thought to reflect CO_2 -degassing of the creek water (see also Pentecost and Spiro, 1990). However, it is difficult to conclude solely on these results that tufa stromatolites precipitate in carbon isotopic equilibrium with creek water DIC. This is because the $\delta^{13}\text{C}$ of spring water in the Westerhöfer Bach probably changes seasonally, which may be attributed to either the ventilation or the mixing ratio between CO_2 from soil and bedrock limestone (Chafetz et al., 1991; Matsuoka et al. 2001; Hori et al. 2008). Indeed, Usdowski et al. (1979) reported 1‰ $\delta^{13}\text{C}$ change between June and August 1977. Seasonal $\delta^{13}\text{C}$ fluctuations of creek water are recorded in tufa stromatolites (Chafetz et al., 1991; Matsuoka et al., 2001), and sometimes co-vary with $\delta^{18}\text{O}$ either negatively or positively,

depending on the aquifer (Smith et al., 2004). The observed seasonal $\delta^{13}\text{C}$ fluctuations of tufa stromatolites in this study (Fig. 10) are also interpreted as reflecting the $\delta^{13}\text{C}$ fluctuations of creek water DIC. Indeed, $\delta^{13}\text{C}$ values of summer laminae are more negative than those in winter laminae, while a reverse relation would be expected if photosynthesis strongly influences $\delta^{13}\text{C}$ records (Pentecost, 1987, 1988; Pentecost and Spiro, 1990). Although photosynthesis causes rapid precipitation, observed precipitation rates in the order of $10^{-6} \text{ mol m}^{-2} \text{ s}^{-1}$ are not expected to have any influence on the carbon isotope fractionation between bicarbonate and calcite (Romanek et al., 1992).

The results indicate that an effect of photosynthesis is not traceable in the carbon isotopic composition of the tufa stromatolites, although photosynthesis-induced calcite precipitation is evident. Therefore, the absence of a photosynthetic signature in carbon isotopes does not necessarily imply an "inorganic" precipitation. Nonetheless, the reason why photosynthetic effects have been detected on the $\delta^{13}\text{C}$ of tufa stromatolite carbonates in sluggish or lower sections of karst-water creeks (Spiro and Pentecost, 1990) and lakes (Andrews et al., 1997, 2000) remains to be explained by future work.

5.4. The relationship between photosynthesis-induced precipitation and annual lamination

The fact that photosynthesis directly drives CaCO_3 precipitation in tufa stromatolites has implications for the mechanisms behind their annual lamination, an understanding of which may provide useful time scale information for palaeoclimate reconstruction (e.g., Kano et al., 2003). Generally, the mechanisms for the formation of annual laminations, suggested by previous studies, can be divided into inorganic and organic factors (for review, see Andrews and Brasier, 2005). Inorganic factors include seasonal changes in water chemistry which cause fluctuations in calcite supersaturation. Indeed, seasonal fluctuations of water chemistry have been reported from a number of temperate tufa-forming creeks (e.g., Matsuoka et al., 2001; Kano et al., 2003; Kawai et al., 2006), including the Westerhöfer Bach (Table 3; Jacobson and Usdowski, 1975). In addition, seasonal changes in water temperature causing variations in the inorganic precipitation rate are suggested to contribute to the formation of annual lamination (Kano et al., 2003, 2007), although it would be restricted on the biofilm-free substrates where microbially controlled precipitation does not occur. Organic factors on the other hand include seasonal variations of the biofilm composition and corresponding EPS properties (Arp et al., 2001b), growth patterns of microorganism (Janssen et al., 1999), and seasonal changes in microbial metabolisms (Pentecost, 1987, 1988).

In addition to these factors, the seasonal changes in diffusion rates are thought to be one of the reasons for annual lamination because the diffusion coefficients are temperature

dependent. For example, at 25°C, the experimental condition of microelectrode measurements in this study, the diffusion coefficient of Ca²⁺ is $7.93 \times 10^{-10} \text{ m}^2 \text{ s}^{-1}$, whereas it decreases to $6.73 \times 10^{-10} \text{ m}^2 \text{ s}^{-1}$ at 18°C, and $3.73 \times 10^{-10} \text{ m}^2 \text{ s}^{-1}$ at 0°C (Li and Gregory, 1974). When water temperature decreases from 18°C to 0°C, Ca²⁺ flux decreases by almost half (Eq. 5.1) even if metabolism rates of microorganisms are constant. Although exact maximum and minimum of water temperature in the Westerhöfer Bach have not been recorded, water temperatures of other temperate tufa-forming creeks vary seasonally by 15°C or more in the lower creek sections (Matsuoka et al., 2001; Kano et al., 2003; Kawai et al., 2006).

Therefore, seasonal variation of diffusion coefficient can be one of the important mechanisms for annual lamination. This effect would be enhanced if photosynthetic activity is high in summer and low in winter, which would result in a dense summer layer and porous winter layer. Of course, care has to be taken when using annual lamination as a seasonal indicator because seasonally fluctuating factors (inorganic and organic) are thought to be complexly involved in lamina formation (see also Andrews and Brasier, 2005). Indeed, some studies have reported a porous summer layer and a dense winter layer (e.g., Monty, 1976; Janssen et al., 1999). From this point of view, it might be difficult to establish a universal mechanism for annual lamination in tufa stromatolites (see also Arp et al., 2001b; Ihlenfeld et al., 2003).

5.5. Fabrics of calcified cyanobacteria and its implication

The occurrence and absence of calcified cyanobacteria in the geological record has been used as an argument for changes in ocean chemistry, especially in the Mg/Ca ratio (Riding, 1982), in CaCO₃ mineral supersaturation (Riding, 1992) and in DIC concentrations (Arp et al., 2001a). This is particularly true for microcrystalline tubular cyanobacterial microfossils (e.g., *Girvanella*), which are thought to result from photosynthesis-induced pH microgradients and corresponding microenvironmental rises in CaCO₃ supersaturation. Based on studies in tufa creeks, Merz-Preiß and Riding (1999) suggested an indicator for recognizing photosynthesis-induced cyanobacterial calcification by means of the resulting carbonate fabrics: cyanobacteria utilize HCO₃⁻ in CO₂-poor sluggish conditions and would induce CaCO₃ precipitation to form microcrystalline sheath impregnations, whereas utilize CO₂ in fast-flowing high pCO₂ conditions such as tufa-forming creeks and would not influence CaCO₃ supersaturation to promote passive external calcification in form of encrusted sheaths.

The present study, however, revealed that photosynthesis induces CaCO₃ precipitation at tufa surfaces even at high-pCO₂ conditions, but nevertheless resulted in the formation of encrusted sheaths (Figs. 3A, B). Further investigations, such as CO₂ microelectrode

measurements, are required to evaluate whether the increasing supersaturation observed in this study was attained by CO₂ assimilation or OH⁻ release resulting from HCO₃⁻ utilization, as suggested by Merz (1992). Nonetheless, cyanobacteria in the Westerhöfer Bach probably utilize HCO₃⁻ as well as CO₂, because 97% of the DIC in the creek is composed of HCO₃⁻, and only 1-2% of CO₂, although pCO₂ is higher than in the atmosphere. In any case, the observed sheath encrustations due to cyanobacterial photosynthesis demonstrate that this style of cyanobacterial calcification is not indicative of an externally forced, physicochemical CaCO₃ precipitation.

6. Conclusions

1. Microelectrode profiles of pH, O₂, Ca²⁺ and CO₃²⁻ demonstrated that tufa stromatolite biofilms, composed mainly of filamentous cyanobacteria, strongly induce CaCO₃ precipitation by photosynthesis, while endolithic biofilms and moss leaf do not.
2. Bulk water chemistry data along the course of the creek as well as a 21 h monitoring did not detect significant effects of photosynthesis in the macroenvironment. Mass balance calculations revealed that about 10-20% of total Ca²⁺ loss in the creek is precipitated by biofilm photosynthesis, the effect of which is undetectable by bulk water analysis as long as water supply dilutes it. The Major cause of Ca²⁺ removal from the creek water is thought to be physicochemical precipitation on biofilm-poor tree branches, leaves and fine-grained calcite particles.
3. Although tufa stromatolites are formed by photosynthesis-induced CaCO₃ precipitation, δ¹³C values of tufa stromatolite carbonates did not exhibit a photosynthetic fractionation. Instead, they probably recorded seasonal δ¹³C fluctuations in bulk creek water DIC. The δ¹⁸O values reflect palaeo-water temperatures, if δ¹⁸O of the creek water is constant.
4. Temperature affects ionic diffusion coefficients and therefore Ca²⁺ flux caused by photosynthesis-induced CaCO₃ precipitation. This is thought to be one important mechanism for annual lamina formation in tufa stromatolites, together with other organic and inorganic factors, such as seasonal fluctuations in creek water chemistry, biofilm compositions and microbial metabolisms.
5. Cyanobacterial sheath encrustation by CaCO₃ can result from photosynthetic activity, and therefore cannot be used as indication of physicochemically-forced CaCO₃

precipitation.

Acknowledgements

This project is the part of the Research Unit 571 "Geobiology of organo- and biofilms", funded by the German Research Foundation (DFG-FOR 571; AR 335/5; publication #21). F.S. is grateful to Dr. Andreas Kronz (University of Göttingen) for introduction to the micromill microsampling device. Mr. Wolfgang Dröse and Mr. Alexander Satmari (University of Göttingen) assisted biofilm sectioning and histological techniques. Dr. Akihiro Kano and Dr. Tatsuya Kawai (Hiroshima University) helped for calculating inorganic precipitation rate. We thank Dr. Lubos Polerecky (MPI, Bremen) for the microprofiling software.

References

- Amann, R.L., Binder, B.J., Olson, R.J., Chisholm, S.W., Devereux, R., Stahl, D.A., 1990. Combination of 16S rRNA-targeted oligonucleotide probes with flow cytometry for analyzing mixed microbial populations. *Appl. Environ. Microbiol.* 56, 1919-1925.
- Andrews, J.E., 2006. Palaeoclimatic records from stable isotopes in riverine tufas: synthesis and review. *Earth-Sci. Rev.* 75, 85-104.
- Andrews, J.E., Riding, R., Dennis, P.F., 1997. The stable isotope record of environmental and climatic signals in modern terrestrial microbial carbonates from Europe. *Palaeogeogr. Palaeoclimatol. Palaeoecol.* 129, 171-189.
- Andrews, J.E., Pedley, M., Dennis, P.F., 2000. Palaeoenvironmental records in Holocene Spanish tufas: a stable isotope approach in search of reliable climatic archives. *Sedimentology* 47, 961-978.
- Andrews, J.E., Brasier, A.T., 2005. Seasonal records of climatic change in annually laminated tufas: short review and future prospects. *J. Quat. Sci.* 20, 411-421.
- Arp, G., Reimer, A., Reitner, J., 2001a. Photosynthesis-induced biofilm calcification and calcium concentrations in Phanerozoic oceans. *Science* 292, 1701-1704.
- Arp, G., Wedemeyer, N., Reitner, J., 2001b. Fluvial tufa formation in a hard-water creek (Deinschwanger Bach, Franconian Alb, Germany). *Facies* 44, 1-22.
- Awramik, S.M., 1984. Ancient stromatolites and microbial mats. In: Cohen, Y., Castenholtz, R.W., Halvorson, H.O. (Eds.), *Microbial Mats: Stromatolites*. Alan R. Liss Inc., New York, pp. 1-22.
- Badger, M.R., Price, G.D., 1994. The role of carbonic anhydrase in photosynthesis. *Ann. Rev. Plant. Physiol. Plant. Mol. Biol.* 45, 369-392.
- Bissett, A., de Beer, D., Schoon, R., Shiraishi, F., Reimer, A., Arp, G., in press. Microbial mediation of stromatolite formation in karst-water creeks. *Limnol. Oceanogr.* submitted.
- Broecker, W.S., Peng, T.H., 1974. Gas exchange rates between air and sea. *Tellus* 26, 21-35.

- Buhmann, D., Dreybrodt, W., 1985. The kinetics of calcite dissolution and precipitation in geologically relevant situations of karst areas, 1. Open system. *Chem. Geol.* 48, 189-211.
- Chafetz, H.S., Utech, N.M., Fitzmaurice, S.P., 1991. Differences in the $\delta^{18}\text{O}$ and $\delta^{13}\text{C}$ signatures of seasonal laminae comprising travertine stromatolites. *J. Sediment. Petrol.* 61, 1015-1028.
- Chen, J., Zhang, D.D., Wang, S., Xiao, T., Huang, R., 2004. Factors controlling tufa deposition in natural waters at waterfall sites. *Sediment. Geol.* 166, 353-366.
- Dandurand, J.L., Gout, R., Hoefs, J., Menschel, G., Schott, J., Usdowski, E., 1982. Kinetically controlled variation of major components and carbon and oxygen isotopes in a calcite-precipitating spring. *Chem. Geol.* 36, 299-315.
- de Beer, D., Kühl, M., Stambler, N., Vaki, L., 2000. A microsensor study of light enhanced Ca^{2+} uptake and photosynthesis in the reef-building hermatypic coral *Favia* sp. *Mar. Ecol. Prog. Ser.* 194, 75-85.
- Dreybrodt, W., Buhmann, D., 1991. A mass transfer model for dissolution and precipitation of calcite from solutions in turbulent motion. *Chem. Geol.* 90, 107-122.
- Dreybrodt, W., Buhmann, D., Michaelis, J., Usdowski, E., 1992. Geochemically controlled calcite precipitation by CO_2 outgassing: field measurements of precipitation rates in comparison to theoretical predictions. *Chem. Geol.* 97, 285-294.
- Emeis, K.C., Richnow, H.H., Kempe, S., 1987. Travertine formation in Plitvice National Park, Yugoslavia: chemical versus biological control. *J. Sediment. Petrol.* 34, 595-609.
- Erez, L., Luz, B., 1983. Experimental paleotemperature equation for planktonic foraminifera. *Geochim. Cosmochim. Acta* 47, 1025-1031.
- Ford, T.D., Pedley, H.M., 1996. A review of tufa and travertine deposits of the world. *Earth-Sci. Rev.* 41, 117-175.
- Freytet, P., Plet, A., 1996. Modern freshwater microbial carbonates: the *Phormidium* stromatolites (tufa-travertine) of Southeastern Burgundy (Paris basin). *Facies* 34, 219-238.
- Gieseke, A., de Beer, D., 2004. Use of microelectrodes to measure in situ microbial activities in biofilms, sediments, and microbial mats. In: Kowalchuk, G.G., de Bruijn, F.J., Head, I.M., Akkermans, A.D., van Elsas, J.D. (Eds.), *Molecular Microbial Ecology Manual*. 2nd edition. Springer-Verlag, Berlin-Heidelberg, pp. 1581-1612.
- Golubic, S., 1973. The relationship between blue-green algae and carbonate deposits. In: Carr, N.G., Whitton, B.A. (Eds.), *The biology of Blue-Green Algae*. Bot. Monogr. 9, Blackwell, Oxford, pp. 434-472.
- Grasshoff, K., Erhardt, M., Kremling, K., 1983. *Methods of Seawater Analysis*. Verlag Chemie, Weinheim.
- Grotzinger, J.P., Knoll, A.H., 1999. Stromatolites in Precambrian carbonates: evolutionary mileposts or environmental dipsticks? *Annu. Rev. Earth Planet. Sci.* 27, 313-358.
- Hori, M., Hoshino, K., Okumura, K., Kano, A., 2008. Seasonal patterns of carbon chemistry and isotopes in tufa depositing groundwaters of southwestern Japan. *Geochim. Cosmochim. Acta* 72, 480-492.
- Ihlenfeld, C., Norman, M., Gagan, M., Drysdale, R., Maas, R., Webb, J., 2003. Climatic significance of seasonal trace element and stable isotope variations in a modern freshwater tufa. *Geochim. Cosmochim. Acta* 67, 2341-2357.
- Jacobson, R.L., Usdowski, E., 1975. Geochemical controls on a calcite precipitating spring. *Contrib. Mineral. Petrol.*

- 51, 65-74.
- Janssen, A., Swennen, R., Podoor, N., Keppens, E., 1999. Biological and diagenetic influence in Recent and fossil tufa deposits from Belgium. *Sediment. Geol.* 126, 75-95.
- Jørgensen, B.B., Revsbech, N.P., 1985. Diffusive boundary layers and the oxygen uptake of sediments and detritus. *Limnol. Oceanogr.* 30, 111-122.
- Kano, A., Matsuoka, J., Kojo, T., Fujii, H., 2003. Origin of annual laminations in tufa deposits, southwest Japan. *Palaeogeogr. Palaeoclimatol. Palaeoecol.* 191, 243-262.
- Kano, A., Kawai, T., Matsuoka, J., Ihara, T., 2004. High-resolution records of rainfall events from clay bands in tufa. *Geology* 32, 793-796.
- Kano, A., Hagiwara, R., Kawai, T., Hori, M., Matsuoka, J., 2007. Climatic conditions and hydrological change recorded in a high-resolution stable isotope profile of a recent laminated tufa on a subtropical island, southern Japan. *J. Sediment. Res.* 77, 59-67.
- Kawaguchi, T., Decho, A.W., 2002. Isolation and biochemical characterization of extracellular polymeric secretions (EPS) from modern soft marine stromatolites (Bahamas) and its inhibitory effect on CaCO₃ precipitation. *Prep. Biochem. Biotechnol.* 32, 51-63.
- Kawai, T., Kano, A., Matsuoka, J., Ihara, T., 2006. Seasonal variation in water chemistry and depositional processes in a tufa-bearing stream in SW-Japan, based on 5 years of monthly observations. *Chem. Geol.* 232, 33-53.
- Li, Y.H., Gregory, S., 1974. Diffusion of ions in sea water and in deep-sea sediments. *Geochim. Cosmochim. Acta* 38, 703-714.
- Matsuoka, J., Kano, A., Oba, T., Watanabe, T., Sakai, S., Seto, K., 2001. Seasonal variation of stable isotopic compositions recorded in a laminated tufa, SW Japan. *Earth Planet. Sci. Lett.* 192, 31-44.
- Merz, M.U.E., 1992. The biology of carbonate precipitation by cyanobacteria. *Facies* 26, 81-102.
- Merz-Preiß, M., Riding, R., 1999. Cyanobacterial tufa calcification in two freshwater streams: ambient environment, chemical thresholds and biological processes. *Sediment. Geol.* 126, 103-124.
- Michaelis, J., Usdowski, E., Menschel, G., 1985. Partitioning of ¹³C and ¹²C on the degassing of CO₂ and the precipitation of calcite—Rayleigh-type fractionation and a kinetic model. *Am. J. Sci.* 285, 318-327.
- Monty, C.L.V., 1976. The origin and development of cryptalgal facies. In: Walter, J. (Ed.), *Stromatolites. Development of Sedimentology* 20, Elsevier, Amsterdam, pp. 193-249.
- Parkhurst, D.L., Appelo, C.A.J., 1999. User's guide to PHREEQC (version 2)—a computer program for speciation, batch-reaction, one-dimensional transport, and inverse geochemical calculations. *Water-Resources Investigations Report 99-4259*, U.S. Geological Survey, Denver.
- Pedley, M., 2000. Ambient temperature freshwater microbial tufas. In: Riding, R., Awramik, S.M. (Eds.), *Microbial Sediments*. Springer-Verlag, Berlin-Heidelberg, pp. 179-186.
- Pentecost, A., 1987. Growth and calcification of the freshwater cyanobacterium *Rivularia haematites*. *Proc. Roy. Soc. London Ser. B* 232, 125-136.

- Pentecost, A., 1988. Growth and calcification of the cyanobacterium *Homoeothrix crustacea*. *J. General Microbiol.* 134, 2665-2671.
- Pentecost, A., Riding, R., 1986. Calcification of cyanobacteria. In: Leadbeater, B.S.C., Riding, R. (Eds.), *Biom mineralization in Lower Plants and Animals*. Systematic Assoc. Spec. Vol. 30, Clarendon Press, Oxford, pp. 73-90.
- Pentecost, A., Spiro, B., 1990. Stable carbon and oxygen isotope composition of calcites associated with modern freshwater cyanobacteria and algae. *Geomicrobiol. J.* 8, 17-26.
- Plummer, L.N., Wigley, T.M.L., Parkhurst, D.L., 1978. The kinetics of calcite dissolution in CO₂-water systems at 5° to 60°C and 0.0 to 1.0 atm CO₂. *Am. J. Sci.* 278, 179-216.
- Plummer, L.N., Parkhurst, D.L., Wigley, T.M.L., 1979. Critical review of the kinetics of calcite dissolution and precipitation. In: Janne, E. (Ed.) *Chemical Modelling in Aqueous Systems: Speciation, Sorption, Solubility and Kinetics*. American Chemical Society, Washington DC, pp. 537-573.
- Plummer, L.N., Busenberg, E., 1982. The solubilities of calcite, aragonite and vaterite in CO₂-H₂O solutions between 0 and 90°C, and an evolution of aqueous model for the system CaCO₃-CO₂-H₂O. *Geochim. Cosmochim. Acta* 46, 1011-1040.
- Reddy, M.M., Plummer, L.N., Busenberg, E., 1981. Crystal growth of calcite from calcium bicarbonate solutions at constant pCO₂ and 25°C: a test of the calcite dissolution model. *Geochim. Cosmochim. Acta* 45, 1281-1291.
- Revsbech, N.P., 1989. An oxygen microsensor with a guard cathode. *Limnol. Oceanogr.* 34, 474-478.
- Riding, R., 1982. Cyanophyte calcification and changes in ocean chemistry. *Nature* 299, 814-815.
- Riding, R., 1992. Temporal variation in calcification in marine cyanobacteria. *J. Geol. Soc. London* 149, 979-989.
- Riding, R., 2000. Microbial carbonates: the geological record of calcified bacterial-algal mats and biofilms. *Sedimentology* 47, 179-214.
- Riding, R., 2006. Cyanobacterial calcification, carbon dioxide concentrating mechanisms, and Proterozoic-Cambrian changes in atmospheric composition. *Geobiology* 4, 299-316.
- Romanek, C.S., Grossman, E.L., Morse, J.W., 1992. Carbon isotopic fractionation in synthetic aragonite and calcite: effects of temperature and precipitation rate. *Geochim. Cosmochim. Acta* 56, 419-430.
- Shiraishi, F., Bissett, A., de Beer, D., Reimer, A., Arp, G., in press. Photosynthesis, respiration and exopolymer calcium-binding in biofilm calcification (Westerhöfer and Deinschwanger Creek, Germany). *Geomicrobiol. J.* submitted.
- Skelland, A.H.P., 1974. *Diffusional Mass Transport*. Wiley, New York.
- Smith, J.R., Giegengack, R., Schwarcz, H.P., 2004. Constraints on Pleistocene pluvial climates through stable-isotope analysis of fossil-spring tufas and associated gastropods, Kharga Oasis, Egypt. *Palaeogeogr. Palaeoclimatol. Palaeoecol.* 206, 157-175.
- Spiro, B., Pentecost, A., 1991. One day in the life of a stream—a diurnal inorganic carbon mass balance for a travertine-depositing stream (Waterfall Beck, Yorkshire). *Geomicrobiol. J.* 9, 1-11.
- Turner, E.C., Jones, B., 2005. Microscopic calcite dendrites in cold-water tufa: implications for nucleation of micrite

Microbial effects on bulk water chemistry, stable isotopes and fabrics

and cement. *Sedimentology* 52, 1043-1066.

Uzdowski, E., Hoefs, J., Menschel, G., 1979. Relationship between ^{13}C and ^{18}O fractionation and changes in major element composition in a recent calcite-depositing spring—a model of chemical variations with inorganic CaCO_3 precipitation. *Earth Planet. Sci. Lett.* 42, 267-276.

Chapter 6

In situ co-localization of microorganisms and calcite in
calcified biofilms by using FISH and CARD–FISH

***In situ* co-localization of microorganisms and calcite in calcified biofilms by using FISH and CARD–FISH**

Fumito Shiraishi, Barbara Zippel, Thomas R. Neu, Gernot Arp

Abstract

Modified protocols of fluorescence *in situ* hybridization (FISH) and catalyze reporter deposition fluorescence *in situ* hybridization (CARD–FISH) were developed to perform a simultaneous detection of microorganisms and calcite crystals in stromatolite-forming biofilms. Smooth, well-preserved thin sections of calcified biofilms (~5 µm thin, vertical sectioning of ~1 cm deep) were obtained by cryo-sectioning with adhesive-tape-stabilization. A modified hybridization buffer was applied during hybridization to prevent calcite dissolution as well as false binding of oligonucleotide probes to the charged mineral surfaces. Particularly, bright and specific CARD–FISH signals allowed the detection of microorganisms in intensively calcified biofilms even at low magnification, which is suitable for investigating millimeter- to centimeter-scale depth distribution pattern of microorganisms.

1. Introduction

Fluorescence *in situ* hybridization (FISH) is a powerful technique to detect and identify bacteria *in situ* inside microbial aggregates and microbial films without cultivation (e.g., Amann et al., 1995; Moter and Göbel, 2000). During the last years, FISH has been applied for various types of samples including environmental biofilms. However, they sometimes closely relate with mineral matrices such as rocks, clays and sediments, which impede the application of FISH to environmental samples by three crucial problems: First, the co-occurrence of soft organic material and hard minerals disturbs the sectioning in standard methods, so that millimeter- to centimeter-scale distribution pattern of microorganisms could not be retained. Second, false binding of negatively charged oligonucleotide probes to positively charged mineral surfaces such as calcite falsifies the specific detection of microorganisms by FISH (Harmsen et al., 1997; Schrenk et al., 2003). Third, FISH signals are sometimes hindered by strong autofluorescence of phototrophic microorganisms (Schönhuber et al., 1997) and minerals (Vesey et al., 1997).

However, mineralizing biofilms are of special interest in geobiology because they

potentially form stromatolites (Kalkowsky, 1908), laminated microbial rocks, which were widespread for two billion years in the early Earth history. While extant stromatolites are rare in the recent marine settings and restricted to a few examples of coarse-agglutinated varieties (e.g. Shark Bay, Bahamas), non-marine settings exhibit a wide variety of stromatolites formed by intensively calcifying biofilms, similar to many fossil counterparts (e.g., Awramik, 1984). One type of non-marine stromatolite is formed in karst hard water creeks, also known as tufa. Recent investigations revealed that the cyanobacterial biofilms of this freshwater stromatolite induce calcite precipitation by photosynthesis, thereby causing stromatolite formation (Shiraishi et al., in press; Bissett et al., in press). However, the role of heterotrophic bacteria, which generally occur in cyanobacterial biofilms, remains unclear. They may either promote or inhibit precipitation and/or cause dissolution of carbonate minerals (Visscher et al., 2000; Dupraz and Visscher, 2005), and FISH investigations are required to understand the roles of heterotrophs in these mineralized biofilms.

The present study describes embedding, sectioning and hybridization protocols for simultaneous *in situ* detection of microorganisms and calcite crystals. Strong autofluorescence of phototrophs and minerals was overcome by applying catalyze reporter deposition FISH (CARD-FISH) using tyramide signal amplification (TSA), which allows 10- to 20-fold amplification of FISH signal (Schönhuber et al., 1997). Thin sectioning of calcified stromatolite biofilms was achieved by cryo-sectioning combined with the adhesive tape technique (Kawamoto et al., 2003), and false binding and calcite dissolution were avoided by applying modified hybridization protocol. In addition, other sectioning methods were tested and their applicability was checked by CARD-FISH as well as FISH.

2. Materials and methods

2.1. Sample fixation

Samples of freshwater tufa stromatolites were collected from the Westerhöfer Creek, central Germany (see Shiraishi et al., in press for further detail of this creek) in October 2006, and immediately fixed with PBS (phosphate buffered saline) buffered 3.7% formaldehyde, and kept cool and dark for two days. Samples were transferred to 50% ethanol in PBS, and stored at 5°C in the dark until further processing. In addition, non-fixed and frozen samples were prepared for comparison.

2.2. Sample embedding and sectioning

Samples for the adhesive tape sectioning were kept at 5°C overnight in 4% CMC

(carboxymethyl cellulose; FINETEC Co. Ltd.) gel for infiltration, embedded in fresh CMC at -25°C , and sectioned by a cryotome (Leica CM3050S) equipped with disposable blades (Leica DB80L) as described by Kawamoto (2003). In this study, sections were obtained by using Cryofilm Type 1 and Transferfilm (FINETEC Co. Ltd.). Sections obtained by Cryofilm Type 1 were supported by mounting on glass slides by means of double-sided tape, and used for further processing. Sections obtained by Transferfilm were transferred on the silanized glass slides in n-hexan for 12 h by following the instructions of the manufacturer.

In order to check the applicability of the modified hybridization protocol in the present study (see below) other embedding and sectioning methods, resin embedded and decalcified paraffin section were prepared. For resin embedding, samples were embedded in Technovit 7100 as described by Manz et al. (2000), and sectioned by a rotary microtome. For paraffin embedding, samples were decalcified in 20% Formical-2000 (Decal Chemical Co. Ltd.), and embedded and sectioned as described by Hoffmann et al. (2003).

2.3. Hybridization

For FISH and CARD-FISH, the mixture of 16S rRNA targeted oligonucleotide probes EUB338 (5'-GCTGCCTCCCGTAGGAGT-3'), EUB338II (5'-GCAGCCACCCGTAGGTGT-3') and EUB338III (5'-GCTGCCACCCGTAGGTGT-3') were applied for eubacteria (Daims et al., 1999). Probes were labeled either by Cy3 for FISH or horseradish peroxidase (HRP) for CARD-FISH. Negative controls were performed by non-EUB338, the complementary sequence of EUB338 (Wallner et al., 1993).

Through the hybridization, 5 mM CaCl_2 and 5 mM NaHCO_3 were added to most of experimental solutions to avoid calcite dissolution. For CARD-FISH, modified protocols of Pernthaler et al. (2002) and Manz et al. (2000) were developed. For cell wall permeabilization, sections were incubated in proteinase K ($50\ \mu\text{g ml}^{-1}$, 5 mM CaCl_2 , 5 mM NaHCO_3) at 37°C for 2 h, and washed with MilliQ. Then, 40 μl of hybridization buffer [0.9 M NaCl, 20 mM Tris (pH 7.5), 10% dextran sulfate (wt/vol), 0.02% SDS, 35% Formamide (vol/vol), 1% Blocking reagent (wt/vol), 0.5 mg fish sperm DNA ml^{-1} , 0.5 mg *Escherichia coli* tRNA ml^{-1} , 5 mM CaCl_2 , 5 mM NaHCO_3 ; modified from Pernthaler et al., 2002] and 5 μl of probe ($50\ \text{ng}\ \mu\text{l}^{-1}$) were dropped onto the sections, and hybridized in a moist chamber at 37°C for 2 h. Unbound probes were removed by $\sim 1\ \text{ml}$ washing buffer [88 mM NaCl, 20 mM Tris (pH 8.0), 0.01% SDS, 5 mM CaCl_2 , 5 mM NaHCO_3], and incubated at 37°C for 10 min., followed by three times MilliQ washing. Freshly prepared amplification solution (1 μl of tyramide-Cy3 and 49 μl of amplification buffer; TSA Plus Fluorescence Systems, Perkin Elmer Inc.) was immediately pipetted onto the slides and incubated at room temperature in

the dark for 10 min. Slides were then washed with TNT buffer [0.1 M Tris (pH 7.5), 0.15 M NaCl, 0.05% Tween20, 5 mM CaCl₂, 5 mM NaHCO₃] for 15 min, rinsed with MilliQ three times, and enclosed in mounting media [5.5 parts of Citifluor, 1 part of VectaShield, 0.5 parts of 1 × PBS, DAPI (4',6'-diamidino-2-phenylindole) at a final concentration of 1 µg ml⁻¹; Pernthaler et al., 2002].

For FISH, the protocol of Manz et al. (2000) was applied with the following modifications. First, above-mentioned hybridization buffer for CARD-FISH was used. Second, 2 h pretreatment by hybridization buffer was carried out. Third, 5 mM of CaCl₂ and NaHCO₃ were added to the washing buffer.

2.4. Epifluorescence microscopy

Hybridized sections were observed by epifluorescence microscopy equipped with a cross-polarization system (Zeiss, Jena). The following filter sets were used: Zeiss 01 (exciter 359–371 nm, dichroic mirror 395 nm, emitter >397 nm; Carl Zeiss MicroImaging) for the detection of DAPI, XF204 M-FISH (exciter 540–550 nm, dichroic mirror 555 nm, emitter 570–600 nm; Omega Optical) for the detection of Cy3, and XF70 (exciter 520–640 nm, dichroic mirror 660 nm, emitter 675–725 nm; Omega Optical) for autofluorescence. Images were acquired using CCD camera (PCO Computer Optics), and processed by Adobe Photoshop 6.0 software (Adobe Systems).

3. Results and discussions

3.1. Optimum hybridization protocols for freshwater stromatolites

The modified CARD-FISH protocol used in the present study which was mostly based on Manz et al. (2000) and Pernthaler et al. (2002), could successfully detect microorganisms and calcite simultaneously without calcite dissolution and false binding (Figs. 1A–C). This protocol was also useful for CARD-FISH of decalcified paraffin sections (Table 1). However, the original protocols mentioned above could not solely yield good results even if calcite dissolution was avoided by adding CaCl₂ and NaHCO₃. For example, hybridization buffer of Manz et al. (2000) could not avoid false binding. Although hybridization buffer of Pernthaler et al. (2002) could avoid false binding, their permeabilization protocol by using lysozyme was too weak whereas their washing procedures were too strong for stromatolite samples investigated in this study. They also could not solely yield good results even if decalcified paraffin sections were used. Apart from these two references, we tried to apply the modified hybridization buffer of Schrenk et al. (2003), which includes poly(A) and bovine serum albumin to reduce false binding by minerals, but false binding was still severe (data not

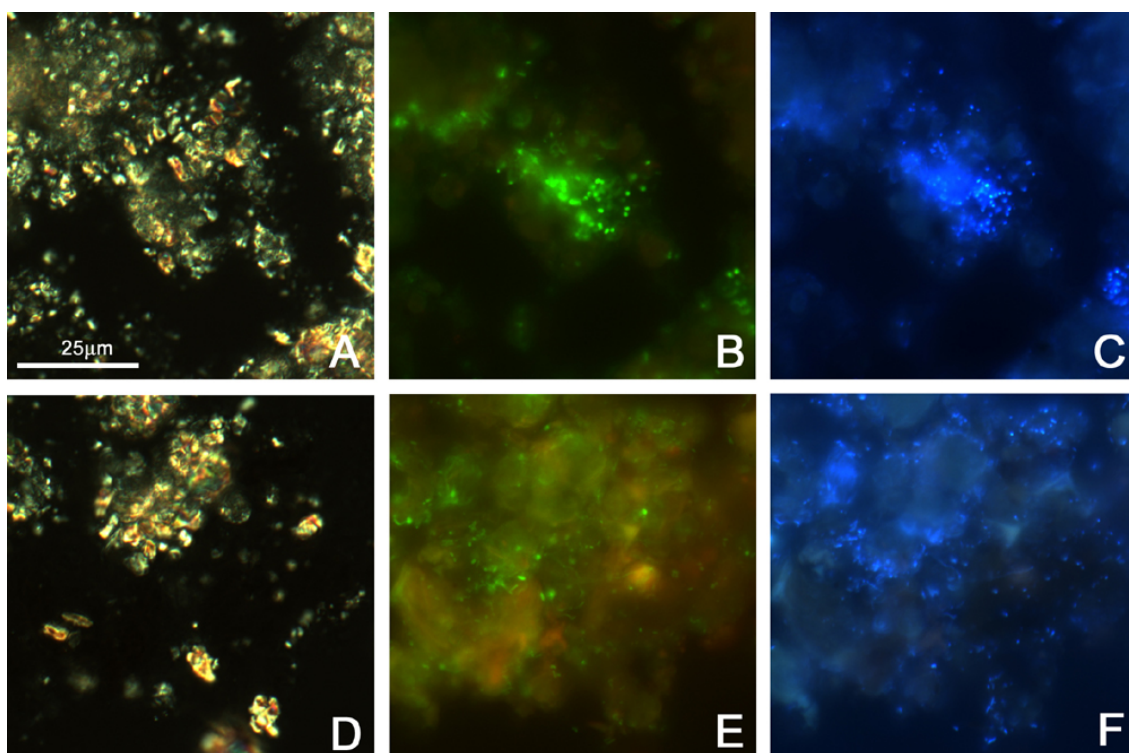


Fig. 1 Photomicrographs of CARD-FISH (A–C) and FISH (D–F) in freshwater stromatolite (tufa) sectioned with adhesive tape (Cryofilm Type 1). Each series shows identical microscopic fields. A and D are cross-polarized microscopy images, B and E are color combinations showing FISH and CARD-FISH signals (EUB338I–III) in green color. C and F represent DAPI staining. Both series were recorded with the same conditions except for E which was taken using a two times longer exposure time if compared to B.

shown).

By introducing a modified hybridization buffer of CARD-FISH into the protocol of Manz et al. (2000) and by adding CaCl_2 and NaHCO_3 , we could also detect microorganisms by FISH without false binding and calcite dissolution (Figs. 1D–F; Table 1).

3.2. Sample embedding and sectioning

For sectioning with adhesive tape, the best result was obtained by using fixed samples with overnight infiltration of 4% CMC, whereas frozen and fresh samples did not yield good quality of sections even if overnight infiltration in CMC was done. Sections obtained by Cryofilm Type 1 achieved good section quality of calcified biofilms, and there was no deformation and bacterial loss that usually occurred during the preparation of decalcified paraffin section due to bubble generation. This tape has no polarization property and hence is suitable for mineral detection. Although this tape caused slightly high background of DAPI, it was not severe for signal detection. The best section thickness was 5 μm and it was more difficult to detect hybridization signals from thicker sections. It is possible to transfer the section from the tape to the glass slide by using Transferfilm, although the quality of the

Table 1 Comparison of sectioning methods and results of modified hybridization protocols

	sectioning	section quality	FISH	CARD-FISH
<i>decalcified</i>	paraffin	+	++	++
<i>non-decalcified</i>	Technovit 7100	+*	++	-
	Cryofilm type1	++	++	++
	Transfer film	+	++	++

*only possible for very porous samples
 ++ denotes very good; + denotes good; - denotes bad

section got worse during the transferring step if compared to the sections obtained by Cryofilm Type 1 (Table 1). Sections obtained by both types of adhesive tape yielded good results of FISH and CARD-FISH. In this study, the adhesive tape method achieved vertical sections of 1 cm deep, but at least a depth of 3 cm may be achieved if larger samples are used.

For comparison, Technovit embedded sections could not produce well preserved thin sections except for very porous samples. Technovit sections yielded good result by FISH, while it caused severe false binding during CARD-FISH (Table 1).

3.3. Spatial distribution of bacteria in the calcified biofilms

Sectioning with adhesive tape and modified hybridization protocols used in the present study allow simultaneous visualization of the vertical distribution of microorganisms and calcite *in situ* in biofilms. Particularly bright CARD-FISH signals were detectable even at low magnification (e.g. $\times 20$), which is suitable for investigating depth profiles of microorganisms in the range of millimeters to centimeters (Fig. 2). These first results, using a universal probe (EUB338I-III), indicate that filamentous cyanobacteria decrease in number from the surface to deeper parts, whereas non-phototrophic bacteria remain abundant even at a depth of $\sim 900 \mu\text{m}$ below the biofilm surface. The bacteria are located in interstices between calcite crystals and are locally concentrated at the surface of the crystals. This fact implies that heterotrophs are deeply involved in the carbon cycling of the stromatolite biofilms similar to other biofilms, and that their metabolic activities and/or products (e.g. exopolymers) probably have a certain influence on mineral precipitation and/or dissolution.

While universal probes targeted for the domain Bacteria were used for method development during this study, the application of this protocol using probes of higher specificity will reveal a more detailed distribution pattern of different functional bacterial groups in the intensively calcified biofilms in various stromatolite-forming settings. In addition, the modified hybridization protocol of the present study will be applicable for FISH and CARD-FISH analysis of other mineral-containing microbial communities such as soils,

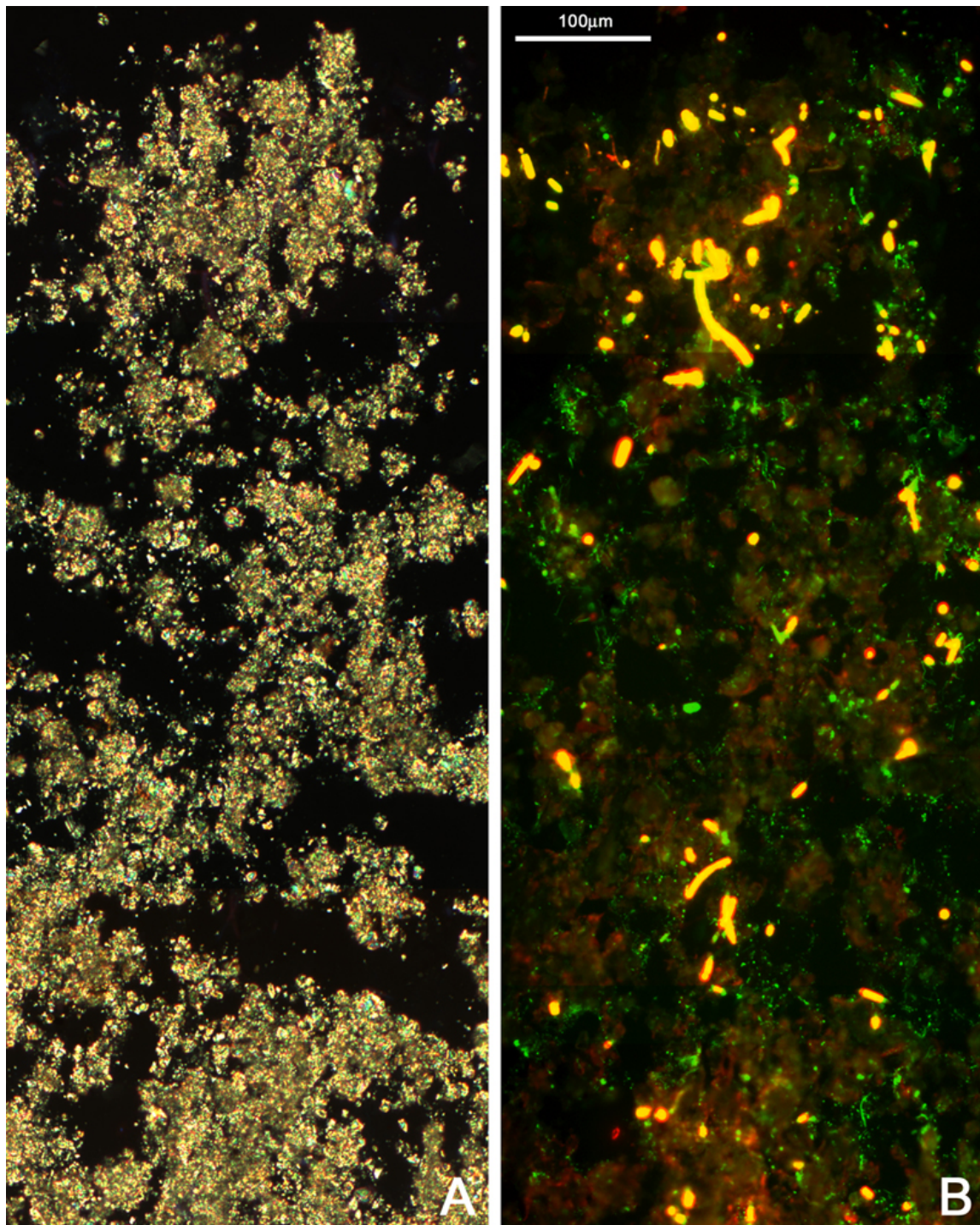


Fig. 2 Photomicrographs of eubacteria and calcite in tufa stromatolite detected by CARD-FISH using adhesive tape (Cryofilm Type 1). (A) Cross-polarized microscopy. (B) Same field of view which shows a color combined image recorded by epifluorescence microscopy. Bright yellow indicates autofluorescence of cyanobacteria, green indicates CARD-FISH signals of EUB338I-III, and dull red indicates autofluorescence of calcite and organic matters.

sediments and calcified sponges. As a consequence a further dissemination of the technique is expected.

Acknowledgements

We acknowledge the support of Dr. Nadia Queric, Mr. Wolfgang Dröse (University of Göttingen) and Dr. Daniel Jackson (University of Queensland) for technical instructions. We also thank to Dr. Tadahumi Kawamoto (Tsurumi University) for advising about adhesive tape methods. This project is the part of the Research Unit 571 "Geobiology of organo- and biofilms", funded by the German Research Foundation (DFG-FOR 571; AR 335/5; publication #30).

References

- Amann, R.I., Ludwig, W., Schleifer, K.-H., 1995. Phylogenetic identification and in situ detection of individual microbial cells without cultivation. *Microbiol. Rev.* 59, 143–169.
- Awramik, S.M., 1984. Ancient stromatolites and microbial mats. In: Cohen, Y., Castenholz, R.W., Halvorson, H.O. (Eds.), *Microbial Mats: Stromatolites*. Alan R. Liss, Inc., New York, pp. 1–22.
- Bissett, A., de Beer, D., Schoon, R., Shiraishi, F., Reimer, A., Arp, G. Microbial mediation of stromatolite formation in karst-water creeks. *Limnol. Oceanogr.* in press.
- Daims, H., Bruhl, A., Amann, R., Schleifer, K.H., Wanger, M., 1999. The domain-specific probe EUB338 is insufficient for the detection of all Bacteria: development and evaluation of a more comprehensive probe set. *Syst. Appl. Microbiol.* 22, 434–444.
- Dupraz, C., Visscher, P.T., 2005. Microbial lithification in marine stromatolites and hypersaline mats. *Trends Microb.* 13, 429–438.
- Harmsen, H.J.M., Prieur, D., Jeanthon, C., 1997. Distribution of microorganisms in deep-sea hydrothermal vent chimneys investigated by whole-cell hybridization and enrichment culture of thermophilic subpopulations. *Appl. Environ. Microbiol.* 63, 2876–2883.
- Hoffmann, F., Janussen, D., Dröse, W., Arp, G., Reitner, J., 2003. Histological investigation of organisms with hard skeletons: a case study of siliceous sponges. *Biotech. Histochem.* 78, 191–199.
- Kalkowsky, E., 1908. Oolith und Stromatolith im norddetschen Buntsandstein. *Dtsch. Geol. Ges.* 60, 68–125.
- Kawamoto, T., 2003. Use of a new adhesive film for the preparation of multi-purpose fresh-frozen sections from hard tissues, whole-animals, insects and plants. *Arch. Histol. Cytol.* 66, 123–143.
- Manz, W., Arp, G., Schumann-Kindel, G., Szewzyk, U., Reitner, J., 2000. Widefield deconvolution epifluorescence microscopy combined with fluorescence in situ hybridization reveals the spatial arrangement of bacteria in sponge tissue. *J. Microbiol. Methods* 40, 125–134.

Development of new hybridization technique for calcified biofilms

- Moter, A., Göbel, U.B., 2000. Fluorescence in situ hybridization (FISH) for direct visualization of microorganisms. *J. Microbiol. Methods* 41, 85–112.
- Pernthaler, A., Pernthaler, J., Amann, R., 2002. Fluorescence in situ hybridization and catalyzed reporter deposition for the identification of marine bacteria. *Appl. Environ. Microbiol.* 68, 3094–3101.
- Schönhuber, W., Fuchs, B., Juretschko, S., Amann, R., 1997. Improved sensitivity of whole-cell hybridization by the combination of horseradish peroxidase-labeled oligonucleotides and tyramide signal amplification. *Appl. Environ. Microbiol.* 63, 3268–3273.
- Schrenk, M.O., Kelley, D.S., Delaney, J.R., Baross, J.A., 2003. Incidence and diversity of microorganisms within the walls of an active deep-sea sulfide chimney. *Appl. Environ. Microbiol.* 69, 3580–3592.
- Shiraishi, F., Bissett, A., de Beer, D., Reimer, A., Arp, G. Photosynthesis, respiration and exopolymer calcium-binding in biofilm calcification (Westerhöfer and Deinschwanger Creek, Germany). *Geomicrobiol. J.* in press.
- Vesey, G., Deere, D., Gauci, M.R., Griffiths, K.R., Williams, K.L., Veal, D.A., 1997. Evaluation of fluorochromes and excitation sources for immunofluorescence in water samples. *Cytometry* 29, 147–154.
- Visscher, P.T., Reid, R.P., Bebout, B.M., 2000. Microscale observations of sulfate reduction: correlation of microbial activity with lithified micritic laminae in modern marine stromatolites. *Geology* 28, 919–922.
- Wallner, G., Amann, R., Beisker, W., 1993. Optimizing fluorescent in situ hybridization with ribosomal-RNA-targeted oligonucleotide probes for flow cytometric identification of microorganisms. *Cytometry* 14, 136–143.

Chapter 7

Discussion: Preconditions of photosynthesis induced
carbonate precipitation

Discussion

Preconditions of photosynthesis induced carbonate precipitation

As presented in the previous chapters, it is revealed that the tufa stromatolites are formed by photosynthesis induced calcite precipitation. However, apparently this phenomenon is not ubiquitous because not all of photosynthetic biofilms are calcified, which probably relate with the rarity of calcareous microbialite in the modern seawater settings. Then, what is the precondition of photosynthesis induced carbonate precipitation? The effects of photosynthetic CO₂ removal on calcite precipitation were simulated by Arp et al. (2001) with using PHREEQC program. They first adjusted the saturation state of model water at 10 by adding Ca²⁺ and DIC, subtracted 200 μmol/l CO₂, and checked the increase of saturation index of calcite (SIc), which is the legalism of Ω defined as followings,

$$SIc \equiv \log \Omega_c = \log \left(\frac{\{Ca^{2+}\}\{CO_3^{2-}\}}{K_{SPc}} \right) \quad (7.1)$$

From this simulation, they presented the DIC dependence of SIc increase by photosynthesis (ΔSIc): it becomes smaller as DIC increase, and vice versa.

In this chapter, further detail of photosynthetic effects on calcite precipitation are examined by changing not only DIC but also pH, which also affects carbonate system. The simulation in this study did not adjust the saturation state to 10 in order to check only the effects of CO₂ removal. Although Arp et al. (2001) subtracted 200 μmol/l CO₂ as an assumption, it is better to apply the similar removal amount of CO₂ caused by actual biofilms. The amount of CO₂ removal is therefore estimated by using pH microprofiles of calcifying biofilms, which fell in the range of ~800 to 1000 μmol/l CO₂ removal by PHREEQC (Fig. 1). In this study, CO₂ removal of 800 μmol/l by PHREEQC was employed throughout

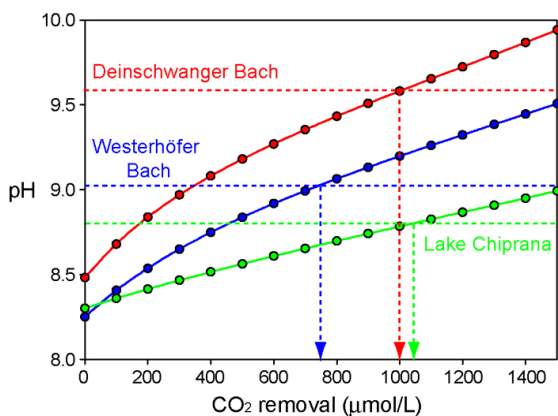


Fig. 1 The relationship between CO₂ removal amount and resulting pH in three settings where photosynthesis induced carbonate precipitation was observed. The amount of CO₂ removal in PHREEQC is estimated by using pH maximums at the top part of biofilms measured by microelectrode, which fell in the range of ~800 to 1000 μmol/l. pH value of Deinschwanger Bach was obtained *in situ* (Shiraishi et al. in press), while values of Westerhöfer Bach (Shiraishi et al. in press) and Lake Chiprana (the profile in light intensity of 500 μmol quanta /m²/s; Ludwig et al., 2005) were obtained *ex situ*. Note that estimated amounts do not represent the actual amount of CO₂ removal by biofilms.

the simulations. The effects of CO_2 removal were expressed by $\Delta\Omega$, not ΔSI , because the latter is not suitable for expressing the photosynthetic effects at low saturation state (for detail calculation, see Methods). $\Delta\Omega$ achieved by CO_2 removal in various DIC and pH is calculated by using standard seawater and tufa spring water as examples of seawater and freshwater respectively. Although complex calculations such as Pitzer equation are required for the precise estimation of ionic activities in the water of high ionic strength like seawater, the difference of Ω calculated by using Pitzer equation is less than 5% if compared to that of Debye–Hückel’s extended equation, which PHREEQC program employed, as indicated by Riding and Liang (2005a). Therefore, the calculation by PHREEQC has no significant effect on the discussion of this study.

The effects of CO_2 removal on $\Delta\Omega$ in various DIC–pH conditions are presented in Fig. 2, which obviously represent the fact that $\Delta\Omega$ depends on not only DIC but also pH. $\Delta\Omega$ pattern of both seawater and freshwater show triangular shape, and the latter is more prominent. The reason of this shape is explained as followings. In high DIC–high pH region where $[\text{CO}_3^{2-}]$ is high, $[\text{CO}_3^{2-}]$ increase caused by photosynthesis is buffered by significant amount of existing $[\text{CO}_3^{2-}]$ (CO_3^{2-} buffering), while in high DIC–low pH region where $[\text{CO}_2]$ is high, the effect of $[\text{CO}_2]$ subtraction by photosynthesis is buffered by significant amount of existing $[\text{CO}_2]$ (CO_2 buffering). In low DIC region on the other hand, the ratio of $[\text{CO}_3^{2-}]$ increase by photosynthetic CO_2 subtraction but total DIC decreases by the subtraction and results in lower $[\text{CO}_3^{2-}]$ (low DIC effect).

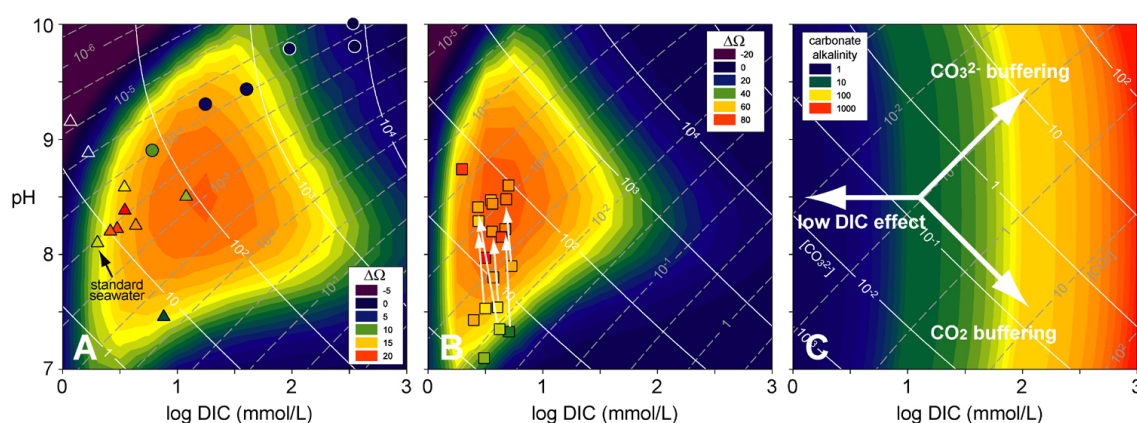


Fig. 2 $\Delta\Omega$ contour plot in various pH–DIC conditions calculated by using standard seawater (A) and tufa spring water of Westerhöfer Bach (B). $\Delta\Omega$ was calculated by subtracting $800\ \mu\text{mol/l}$ CO_2 in PHREEQC program. Temperature of both calculations was set at 25°C to make them comparable. pCO_2 (gray dot lines) and Ω (white solid lines) contours are also shown. For the calculation of Ω contours, $\{\text{Ca}^{2+}\}$ and $\{\text{CO}_3^{2-}\}$ of original water were used ($\{\text{Ca}^{2+}\}$ and $\log \gamma\text{CO}_3^{2-}$ of seawater were 2.305×10^{-3} and -0.677 , $\{\text{Ca}^{2+}\}$ and $\log \gamma\text{CO}_3^{2-}$ of tufa spring water were 1.994×10^{-3} and -0.215 , respectively). In these figures, $\Delta\Omega$ of various water samples are also plotted, and their values are indicated by the same color scale. Triangle symbols represent seawater and halite lakes, circles represent soda lakes and squares represent hardwater lakes and creeks. For their detail chemistries, see Table 1. Arrows in (B) indicate the changes of water chemistry in the tufa creeks from spring sites to lower creek sites. (C) The interpretation of $\Delta\Omega$ patterns. $[\text{CO}_2]$, $[\text{CO}_3^{2-}]$ and carbonate alkalinity contours were calculated by assuming freshwater. For detail calculations, see Methods.

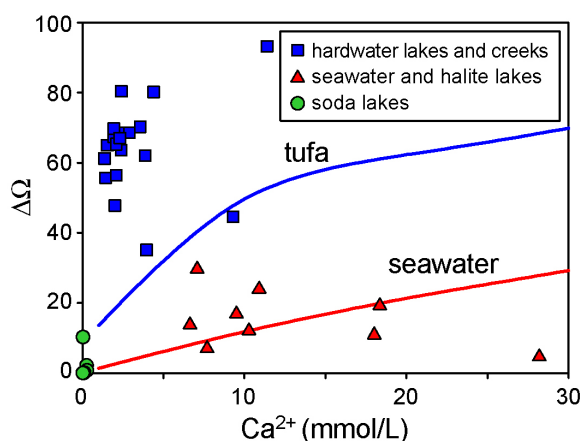


Fig. 3 The relationship between Ca^{2+} concentration and $\Delta\Omega$ attained by $800 \mu\text{mol/l}$ CO_2 subtraction. Lines were drawn by changing Ca^{2+} concentrations of standard seawater and tufa spring water (Westerhöfer Bach).

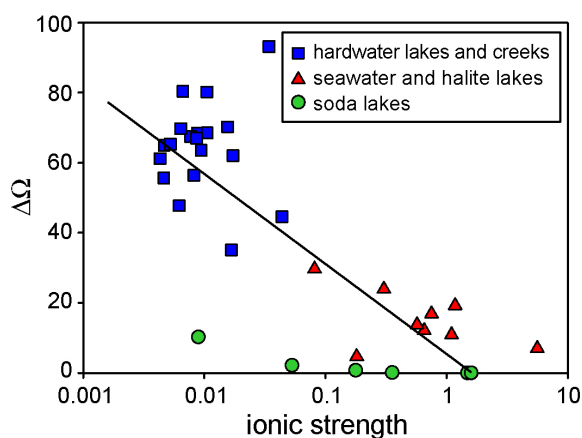


Fig. 4 The relationship between ionic strength and $\Delta\Omega$ attained by $800 \mu\text{mol/l}$ CO_2 subtraction. Water of lower ionic strength tends to attain higher $\Delta\Omega$. The examples of soda lakes significantly deviate from this trend because of their low Ca^{2+} concentration.

Therefore, $\Delta\Omega$ attains the maximum where these three effects are minimum. $\Delta\Omega$ pattern of tufa spring water is much higher than that of seawater because of lower ionic strength (see below).

$\Delta\Omega$ calculated by using various water chemistries are also plotted in Fig. 2 (for the original data, see Table 1). Although the tendency of calculated $\Delta\Omega$ roughly fits to both examples of seawater and tufa creek water, some are deviated and especially $\Delta\Omega$ of soda lakes did not fit at all. This deviation comes mainly from the differences of Ca^{2+} concentration. Fig. 3 shows the relationship between Ca^{2+} concentration and $\Delta\Omega$. $\Delta\Omega$ becomes higher as Ca^{2+} increases in both seawater and freshwater (tufa spring water). In the case of soda lakes, cation concentrations including Ca^{2+} are usually very low, which results in very low $\Delta\Omega$. This fact indicates that photosynthesis induced precipitation does not occur in the environments like soda lake where Ca^{2+} concentration is very low even if DIC–pH condition is suitable for increasing $\{\text{CO}_3^{2-}\}$. Of course, soda lakes tend to have high DIC and high pH where photosynthetic effects on carbonate system would be further inhibited by CO_3^{2-} buffering. On the other hand, Ca^{2+} concentrations of the other examples plotted in Fig. 3 are not extremely low, and therefore Ca^{2+} concentration would not be the limitation for

photosynthesis induced precipitation. The deviation of plotted data from calculated lines in Fig. 3 mostly comes from the differences of DIC and pH as shown in Fig. 2, as well as the differences of ionic strength. Higher ionic strength results in lower $\{\text{CO}_3^{2-}\}$ and $\Delta\Omega$ becomes smaller (Fig. 4), which is also obvious from Fig. 2.

Although optimum DIC–pH condition for achieving higher $\Delta\Omega$ is presented in Fig. 2, this $\Delta\Omega$ pattern does not represent the actual precondition of photosynthesis induced carbonate precipitation because the initial saturation state is not considered. Even if photosynthetic CO_2 removal could cause high $\Delta\Omega$, precipitation does not occur if initial saturation state is low because final Ω achieved by photosynthesis is lower than the threshold of precipitation ($\Omega_{\text{threshold}}$; Fig. 5). In this study, actual effect of photosynthetic CO_2 removal on Ω increase ($\Delta\Omega_{\text{actual}}$) is defined as follows,

$$\Delta\Omega_{\text{actual}} = |\Omega_{\text{after}} - \Omega_{\text{threshold}}| - |\Omega_{\text{before}} - \Omega_{\text{threshold}}| \quad (7.2)$$

Precipitation occurs if $\Delta\Omega_{\text{actual}}$ is >0 , while precipitation does not occur if $\Delta\Omega_{\text{actual}}$ is ≤ 0 (note that the size of minus value does not reflect the unlikelihood of precipitation). $\Omega_{\text{threshold}}$ would be larger than the achieved Ω when $800 \mu\text{mol/l}$ of CO_2 is removed from standard seawater ($\Omega=16.5$) because there is no extensive carbonate microbialite in the recent ocean. In this study, $\Omega_{\text{threshold}}$ is set at 17. The result of $\Delta\Omega_{\text{actual}}$ calculation is presented in Fig. 6. In the case of seawater, $\Delta\Omega_{\text{actual}}$ is ≤ 0 at low pH–DIC region while other parts are almost the same as that of $\Delta\Omega$ pattern. Similar tendency is seen in the case of freshwater although absolute values are higher than that of seawater because of lower ionic strength. Actual $\Omega_{\text{threshold}}$ must be somewhat higher than 17 at least for the freshwater case because the spring site of Westerhöfer Bach attained positive $\Delta\Omega_{\text{actual}}$ although it is free from biofilm calcification. Nonetheless, this pattern well presented the fact that photosynthesis induced precipitation is getting more important as water flows downstream in tufa creeks, which is confirmed by Shiraishi et al. (2008, in press) and Bissett et al. (2008, in press).

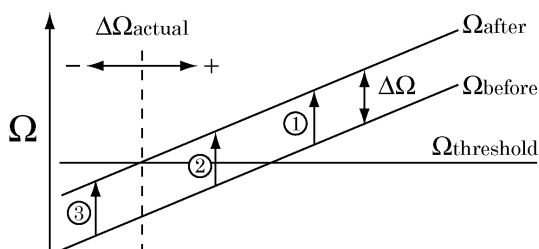


Fig. 5 The concept of actual effect of CO_2 removal for causing precipitation ($\Delta\Omega_{\text{actual}}$). Ω_{before} denotes Ω value before photosynthesis, and Ω_{after} denotes Ω value achieved by photosynthesis. Three examples are presented here, of which $\Delta\Omega$ achieved by photosynthesis is the same. 1) Ω_{before} is higher enough than the threshold ($\Omega_{\text{threshold}}$), and Ω_{after} results in precipitation. 2) Ω_{before} is somewhat lower than the threshold, but Ω_{after} can achieve higher Ω than the threshold, and results in precipitation. 3) Ω_{before} is too low, and Ω_{after} cannot exceed the threshold, and precipitation does not occur.

From discussions above, the preconditions of photosynthesis induced carbonate precipitation are 1) optimum pH–DIC condition where low DIC effect, CO_2 and CO_3^{2-} buffering are not severe, 2) sufficient initial saturation state, 3) Ca^{2+} concentration is not extremely low. In addition, high ionic strength weakens and/or inhibits photosynthesis induced precipitation. Of course, photosynthetic activity of biofilms must be high enough to shift carbonate system on and in the biofilms. Although these preconditions were delivered from the studies of photosynthesis induced carbonate precipitation, most of them are also applicable for carbonate precipitation induced by other types of microbial metabolisms such as sulfate reduction because carbonate precipitation induced by microbial mechanisms are achieved by increasing $\{\text{Ca}^{2+}\}$ and/or $\{\text{CO}_3^{2-}\}$ regardless of metabolic pathways. Therefore, it is concluded that these preconditions would be important keys to understand the formation and distribution of carbonate microbialite through the geologic time.

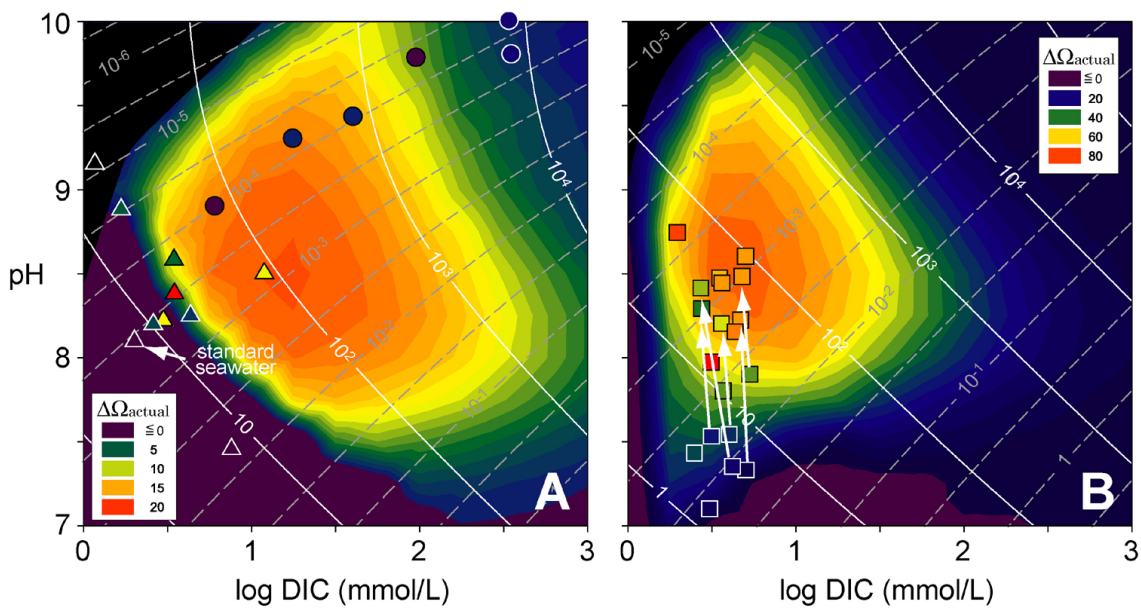


Fig. 6 The contour plots of actual effect of CO_2 removal for causing precipitation ($\Delta\Omega_{\text{actual}}$) in various pH–DIC conditions by using standard seawater (A) and tufa spring water of Westerhöfer Bach (B). Compare the results with the contour plots shown in Fig. 2. $\Delta\Omega_{\text{actual}}$ of low DIC–high pH region was not calculated because of negative $\Delta\Omega$.

location		pH	Ca ²⁺ ($\mu\text{mol/L}$)	Mg ²⁺ ($\mu\text{mol/L}$)	Na ⁺ ($\mu\text{mol/L}$)	K ⁺ ($\mu\text{mol/L}$)	Sr ²⁺ ($\mu\text{mol/L}$)	DIC ($\mu\text{eq/L}$)	Alk ($\mu\text{eq/L}$)	Cl ⁻ ($\mu\text{mol/L}$)	SO ₄ ²⁻ ($\mu\text{mol/L}$)	B ($\mu\text{mol/L}$)	Br ⁻ ($\mu\text{mol/L}$)	F ⁻ ($\mu\text{mol/L}$)	$\Delta\Omega$	$\Delta\Omega_{\text{actual}}$	ref	
hardwater lakes and creeks																		
Westerhöfer Bach	(spring)	May 2006	7.33	3.95	1.72	0.34	0.05		5.40	0.29	2.94				35.1	6.6	(1)	
	(downstream)		8.22	3.57	1.69	0.33	0.05		4.82	0.29	2.87				70.2	68.9	(1)	
Deinshwanggr Bach	(spring)	Oct. 2006	7.90	2.39	0.82	0.44	0.09		5.28	0.70	0.14				63.6	45.0	(1)	
	(downstream)		8.48	2.28	0.78	0.43	0.09		5.00	0.67	0.14				68.5	68.5	(1)	
Shimokuraida	(spring)	Jan. 2002	7.35	2.01	0.06	0.19	0.01		3.86	0.15	0.08				47.7	16.8	(2)	
	(downstream)		8.41	1.53	0.06	0.19	0.01		2.79	0.15	0.08				65.0	49.7	(2)	
Shirokawa	(spring)	Jul. 1999	7.58	1.44	0.06	0.15	0.01		3.01	0.12	0.06				55.7	24.7	(3)	
	(downstream)		8.29	1.36	0.06	0.15	0.01		2.79	0.12	0.06				61.2	40.3	(3)	
Muiga	(spring)	Oct. 2003	7.54	2.08	0.25	1.47	0.06		3.82	1.44	0.28				56.4	26.9	(4)	
	(downstream)		8.20	1.92	0.25	1.46	0.05		3.66	1.35	0.27				67.5	51.0	(4)	
Faytreville Green Lake			7.97	11.39	2.67				3.20		9.30				93.2	87.0	(5)	
Lake Zurich		Jul. 1975	8.74	4.4	0.6				2.22						80.2	80.2	(5)	
Everglades		Aug. 1989	7.43	2.09					2.33						65.3	33.7	(5)	
Flensbrunnbach			8.15	2.4					4.4						80.4	70.7	(5)	
Lake El Mojarral		Jul. 1983	7.1	9.30	4.50	6.20	0.21		2.70	2.90	14.30				44.6	12.9	(5)	
Lake Kozjak Pitvice		Oct. 1983	8.47	3.88	4.32				3.80						62.0	62.0	(5)	
Weissenbach		Sept. 1988	8.6	1.95	0.21				5.28						69.8	69.8	(5)	
River Moosach		Aug. 1996	7.80	2.89	0.98	0.91	0.11		3.63	0.93	0.33				68.5	44.5	(5)	
River Seempt		Feb. 1996	8.44	2.30	1.04	0.19	0.03		3.78	0.40	0.23				67.1	67.1	(5)	
seawater and halite lakes																		
standard seawater																		
Aldabra "Cinq Cases Pools I"		Aug. 1984	8.10	10.28	52.82	469.06	10.21	0.09	2.04		545.86	28.24	0.42	0.84	0.01	12.1	-12.1	(6)
Aldabra "Cinq Cases Pools III"		Aug. 1984	8.88	28.18	63.02				2.51						4.6	4.6	(5)	
		Aug. 1984	9.15	19.50	82.83				2.09						-16.0	n.c.	(5)	
Aldabra Pool "Profond"		Aug. 1984	8.38	7.08	33.66				3.98						29.7	29.7	(5)	
Lake Clifton		Aug. 1998	8.22	10.90	41.97	388	6.94		3.34					23.9	11.8	(5)		
Shark bay		Aug. 1998	8.2	18.35	89.69	852	18.6		2.97	10.10	54.13			19.2	4.1	(5)		
Lake Theis		Aug. 1998	8.25	9.50	50.20	501.0	10.76		4.80	682.2	54.55			16.9	3.1	(5)		
Great Salt Lake, North Arm		Aug. 1997	7.46	7.69	440.2	4372	191.3		7.98	5100	280			6.9	-6.9	(5)		
Satonda		Oct. 1993	8.58	6.64	42.5	423.54	11.46		3.41	417	487.49	18.33		13.8	5.7	(5), (7)		
Lake Chiprana		Oct. 2000	8.5	18	322	497	5		12	309	500			10.9	10.9	(8)		
soda lakes																		
Lake Tanganyika		1985	8.9	0.309	1.868	2.401	0.729		6.60	0.747	0.052			10.3	-5.1	(5)		
Pyramid Lake		May 1996	9.3	0.26	3.29	72.6	2.86		22.08					2.1	2.1	(5)		
Walker Lake		Aug. 1997	9.43	0.28	3.89	173.1	5.05		55.20	56.977	20.092			0.7	0.7	(5)		
Lake Van			9.78	0.115	3.9	336.9	13.0		155.5	157.3	24.4			0.1	-0.1	(5)		
Lake Nuoerta		Sept. 1994	10	0.073	6.15	1495	112		624.3	786	113			0.0	0.0	(5)		
Mono Lake			9.8	0.025	1.32	1422	40.3		618	685	277			0.0	0.0	(5)		

Table 1 The actual effect of CO₂ removal for causing precipitation ($\Delta\Omega_{\text{actual}}$) in various water samples. $\Delta\Omega_{\text{actual}}$ were calculated at 25°C by subtracting 800 $\mu\text{mol/L}$ CO₂. Water chemistry data was obtained from literatures (1 Shirraishi et al. in press; 2 Kawai et al. 2006; 3 Kano et al. unpublished data; 4 Kano et al. 2007; 5 Arp et al. 2001; 6 Zeebe and Wolf-Gladrow 2001; 7 Arp et al. 2003; 8 Jonkers et al. 2003).

Methods

$\Delta\Omega$ contour calculations

$\Delta\Omega$ was calculated by subtracting 800 $\mu\text{mol/L}$ with PHREEQC program in various pH–DIC conditions. pH change ranged from 7.0 to 10.0, and log DIC (mmol/L) ranged from 0.0 to 3.0, and calculated in 0.25 grid (the region of log DIC <-0.0 was impossible to calculate because there is no sufficient DIC). In this study, standard seawater and tufa creek water (Westerhöfer Bach, spring site) were used. Temperature was set at 25°C to exclude the effect of temperature.

Although PHREEQC can calculate saturation state of calcite directly as saturation index, its significant figures are small (e.g., 1.00), which causes severe artifacts in high pH–high DIC region where saturation state tends to high. For example, if very small change in unexpressed figure, generated by CO_2 subtraction, accidentally caused 0.01 of ΔSI , this change account for $\Delta\Omega$ of 0.02 when SI changed from 0.00 to 0.01, while it gets more significant if initial saturation state becomes higher (e.g., SI change of 1.00→1.01 accounts for $\Delta\Omega$ of 0.23, 2.00→2.01 accounts for $\Delta\Omega$ of 2.32). In this study, Ω was calculated by PHREEQC-delivered $\{\text{Ca}^{2+}\}$ and $\{\text{CO}_3^{2-}\}$ as followings,

$$\Omega = \frac{\{\text{Ca}^{2+}\}\{\text{CO}_3^{2-}\}}{K_{\text{sp}}} \quad (7.3)$$

K_{sp} for calcite was given by Plummer and Busenberg (1982), which is consistent with the values used in PHREEQC program. Of course the significant figures of $\{\text{Ca}^{2+}\}$ and $\{\text{CO}_3^{2-}\}$ (four figures) cause slight artifact, but the quality is sufficient for the discussion in this study.

Other contour calculations

$[\text{CO}_2]$ and $[\text{CO}_3^{2-}]$: Contour lines are calculated from equations (1.6) and (1.8), respectively.

p CO_2 : Contour lines are calculated from equation (1.1) and (1.6),

$$\text{DIC} = \text{pCO}_2 K_{\text{H}} \left(1 + \frac{K_1}{[\text{H}^+]} + \frac{K_1 K_2}{[\text{H}^+]^2} \right)$$

DIC is expressed as a function of $[\text{H}^+]$, if p CO_2 is fixed.

Saturation state (Ω): Contour lines are calculated from equations (7.3) and (1.8),

$$\text{DIC} = \frac{\Omega K_{\text{SP}}}{[\text{Ca}^{2+}]} \left(1 + \frac{[\text{H}^+]}{K_2} + \frac{[\text{H}^+]^2}{K_1 K_2} \right)$$

DIC is expressed as a function of $[\text{H}^+]$, if Ω and $[\text{Ca}^{2+}]$ are fixed. To take activities into account, $\{\text{Ca}^{2+}\}$ was applied instead of $[\text{Ca}^{2+}]$, and γCO_3^{2-} was multiplied.

Carbonate alkalinity: Contour is calculated from equations (1.7)–(1.9),

$$\text{CA} = \text{DIC} \left\{ 1 / \left(1 + \frac{[\text{H}^+]}{K_1} + \frac{K_2}{[\text{H}^+]} \right) + 2 / \left(1 + \frac{[\text{H}^+]}{K_2} + \frac{[\text{H}^+]^2}{K_1 K_2} \right) \right\}$$

CA is expressed as a function of $[\text{H}^+]$, if CA and DIC are fixed.

Equilibrium constants

Equilibrium constants of Plummer and Busenberg (1982) were applied for the contour calculations of freshwater setting, and constants of Roy et al. (1993), presented below, were applied for the calculation of seawater settings.

$$\begin{aligned} \ln K_1 = & 2.83655 - 2307.1266 / T - 1.5529413 \ln T - (0.207608410 + 4.0484 / T) \sqrt{S} \\ & + 0.0846834S - 0.00654208S^{\frac{3}{2}} + \ln(1 - 0.001005S) \end{aligned}$$

$$\begin{aligned} \ln K_2 = & -9.226508 - 3351.6106 / T - 0.2005743 \ln T - (0.106901773 + 23.9722 / T) \sqrt{S} \\ & + 0.1130822S - 0.00846934S^{\frac{3}{2}} + \ln(1 - 0.001005S) \end{aligned}$$

where T and S denote absolute temperature and salinity, respectively.

K_{H} for seawater is delivered from Weiss (1974),

$$\ln K_{\text{H}} = 9345.17 / T - 60.2409 + 23.3585 \ln(T / 100) + S \left[0.023517 - 0.00023656T + 0.0047036(T / 100)^2 \right]$$

References

- Arp G, Reimer A, Reitner J. 2001. Photosynthesis-induced biofilm calcification and calcium concentrations in Phanerozoic oceans. *Science* 292:1701–1704.
- Jonkers HM, Ludwig R, de Wit R, Pringault O, Muyzer G, Niemann H, Finke N, de Beer D. 2003. Structural and functional analysis of a microbial mat ecosystem from a unique permanent hypersaline inland lake: ‘La Salada de Chiprana’ (NE Spain). *FEMS Microbiol Ecol* 44:175–189.
- Kano, A., Matsuoka, J., Kojo, T., Fujii, H., 2003. Origin of annual laminations in tufa deposits, southwest Japan.

-
- Palaeogeogr. Palaeoclimatol. Palaeoecol. 191, 243–262.
- Kano, A., Hagiwara, R., Kawai, T., Hori, M., Matsuoka, J., 2007. Climatic conditions and hydrological change recorded in a high-resolution stable isotope profile of a recent laminated tufa on a subtropical island, southern Japan. *J. Sediment. Res.* 77, 59–67.
- Kawai, T., Kano, A., Matsuoka, J., Ihara, T., 2006. Seasonal variation in water chemistry and depositional processes in a tufa-bearing stream in SW-Japan, based on 5 years of monthly observations. *Chem. Geol.* 232, 33–53.
- Ludwig R, Al-Horani F, de Beer D, Jonkers HM. 2005. Photosynthesis-controlled calcification in hypersaline microbial mat. *Limnol Oceanogr* 50:1836–1843.
- Plummer LN, Busenberg E. 1982. The solubilities of calcite, aragonite and vaterite in CO₂-H₂O solutions between 0 and 90°C, and an evolution of aqueous model for the system CaCO₃-CO₂-H₂O. *Geochim Cosmochim Acta* 46:1011–1040.
- Riding R, Liang L. 2005. Geobiology of microbial carbonates: metazoan and seawater saturation state influences on secular trends during the Phanerozoic. *Palaeogeogr Palaeoclimatol Palaeoecol* 219:101–115.
- Roy, R.N., Roy, L.N., Vogel, K.M., Porter-Moore, C., Pearson, T., Good, C.E., Millero, F.J., Campbell, D.M., 1993. The dissociation constants of carbonic acid in seawater at salinities 5 to 45 and temperatures 0 to 45°C. *Marine Chemistry* 44, 249–267.
- Shiraishi, F., Bissett, A., de Beer, D., Reimer, A., Arp, G. Photosynthesis, respiration and exopolymer calcium-binding in biofilm calcification (Westerhöfer and Deinschwanger Creek, Germany). *Geomicrobiol. J.* in press.
- Weiss, R.F., 1974. Carbon dioxide in water and seawater: the solubility of a non-ideal gas. *Mar. Chem.* 2, 203–215.
- Zeebe RE, Wolf-Gladrow D. 2001. CO₂ in seawater: equilibrium, kinetics, isotopes. Elsevier, Amsterdam, 346p.

Summary

In this study, biofilms of two CO₂-degassing karst-water creeks in Germany, which attain high calcite supersaturation during their course downstream, were investigated with regard to the effects of microbial activity on CaCO₃ precipitation, water chemistry of micro- and macroenvironment, stable isotopic records, and tufa fabric formation. *In situ* and *ex situ* microelectrode measurements (pH, O₂, Ca²⁺ and CO₃²⁻) of annually laminated calcified biofilms composed mainly of filamentous cyanobacteria (tufa stromatolites) revealed that they strongly induced CaCO₃ precipitation by photosynthesis under illumination, and inhibited precipitation by respiration in the dark. During illumination, microbial photosynthesis cause a strong pH increase, coupled with Ca²⁺ consumption at the biofilm surface, while the opposite occurred in the dark. Calcite supersaturation at the biofilm surface, calculated from *ex situ* Ca²⁺ and CO₃²⁻ microelectrode measurements, showed that photosynthesis resulted in high Ω values during illumination, while respiration slightly lowered supersaturation values in the dark, compared to values in the water column. Dissociation calculation demonstrated that the potential amount of Ca²⁺ binding by exopolymers would be insufficient to explain the Ca²⁺ loss observed, although Ca²⁺ complexation to exopolymers might be crucial for calcite nucleation. Photosynthesis-induced CaCO₃ precipitation was also confirmed by radioactive isotope (⁴⁵Ca²⁺) uptake studies as well as mass balance calculations.

Oxygen and carbon stable isotopic records of the tufa stromatolites did confirm photosynthetic effects despite the evident photosynthesis-induced calcite precipitation, and therefore, the absence of photosynthetic effect in the isotopic records of carbonate minerals (e.g., heavier $\delta^{13}\text{C}$) does not indicate the absence of photosynthetic effect on the carbonate precipitation. Similarly, fabrics of calcified cyanobacteria (e.g., sheath impregnation or encrustation by CaCO₃) cannot be used to distinguish photosynthesis-induced from physicochemically-induced CaCO₃ precipitation because encrusted cyanobacterial sheaths, that was previously suggested as an indicator of physicochemically-forced precipitation, was observed in tufa stromatolite instead of sheath impregnation, that was previously suggested as an indicator of photosynthesis-induced precipitation.

Although tufa stromatolites are formed by photosynthesis-induced calcite precipitation, mass balance calculations demonstrated that biofilm photosynthesis was responsible for only 10–20% of Ca²⁺ loss in the creek, while remaining Ca²⁺ loss derived from physicochemical precipitation on branches, leaves and fine-grained calcite particles. Therefore, the effects of photosynthesis-induced precipitation are diluted, and undetectable

by conventional water analysis except for the period of low flow rate.

In contrast, endolithic cyanobacterial biofilms and mosses, both can also perform photosynthesis, did not cause photosynthesis-induced precipitation under experimental conditions of *ex situ* microelectrode measurements because of their lower photosynthetic activity. No spontaneous precipitation occurred on biofilm-free limestone substrates under the *ex situ* measurements, despite of high supersaturation, while tufa stromatolites could induce precipitation in the same condition. This fact indicates that photosynthesis is a crucial mechanism to overcome the kinetic barrier for CaCO_3 precipitation, even in highly supersaturated settings.

The simulations of photosynthetic effects in various pH, DIC and Ca^{2+} concentration revealed the preconditions of photosynthesis-induced carbonate precipitation are 1) optimum pH–DIC condition where low DIC effect, CO_2 and CO_3^{2-} buffering are not severe, 2) sufficient initial saturation state, 3) Ca^{2+} concentration is not extremely low. In addition, high ionic strength weakens and/or inhibits photosynthesis-induced precipitation. Of course, photosynthetic activity of biofilms must be high enough to shift carbonate system on and in the biofilms. Most of these preconditions are also applicable for the carbonate precipitation induced by other types of microbial metabolisms such as sulfate reduction. Therefore, it is concluded that these preconditions would be the important keys to understand the formation and distribution of carbonate microbialite through the geologic time.

Lebenslauf Fumito Shiraishi

3. Juli 1979	geboren in Imabari, Japan
April 1986– März 1992	Kusukawa Grundschule in Toyo, Japan
April 1992– März 1995	Kahoku Mittelschule in Toyo, Japan
April 1995– März 1998	Saijo Oberschule in Saijo, Japan
April 1998– März 2002	Geologe-Studium an der Universität Hiroshima
März 2002	Bachelor of Science (B.Sc.)
April 2002– März 2004	Geologe-Studium an der Universität Hiroshima
März 2004	Master of Science (M.Sc.)
Juni 2005– März 2008	wissenschaftlicher Mitarbeiter am Geowissenschaftlichen Zentrum der Georg-Augst-Universität Göttingen